May 2017

Applications of Elpasolites as a Multimode Radiation Sensor

Amber Lynn Guckes
University of Nevada, Las Vegas, shield39@unlv.nevada.edu

APPLICATIONS OF ELPASOLITES AS A MULTIMODE RADIATION SENSOR

By

Amber Guckes

Bachelor of Science – Mechanical Engineering
University of Nevada, Las Vegas
2013

Master of Science – Materials and Nuclear Engineering
University of Nevada, Las Vegas
2014

A dissertation submitted in partial fulfillment
of the requirements for the

Doctor of Philosophy – Mechanical Engineering

Department of Mechanical Engineering
Howard R. Hughes College of Engineering
The Graduate College

University of Nevada, Las Vegas
May 2017

This research was supported by National Security Technologies, LLC, under Contract No. DE AC52-06NA25946 with the U.S. Department of Energy. The United States Government retains and the publisher, by accepting the article for publication, acknowledges that the United States Government retains a non-exclusive, paid-up, irrevocable, world-wide license to publish or reproduce the published form of this manuscript, or allow others to do so, for United States Government purposes. DOE/NV/25946—3083.

UNLV | GRADUATE COLLEGE

Dissertation Approval

The Graduate College
The University of Nevada, Las Vegas

April 5, 2017

This dissertation prepared by

Amber Guckes

entitled

Applications of Elpasolites as a Multimode Radiation Sensor

is approved in partial fulfillment of the requirements for the degree of

Doctor of Philosophy – Mechanical Engineering
Department of Mechanical Engineering

Alexander Barzilov, Ph.D.
Examination Committee Chair

Kathryn Hausbeck Korgan, Ph.D.
Graduate College Interim Dean

William Culbreth, Ph.D.
Examination Committee Member

Charles Martin, Ph.D.
Examination Committee Member

Paul Guss, Ph.D.
Examination Committee Member

Ke-Xun Sun, Ph.D.
Graduate College Faculty Representative

ABSTRACT

APPLICATIONS OF ELPASOLITES AS A MULTIMODE RADIATION SENSOR

By

Amber Guckes

Dr. Alexander Barzilov, Examination Committee Chair

Associate Professor of Mechanical Engineering

University of Nevada, Las Vegas

This study consists of both computational and experimental investigations. The computational results enabled detector design selections and confirmed experimental results. The experimental results determined that the CLYC scintillation detector can be applied as a functional and field-deployable multimode radiation sensor.

The computational study utilized MCNP6 code to investigate the response of CLYC to various incident radiations and to determine the feasibility of its application as a handheld multimode sensor and as a single-scintillator collimated directional detection system. These simulations include:

- Characterization of the response of the CLYC scintillator to gamma-rays and neutrons;
- Study of the isotopic enrichment of ^{7}Li versus ^{6}Li in the CLYC for optimal detection of both thermal neutrons and fast neutrons;
- Analysis of collimator designs to determine the optimal collimator for the single CLYC sensor directional detection system to assay gamma rays and neutrons;

- Simulations of a handheld CLYC multimode sensor and a single CLYC scintillator collimated directional detection system with the optimized collimator to determine the feasibility of detecting nuclear materials that could be encountered during field operations. These nuclear materials include depleted uranium, natural uranium, low-enriched uranium, highly-enriched uranium, reactor-grade plutonium, and weapons-grade plutonium.

The experimental study includes the design, construction, and testing of both a handheld CLYC multimode sensor and a single CLYC scintillator collimated directional detection system. Both were designed in the Inventor CAD software and based on results of the computational study to optimize its performance.

The handheld CLYC multimode sensor is modular, scalable, low-power, and optimized for high count rates. Commercial-off-the-shelf components were used where possible in order to optimize size, increase robustness, and minimize cost. The handheld CLYC multimode sensor was successfully tested to confirm its ability for gamma-ray and neutron detection, and gamma-ray and neutron spectroscopy. The sensor utilizes wireless data transfer for possible radiation mapping and network-centric deployment. The handheld multimode sensor was tested by performing laboratory measurements with various gamma-ray sources and neutron sources.

The single CLYC scintillator collimated directional detection system is portable, robust, and capable of source localization and identification. The collimator was designed based on the results of the computational study and is constructed with high density polyethylene (HDPE) and lead (Pb). The collimator design and construction allows for the directional detection of gamma rays and fast neutrons utilizing only one scintillator which is interchangeable. For this study, a CLYC-7 scintillator was used. The collimated directional detection system was tested by

performing laboratory directional measurements with various gamma-ray sources, ^{252}Cf and a ^{239}PuBe source.

ACKNOWLEDGEMENTS

I have looked back at the last seven years of my life and have wondered how have I gotten this far? Yes, I put in the time, the hard work, the sweat, the tears, but there was something more: I did not do it alone. It has been by the support of my family, friends, peers, professors, coworkers, and mentors, that I was able to do it. I am eternally grateful for them.

I would first like to thank Dr. Barzilov, my committee chair. Dr. Barzilov you have helped me grow technically as an engineer and have provided the tools for me to innovate and to be successful in doing so. I hope that after I graduate, we can collaborate and help other young nuclear engineers achieve their dreams.

To my remaining dissertation committee members, Dr. Sun, Dr. Culbreth, Dr. Guss, and Dr. Martin, I thank you all for your time and support as I have pursued my dissertation. During my prospectus defense I was in awe as to how much knowledge, experience, and respect was felt from you all. I hope to work with you all again someday as a peer.

To my coworkers at NSTec, you may now call me doc. I am only teasing! Thank you for your inspiration and motivation. Also, thank you for challenging me as a leader. I feel now that I have the tools to not only be a successful nuclear engineer, but to be a successful leader.

I owe a big thank you to my mentor Dennis Fulkerson. Dennis, thank you for taking me under your wings and mentoring me where I really needed it the most. I recall you first thinking how am I supposed to help her be a better engineer. However, you have certainly helped me become a stronger communicator and leader.

Thank you to my supervisor, Eric Loros, and my director, Ron Piburn, for allowing me to pursue my PhD degree while working full time for you. Your understanding, encouragement, and support have helped me successfully complete this work.

Thank you to Terry Kell and Jake from the UNLV Machine Shop. I greatly appreciate all of the hours you both spent consulting with me on the design of my detectors, teaching me how to use and clean all of the machines, allowing me to use raw materials from the shop, and for helping me bring to life my collimated directional radiation detection system.

Thank you Kason Knight of i-SOLIDS 3-D printing hub and Knight Engineering Solutions, LLC, for the 3-D printing of the handheld detector housing. Your customer service and work is fantastic. I will certainly come back to you for business in the future.

Thank you to Melinda Sweany of Sandia National Laboratory for the advice concerning the MLEM algorithm and discussing with me the approach used by her team to implement it in their journal publication "Demonstration of two-dimensional time-encoded imaging of fast neutrons." Without your direction, I would still probably be working on the MLEM algorithm for this work.

Thank you to my mother and father who have never doubted me and have always encouraged me to go after my dreams, no matter how unattainable they may have seemed. The two of you together are my rock and I am uncertain what I would ever do without you. I am so thankful and joyous that you two are able to share this significant moment in my life. Besides your support, one thing that I forever will be thankful for is that you taught to Sean and me morals: to know the difference between right and wrong, to stand for what you believe in, and that the only way to make something of yourself is through hard work. I love you both very much.

To my brother Sean, I am so very happy that you came home and that I have been able to share my journey with you. I am thankful that we get spend more time together, especially when it gives me a break from working relentlessly on my dissertation. Also, thanks to your amazing mechanical mind and skills, I could actually bring my ideas to life. I love you brother.

To my dogs Balto and Athena, I understand that you will never read this because you can't read, but nonetheless I owe a lot to the two of you. Balto, you area real sweetheart and always give me doggy kisses when I need them the most and bite me in my bottom when I need a wake-up call. Athena, you are this girl's best friend indeed. Since Jared and I picked you up you have held our hearts. You make every day special and I can't wait to graduate and share more time together. I love you both.

To my husband Jared and I am thankful for many things. Thank you for letting me spend time on my dissertation instead of with you. Thank you for teaching me to stick-up for myself and to care less about what other people think of me. Thank you for teaching me when to work hard and when to relax and let-loose. Most of all, thank you for the unwavering love that you have given to me. I look forward to all the adventures we will have together once I have my weekends back. I love you.

My family can tell you that I am a very determined and motivated individual. Once I set my eyes on a goal, I will put everything I have got into that goal until I have achieved it. I have dreamed of becoming a nuclear engineer and to earn a PhD degree for years. To finally see this come to fruition is quite humbling. Although this chapter of my life has come to an end, this is only the beginning for me as a nuclear engineer and I cannot wait to face the challenges and opportunities that lay before me.

DEDICATION

To my mother and father.

"Nothing in life is to be feared, it is only to be understood. Now is the time to understand more, so that we may fear less." – Marie Curie

TABLE OF CONTENTS

LIST OF TABLES

LIST OF FIGURES

CHAPTER 1

INTRODUCTION

1.1 Motivation for Study

The progress in advancing radiation detection capabilities within the last few years has been outstanding. The motivation behind this progress is to address nuclear safeguards and security challenges and support nonproliferation efforts. Radiological and nuclear threats around the world continue to grow as terrorist groups rise and rogue states grow. Radioactive or nuclear material in the wrong hands could mean devastating results for all.

The advancement of radiation detection technologies allows for more efficient means to detect and perhaps mitigate or prevent such disasters from occurring. Sodium iodide (NaI) gamma-ray scintillators and helium-3 (^{3}He) gaseous detectors were once looked to as the gold standards in radiation detection. Recent discovery and development of novel radiation detection materials are beginning to challenge these standards. New materials, such as the elpasolite $Cs_2LiYCl_6:Ce^{3+}$ (CLYC), offer the ability to perform gamma-ray spectroscopy with an energy resolution better than that of NaI, to detect thermal neutrons as does ^{3}He, to perform fast neutron spectroscopy, and be able to detect and discriminate all three of these radiation types in a single scintillator sensor.

The ability to detect and discriminate gamma rays, thermal neutrons and fast neutrons provides CLYC the designation of multimode radiation-detecting scintillator. The application of CLYC as a field-deployable scintillator is emergent, but not yet complete. Various handheld detectors and directional detection systems utilizing CLYC as a thermal neutron/gamma-ray sensor have been investigated; only a few have been commercially produced or deployed. Application of CLYC as a multimode sensor capable of simultaneously detecting thermal neutrons, fast neutrons, and gamma rays has yet to be investigated.

It is the goal of this study to perform independent review of the characteristics of CLYC and to apply this scintillator as a multimode radiation sensor in the form of a handheld detector and a directional detection system.

1.2 Background

The CLYC scintillator has proven to demonstrate a gamma-ray energy resolution at 662 keV of less than 5% [1]. This energy resolution is 25 – 30% better than a typical NaI scintillator [2]. The energy resolution of the thermal neutron peak appearing at approximately 3.2 MeV gamma-ray equivalent energy (GEE) is between 2.5% and 3.1% [3]. The thermal neutron cross-section of the ^{6}Li isotope present in CLYC is 940 barns [4]. The cross-section of ^{6}Li is 2.3 times higher than ^{3}He at 10 atmospheres (atm) [5]. The higher the total neutron cross-section is, the higher the probability that a neutron will interact with the target material (in this case the CLYC crystal). Thermal neutrons interact with ^{6}Li in CLYC via the following reaction:

$$^{6}\text{Li} + \text{n} \rightarrow {}^{3}\text{H} + {}^{4}\text{He (Q-value = 4.8 MeV)} \qquad \textbf{Equation 1}$$

CLYC is also capable of fast neutron detection and spectroscopy. Fast neutron interactions with the chlorine-35 (^{35}Cl) isotope in CLYC produced protons via the following reaction:

$$^{35}\text{Cl} + \text{n} \rightarrow {}^{35}\text{S} + \text{p (Q-value = 615 keV)} \qquad \textbf{Equation 2}$$

The emitted proton's energy is 615 keV plus the incident neutron's energy, so the proton energy varies linearly with the incident neutron energy which enables fast neutron spectroscopy with CLYC [3]. The fast neutron cross-section of ^{35}Cl present in CLYC varies with neutron energy, but is on the order of millibarns [6]. However, by comparing the effective cross-sections (defined as the cross-section multiplied by the isotopic abundance and atom fraction) of ^{6}Li and ^{35}Cl, it is

determined that ^{35}Cl is much better suited for the detection of fast neutrons [3]. The thermal neutron peak that appears at approximately 3.2 MeV GEE will interfere with the proton-induced peaks in this energy region. Reducing the ^{6}Li enrichment in CLYC can help the spectral analysis of fast neutron induced protons, while keeping the thermal neutron detection capability. By enriching the CLYC scintillator with ^{7}Li and depleting it of ^{6}Li, the thermal neutron signature is suppressed and the ability to detect fast neutrons is optimized.

Pulse shape discrimination (PSD) can be utilized to separate gamma-rays and neutrons detected within the CLYC scintillator [7]. The CLYC scintillation light emission consists of three components [7]. The first two components to appear are due to gamma-ray interactions in the scintillator and include the core-to-valence luminescence (CVL) and the Ce^{3+} emission. The third component appears due to thermal neutron interaction within the CLYC and is due to the cerium self-trapped excitation (Ce-STE). The significant difference in the decay times of the gamma-ray versus neutron-induced emission components allow for excellent PSD capabilities. The gamma-ray emission components, CVL and Ce^{3+}, have decay times of 1 ns and 50 ns, respectively [8]. The neutron emission component, Ce-STE, has a much longer decay time of 1000 ns [8].

1.3 Thematic Statement

This study is two-fold: first, to characterize CLYC as a multimode radiation sensor and second, to apply CLYC as a multimode radiation sensor. Both characterization and application modeled computationally and performed experimentally. Collectively, these investigations provided the basis for implementing CLYC as a multimode radiation sensor capable of neutron and gamma-ray measurements, fast neutron and gamma-ray spectroscopy, neutron/photon PSD, and the radiation source localization to be used by first responders, port authorities, scientists, and engineers across the globe.

1.4 Significance of the Study

The radiological and nuclear threat is real. Radioactive sources have gone missing or have been stolen and have irradiated those nearby. Nuclear reactors have melted-down and have exposed the public to above-normal levels of radiation. Terrorists can obtain radiological or nuclear materials to create a radiological dispersal device or nuclear weapon. However, radiation cannot be seen; it can only be detected. So, first responders rely on the radiation detection to deter these threats.

First responders require portable or handheld systems to detect and distinguish between gamma rays, thermal neutrons and high-energy neutrons, and determine the gamma-ray and neutron energy spectra "on the go." Current handheld detectors are limited to the detection of a single radioactive type at a time (i.e., only gamma rays or only thermal neutrons). Often two independent detection systems are used to detect gamma rays and thermal neutrons or gamma rays and fast neutrons which complicates detection systems in particular field deployed technologies.

CLYC applied as a multimode radiation sensor has the capability to detect gamma rays, thermal neutrons and fast neutrons all within a single scintillator cell. In addition to detection, CLYC enables the gamma-ray and fast neutron spectroscopy, source localization and imaging, and pulse shape signal analysis.

With the aforementioned capabilities of CLYC, first responders will be able to collect gamma-ray, thermal neutron and fast neutron data in a single scintillator simultaneously thereby increasing the functionality of the system and decreasing the size, weight, and power (SWaP). Having the ability to determine gamma-ray and neutron counting rates, dose and neutron/gamma-ray spectra allows first responders to have more information and analysis capabilities at their fingertips. Critical decisions can be more readily made in order to find a stolen radioactive source,

to evacuate a high radiation area due to a nuclear accident or mitigate the threat of nuclear terrorism.

In addition to radiological emergency response efforts, CLYC applied as a multimode sensor can also contribute to nuclear non-proliferation and nuclear safeguards and security efforts. CLYC can be used to locate and image radiological or nuclear material utilizing both neutron and photon emissions. Nuclear facilities, processing facilities, and enrichment facilities at home and abroad can all be monitored by a system utilizing CLYC as the detection medium to observe the throughput and movement of radiological and nuclear material.

CHAPTER 2

LITERATURE REVIEW

2.1 Introduction

The following sections provide an overview of radiation detection fundamentals, the current literature on multimode radiation detectors and performance of CLYC as a multimode sensor, and a review of currently deployed handheld radiation detectors and directional detection systems. This information is pertinent to understanding the science and engineering behind the efforts of this study and the importance and impact that the subject of this study has on the advancement of radiation detection capabilities.

2.2 Radiation Detection Fundamentals

All matter that exists is made up of atoms. Atoms consist of a nucleus made up of neutrons and protons (nucleons). A cloud of moving electrons surrounds the nucleus. Unstable atoms will emit particles and electromagnetic waves in order to reach a stable state. Materials consisting of unstable atoms are called radioactive materials. The particles and photons they emit are called radiation.

There are four common types of radiation encountered in nuclear engineering and safeguards applications: beta particles, alpha particles, gamma rays, and neutrons. Beta particles, i.e., electrons and positrons, are emitted in beta decay via the following reactions:

$$ {}^{A}_{Z}X \rightarrow {}_{Z+1}{}^{A}Y + \beta^{-} + \bar{\nu} \qquad \textbf{Equation 3} $$

$$ {}^{A}_{Z}X \rightarrow {}_{Z-1}{}^{A}Y + \beta^{+} + \nu \qquad \textbf{Equation 4} $$

where *A* is the atomic mass and *Z* is the atomic number, *X* is the symbol of the atom prior to decay and *Y* is the symbol of the atom after decay, β^{-} is the electron, $\bar{\nu}$ is an antineutrino, $\beta^{+}$is the

positron, and v is a neutrino [9]. The beta-particle emitting radioactive isotopes include, for example, tritium (^{3}H), sulfur-35 (^{35}S), and technicium-99 (^{99}T). Due to the energy sharing between three particles in the beta decay, the electron energy spectrum exhibits the wide distribution (not peaks). Each beta-particle emitter has different characteristic endpoint energies in the electron spectrum which enable the identification of the radioactive isotope. Beta particles can be absorbed or backscattered when interacting with matter [9].

Alpha particles, or ionized helium-4 (^{4}He^{+2}), are emitted in alpha decays via the following reaction:

$$ {}^{A}_{Z}X \rightarrow {}^{A-4}_{Z-2}Y + {}^{4}_{2}\alpha \qquad \textbf{Equation 5} $$

where ${}^{4}_{2}\alpha$ is the alpha particle [9]. The alpha particle-emitting radioactive isotopes include uranium-235 (^{235}U), ^{236}U, ^{238}U, plutonium-239 (^{239}Pu), and ^{240}Pu. Alpha-particle emitters have different characteristic alpha-particle kinetic energies. Alpha particles interact with matter via the coulomb forces between their positive charge and the electrons in surrounding atoms [9].

Gamma rays are electromagnetic waves; they have no charge, no mass, and are typically emitted when an excited nucleus de-excites. This de-excitation for example often occurs following beta and alpha decays. Photons are also produced when an electron and a positron are annihilated, or as a result of bremsstrahlung interactions [9]. Common gamma-ray emitters include cobalt-60 (^{60}Co), cesium-137 (^{137}Cs), and sodium-22 (^{22}Na). Gamma-ray emitters have different characteristic gamma-ray energies. Gamma rays can interact with matter via three reactions: photoelectric absorption, Compton scattering, and pair production (above the 1.022 MeV energy threshold).

Neutrons have no charge, but do have mass, magnetic moment, and spin. Neutrons are most commonly created by spontaneous fission, induced fission, (α, n) reactions, accelerated

charged particle reactions, and photoneutron reactions. Neutrons created from spontaneous fission, induced fission, and (α, n) reactions do not have single characteristic energies. Instead, neutrons are generated over a span of energies (a neutron spectrum). Neutrons created in accelerated charged particle reactions can possess single characteristic neutron energies. Neutrons can interact with matter by absorption (fission, (n,α), neutron-proton (n,p), neutron-deuteron (n.d), neutron-triton (n,t), neutron-neutron (n, xn)), and inelastic or elastic scattering.

Each of these four common radiation types can be detected through various mediums. One of the most common detection mediums is a scintillator. Ionizing radiation interacting in a scintillating material creates charged particles which are converted into a detectable light that is proportional to the energy of the incident radiation [9]. This detectable light is converted to an electrical signal using an optical readout, most commonly by means of a photomultiplier tube (PMT) or a solid-state silicon photomultiplier (SiPM). This electrical signal is conditioned and digitized through subsequent electronics to enable analysis of the detected radiation by the end user.

Two indicators of how well scintillators perform are the energy resolution and the detection efficiency. The energy resolution, also known as the full width half maximum (FWHM), is defined as the width of a characteristic peak captured in an energy spectrum at half the maximum height of that peak. The smaller the FWHM, the better characteristic peaks of detected radiation can be resolved. The absolute detection efficiency is defined as the number of pulses measured by the detector compared to the number of radiation particles emitted from the measured source. For photons, the absolute detection efficiency is the ratio of the total number of detected photons in the full-energy peak to the total number of photons emitted from the source.

There are two types of scintillators: organic and inorganic. Organic scintillators are composed primarily of carbon and hydrogen. Inorganic scintillators typically do not contain hydrogen. The most notable organic scintillators include benzene, plastic scintillators, and liquid scintillators. Common inorganic scintillators include sodium iodide doped with thallium (NaI:Tl), cesium iodide (CsI), and bismuth germanate (BGO).

A relatively novel group of inorganic scintillators known as elpasolites have risen to popularity in the field of radiation detection. Elpasolites offer the ability to detect gamma rays and neutrons simultaneously and furthermore, discriminate one from the other. One elpasolite in particular, $Cs_2LiYCl_6:Ce^{3+}$ (CLYC), stands out among the rest for its remarkable ability to enable pulse shape discrimination between gamma rays and neutrons.

CLYC has a thermal neutron energy resolution typically between 2.5% and 3.1% at the thermal neutron peak occurring at 3.2 GEE [3]. This response is resultant of neutrons incident on ^{6}Li by means of the $^{6}Li(n,\alpha)^{3}H$ reaction. CLYC has the capability to detect fast neutrons resultant of fast neutrons incident on chlorine-35, ^{35}Cl, by means of the following reactions:

$$^{35}Cl + n \rightarrow {}^{35}S + {}^{1}H \qquad \textbf{Equation 6}$$

$$^{35}Cl + n \rightarrow {}^{35}P + {}^{4}He \qquad \textbf{Equation 7}$$

The energy of the proton (^{1}H) and alpha (^{4}He) resultants of these reactions scales linearly with the energy of the incident fast neutron [10]. This response is optimized by reducing the ^{6}Li content of CLYC and increasing the ^{7}Li content. This suppresses the thermal neutron response of CLYC and enables a better response of CLYC to fast neutrons and fast neutron spectroscopy. CLYC enriched in ^{6}Li is known as CLYC-6. CLYC enriched in ^{7}Li is known as CLYC-7.

Both CLYC-6 and CLYC-7, collectively referred to as CLYC, have a gamma-ray energy resolution of approximately 4% at 662 keV (the gamma-ray energy from cesium-137 (^{137}Cs) decays [11]. This gamma-ray energy resolution is approximately 3% better than that of the gamma-ray gold standard, the sodium iodide (NaI) scintillator.

Table 1. CLYC material characteristics **[8]**

Material Property	Value
Melting Point	640 °C
Density	3.31 g/cm^3
Crystal Structure	Cubic
Water Solubility	Hygroscopic
Refractive Index	1.81 ± 0.037 @ 405 nm
Coefficient of Thermal Expansion	34.34 × 10^{-6} / °C @ 30°C
Emission Spectral Range	275 – 450 nm
Peak Scintillation Wavelength	370 nm
Decay Constants (CVL, Ce^{3+}, Ce-STE)	1 ns, 50 ns, 1000 ns
Scintillation Light Yield	20,000 photons/MeV
GEE for Thermal Neutrons	3.2 MeV

Discrimination between gamma rays and thermal neutrons and between gamma rays and fast neutrons utilizing CLYC has yielded a figure of merit (FOM) as good as 4.83 [11]. A FOM of 1.5 is considered good and indicates that the particles (gamma ray versus neutron) are separated [10].

Other elpasolites offering similar capabilities include Cs_2LiYBr_6:Ce (CLYB), $Cs_2LiLaBr_6$:Ce (CLLB), $Cs_2LiLa\ Cl_6$:Ce (CLLC), and most recently investigated, Tl_2LiYCl_6:Ce (TLYC).CLYB has a higher neutron absorption cross-section than other chlorine-based elpasolites which yields a thermal detection efficiency of approximately 90% as compared to 80% for CLYC [12]. It has a similar response to gamma-rays as CLYC with a 662 keV gamma-ray energy resolution of 4.1% and a light yield of 24,000 photons/MeV. However, CLYB is inferior to CLYC for PSD with a FOM of only 1.2.

CLLB is one of the brightest elpasolite scintillators with a light yield of approximately 55,000 photons/MeV [13]. It also has one of the best 662 keV gamma-ray energy resolutions of 2.9% [12]. However, CLLB falls short as a medium for PSD with a FOM of 1.2 [12].

CLLC has a light yield of 35,000 photons/MeV and a 662 keV gamma-ray energy resolution of 3.4%, both values of which are substantial for gamma-ray spectroscopy [12]. However, it too falls short of CLYC for PSD capability with a FOM of only 1.5 [12].

The most recently investigated elpasolite, TLYC, shares similar gamma-ray response properties with CLYC. The incorporation of thallium (Tl) enables better photon and neutron detection [14]. It has a 662 keV gamma-ray energy resolution of 4.8% and a light yield of 30,500 photons/MeV [14]. The neutron detection and PSD capabilities of TLYC have yet to be studied. Additionally, large TLYC crystals have yet to be grown successfully.

CLYC remains the most studied, well-understood, and furthest developed elpasolite. Only recently CLYC was considered capable of the multimode sensing of gamma rays, thermal neutrons, and fast neutrons simultaneously. Other elpasolites have yet to be considered as a multimode sensor. CLYC is a compelling alternative to radiation detection systems currently used by first responders, scientists, engineers, and other users of radiation detection technologies and it offers significant advantages. Radiation detection technologies currently employed in the field and under research and development, including the application of CLYC, are discussed in the subsequent sections.

2.3 Current Multimode Detection Capabilities

Typically, two detection units are employed in the field to detect gamma rays and neutrons separately. NaI:Tl gamma-ray scintillators dominate units used for gamma-ray detection and spectroscopy in the field. Helium-3 (^{3}He) gas proportional counters are popular for neutron detection in the field. Due to shortages of ^{3}He gas and the increased need to advance radiation detection technologies to achieve higher quality and faster results, alternative capabilities have been studied and developed [15]. This includes the ability to detect gamma rays, thermal neutrons, and fast neutrons within a single detector. Very few materials have been studied for applicability as multimode sensors. These materials include a combination of Eljen Technologies scintillators, ^{6}Li-loaded organic scintillators, ^{10}B-loaded scintillators, and CLYC.

By combining the Eljen Technologies EJ-240 and EJ-299-33A scintillators as shown in Figure 1, a multimode sensor was designed [16]. The detector assembly consists of one EJ-420 plastic scintillator, optically coupled with an EJ-560 optical coupling pad to an EJ-299-33A plastic scintillator, which in turn is optically coupled to an H12700 Hamamatsu PMT. This assembly was not permanently enclosed in a housing, but rather wrapped in Tyvek-reflective sheet and black

tape so that light could not enter the assembly. Scintillations were read-out by a CAEN V1720 waveform digitizer. Custom software from the University of Padova was used for data acquisition and analysis.

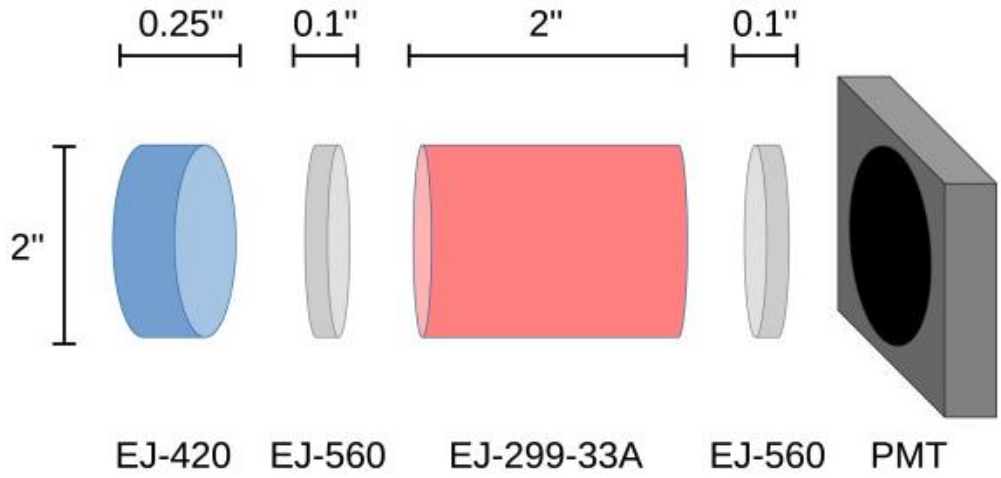

Figure 1. Coupled EJ-240, EJ-299-33A Detector **[16]**

This assembly was used to measure the energy spectrum of a sodium-22 (^{22}Na) gamma-ray source and neutron/gamma-ray discrimination of a californium-252 (^{252}Cf) neutron source. The resultant ^{22}Na gamma-ray energy spectra and ^{252}Cf PSD plots are shown in Figure 2 and Figure 3, respectively. The resolution of the 511 keV and 1.275 MeV characteristic gamma-ray peaks of ^{22}Na were 10.6% and 7.8%, respectively. These values are larger than that of CLYC (approximately 4%) for 662 keV. A truer comparison can be made if the resolutions of the same characteristic gamma-ray peaks are compared instead. The PSD plots of the ^{252}Cf source visibly separate thermal neutrons (top "cloud" in Figure 3), fast neutrons (the middle "cloud" of Figure 3), and gamma rays (the bottom "cloud" of Figure 3). It was reported that the highest FOM achieved was approximately 1.1. The FOM is a function of the threshold energy and increases as the threshold energy increases. At lower threshold energies, the FOM is as low as 0.3. This FOM is much less than that of CLYC.

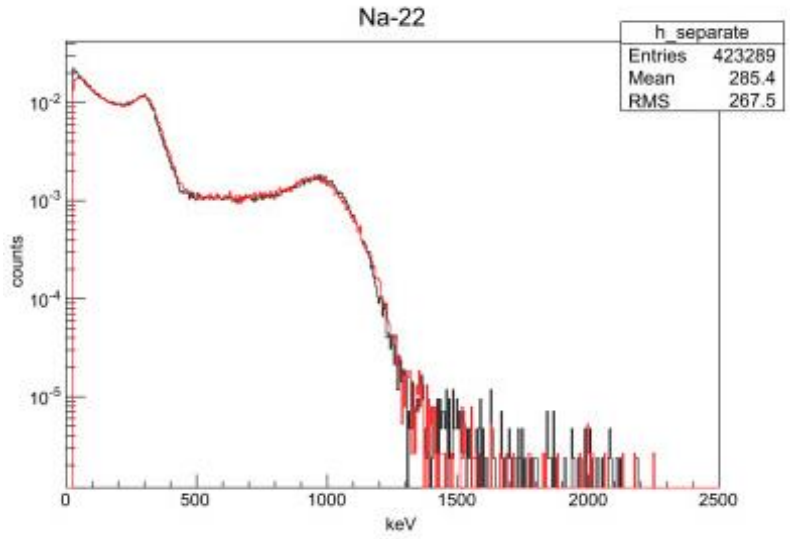

Figure 2. Coupled EJ-240, EJ-299-33A Detector ^{22}Na energy spectra **[16]**

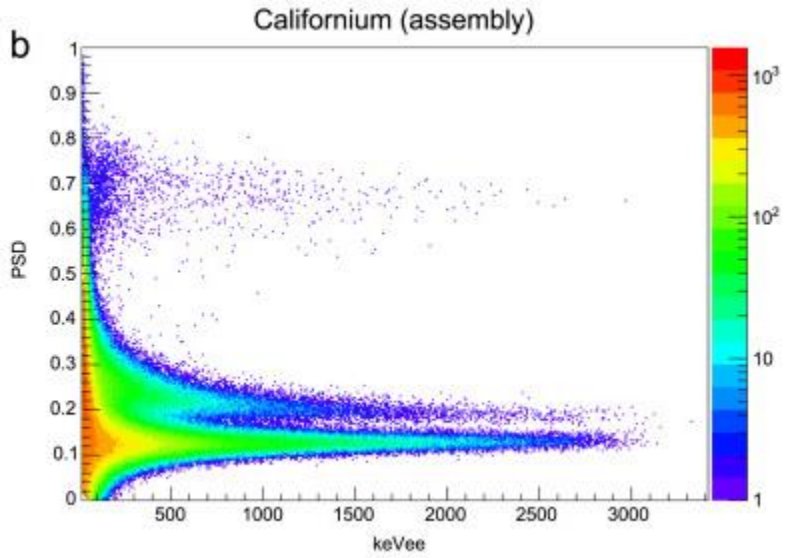

Figure 3. Coupled EJ-240, EJ-299-33A Detector ^{252}Cf PSD Plot **[16]**

The advantages of this assembly are that it is affordable due to the lower cost of plastic scintillators and it is more rugged due to the material properties of plastic. This assembly has proven to be capable of detecting thermal neutrons, fast neutrons, and gamma rays with the capability to discriminate all three from one another. However, gamma-ray spectroscopy is inferior

to other available scintillators and fast neutron spectroscopy has not been demonstrated. Furthermore, this assembly is not commercially available and has only been assembled and tested in a laboratory environment.

Boron-10 (^{10}B) has an excellent cross-section for the capture of thermal neutrons as seen in Figure 4. Introducing ^{10}B into a plastic or liquid scintillator enables the detection of thermal neutrons whereas only the detection of fast neutrons and/or gamma-rays would be possible. However, increasing the ^{10}B content in a plastic or liquid scintillator will decrease its light yield [9]. Organic scintillators, including plastic and liquid scintillators, are well known for their superior light yield.

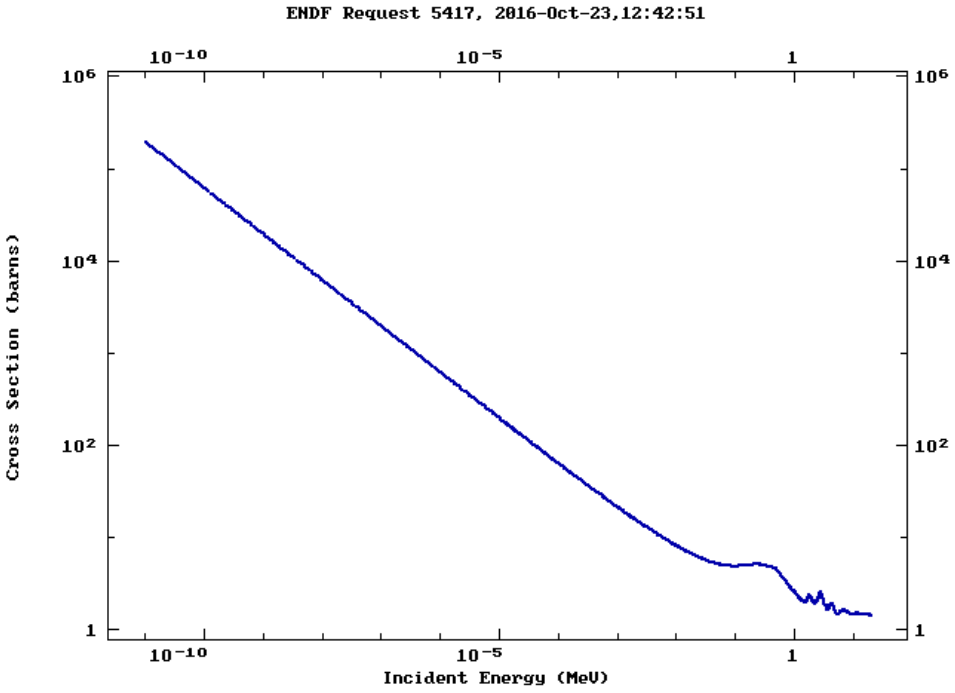

Figure 4. Total neutron cross-section for ^{10}B **[17]**

Two such boron-loaded scintillator detectors are discussed: the first is a capture-gated detector. The capture-gated boron-loaded scintillator detector replaces the continuum created from fast neutrons in the energy spectra with a single photopeak enabling fast neutron spectroscopy. Fast neutrons create a pulse in an organic scintillator which is resultant of multiple recoil protons [9]. A second pulse is created when the moderated fast neutrons are captured as thermalized neutrons on ^{10}B [9]. This is the signature of fast neutrons interacting in a boron-loaded organic scintillator. The energy of the incident fast neutron plus the Q-value (2.79 MeV) of its capture on ^{10}B after subsequent thermalization equals the energy of the photopeak created in the resultant energy spectrum.

The investigation of a capture-gated boron-loaded scintillator by Holm, et al, utilized an EJ-254 boron-loaded plastic scintillator optically coupled to a Scionix ETL 9305 PMT [18]. The measurements were read-out by a Canberra Osprey digital MCA. Data acquisition and analysis was performed using STUK software [18]. The assembly is presented in Figure 5.

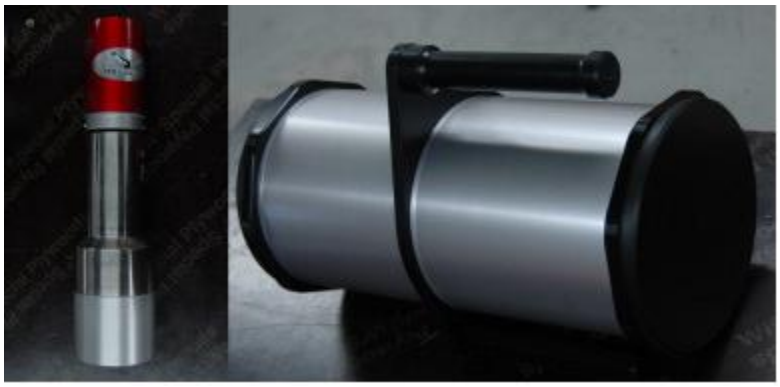

Figure 5. Capture-gated boron-loaded scintillator assembly **[18]**

Measurements were carried out using a ^{252}Cf source and an americium -beryllium (AmBe) source. Various lead (Pb) and borated polyethylene were used to achieve optimal results. The ^{252}Cf and AmBe spectra collected are presented in Figure 6. It was observed that the energy resolutions of both the neutron and gamma-ray peaks are poor. These "peaks" rather appear as continuum distributions.

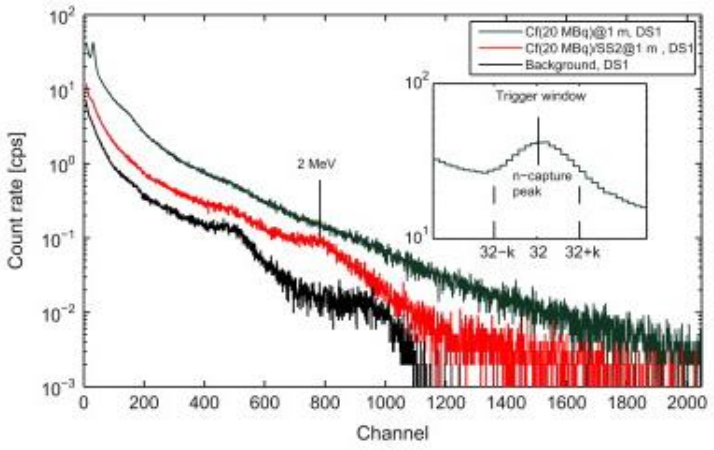

(a)

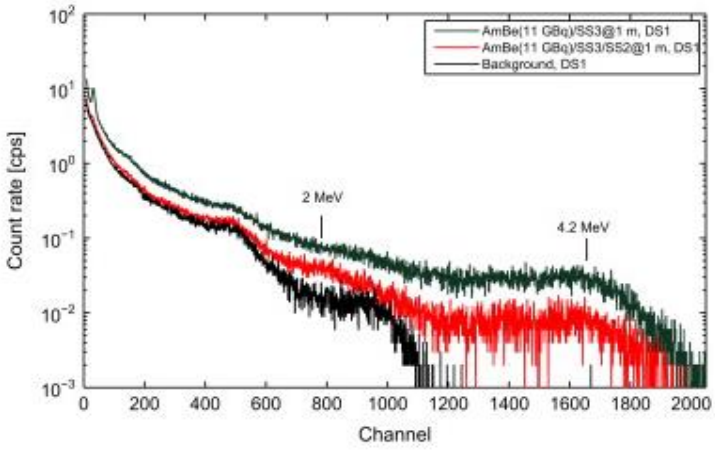

(b)

Figure 6. Capture-gated boron-loaded scintillator (a) ^{252}Cf and (b) AmBe spectra **[18]**

This investigation proved that fast neutron spectroscopy is possible with the EJ-254 boron-loaded plastic scintillator. However, the resolution of the resultant peaks in the energy spectra was poor. Furthermore, PSD and thermal neutron detection was not investigated. Advantages of this assembly and capture-gated technique include the ability to discern between fission neutrons and Be-reaction neutrons, to determine the presence and type of shielding surrounding a source, and to discern between a soft-spectrum and a hard spectrum. The ability of this assembly to perform as a multimode sensor has yet to be determined.

Another boron-loaded scintillator investigation conducted by Pino, et al, does address the ability of such a detector to detect thermal neutrons, fast neutrons, and gamma rays [19]. The EJ-339A boron-loaded liquid scintillator is the selected scintillator for this study. The EJ-339A scintillator can be employed for gamma-ray spectroscopy, PSD, and capture-gating techniques for fast neutron spectroscopy [19]. For this investigation, the EJ-339A scintillator was optically coupled to a H1949-51 Hamamatsu PMT via an EJ-560 optical coupler [19]. Measurements were read out utilizing a CAEN V1720 digitizer [19]. The software used to perform data acquisition and analysis was undisclosed. One ^{22}Na and one americium-241 (^{241}Am) gamma-ray source were used for energy calibration. A ^{252}Cf source moderated by polyethylene blocks was measured for the purposes of thermal neutron and fast neutron detection. The neutrons produced from the ^{252}Cf source were discriminated from background gamma-rays. The PSD plot for this study is shown in Figure 7. It is observable that the thermal neutrons, fast neutrons, and gamma rays are separated in Figure 7 (b) but not in (a). Figure 7 (a) plots the PSD parameter (i.e., PID) versus electron equivalent energy whereas, in Figure 7 (b), plots the delayed component (defined as the short gate integration minus the long gate integration) versus the electron equivalent energy. It is by the method in Figure 7 (b) only for which thermal neutrons, fast neutrons, and gamma rays can be

discriminated. The highest FOM is approximately 1.7 for gamma rays versus neutrons for the EJ-339A scintillator in this study. Again, the FOM is a function of the energy (the light output) threshold and decreases with decreasing energy threshold.

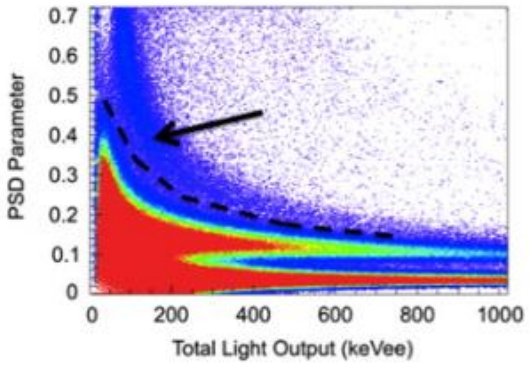

(a)

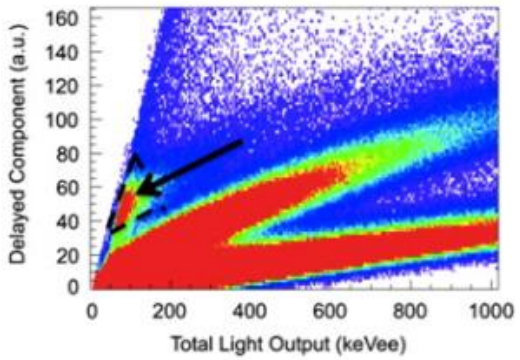

(b)

Figure 7. EJ-339A PSD plots for polyethylene-moderated ^{252}Cf source **[19]**

Beyond PSD between thermal neutrons, fast neutrons, and gamma rays, it is possible for the EJ-339A to discriminate between thermal neutrons and low-energy gamma rays. This is important since the thermal neutron peak appears at approximately 50 keVee and plutonium (Pu) isotopes have a characteristic photopeak in close proximity at 59 keVee [19]. This is accomplished by comparing the ratio of the gamma-ray yield in a low-energy region to that in a high energy

region to the same ratio for neutrons. The results for the ^{252}Cf source examined in this study are presented in Figure 8.

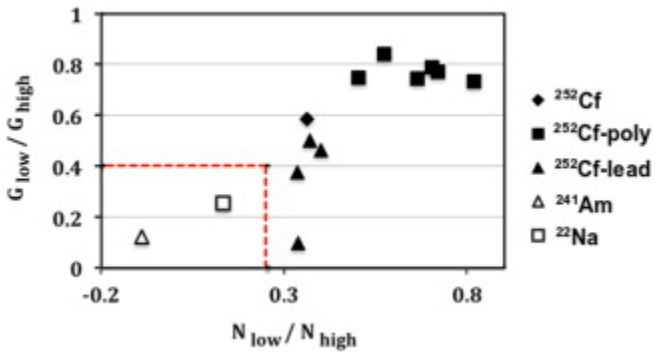

Figure 8. EJ-339A discrimination of thermal neutrons and low-energy gamma rays **[19]**

This investigation demonstrates the ability of a boron-loaded organic scintillator to be used for PSD purposes to discriminate between thermal neutrons, fast neutrons, and gamma rays, albeit with an inferior FOM to that of CLYC. Coupled with the results of the Holm, et al, investigation, boron-loaded organic scintillators can be used to detect and discriminate thermal neutrons, fast neutrons, and gamma rays, and perform fast neutron spectroscopy [18]. The capability of boron-loaded organic scintillators to perform gamma-ray spectroscopy has yet to be characterized in detail. The capabilities of boron-loaded organic scintillators are similar, but inferior to both lithium-loaded scintillators and CLYC scintillators still yet to be discussed.

For purposes of PSD, lithium-loaded organic scintillators are superior to their boron-loaded counterparts [16]. The Q-Value for ^{6}Li (4.78 MeV is approximately twice as large as that of ^{10}B (2.30 MeV). The higher Q-value results in a higher threshold energy and thus, a better FOM.

Single peaks are created in the energy spectra when fast neutrons interact with ^{6}Li [16]. The energy of these peaks is equal to the Q-value of the fast neutron reaction with ^{6}Li plus the

energy of the incident neutron [16]. However, only fast neutrons having energy of several hundred keV can create these peaks enabling spectroscopy [16].

There are a variety of lithium-loaded organic scintillators. Two of such are discussed herein. A study conducted by Zaitseva, et al, investigated the performance of Li-salt of 3-phenylsalicylic acid (Li-3-PSA) incorporated into a plastic scintillator, a liquid scintillator, and a crystal. The dissolution of Li-3-PSA into these three different mediums enables the simultaneous detection of thermal and fast neutrons while discriminating gamma rays from them [20]. Each of the three Li-3-PSA-based detection mediums was utilized to measure a ^{252}Cf source.

The 5% Li-3-PSA plastic scintillator coupled with a high density polyethylene (HDPE) moderator boasted a FOM of 3.19 for discrimination of thermal neutrons from gamma rays [20]. The pulse and PSD plots generated by the 5% Li-3-PSA plastic scintillator measurement of the ^{252}Cf source is presented in Figure 9. The same scintillator yielded a FOM of 2.47 for separation of fast neutrons from gamma rays [20].

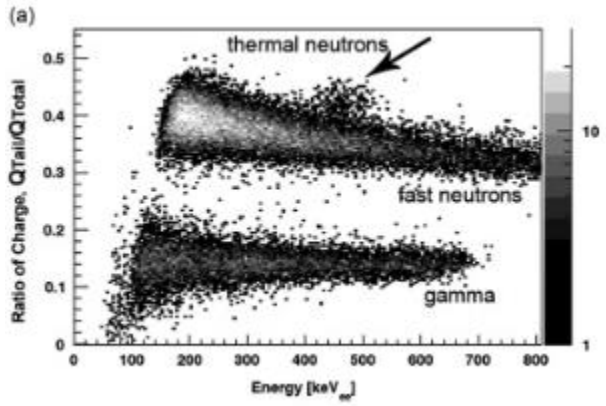

Figure 9. 5% Li-3-PSA plastic scintillator PSD plot for ^{252}Cf **[20]**

The Li-3-PSA liquid scintillator did not perform as well as expected and performed worse than the plastic scintillator. It only obtained a FOM of 1.67 for total (thermal and fast) neutrons separated from gamma rays [20]. This poor separation is presented in the PSD plot of Figure 10. The fast and thermal neutrons are in a single "cloud" in very close proximity to the gamma-ray "cloud." It is hypothesized by the Zaitseva, et al, that this unexpected poor PSD performance could be the result of a less than optimal combination of constituents in the liquid scintillator.

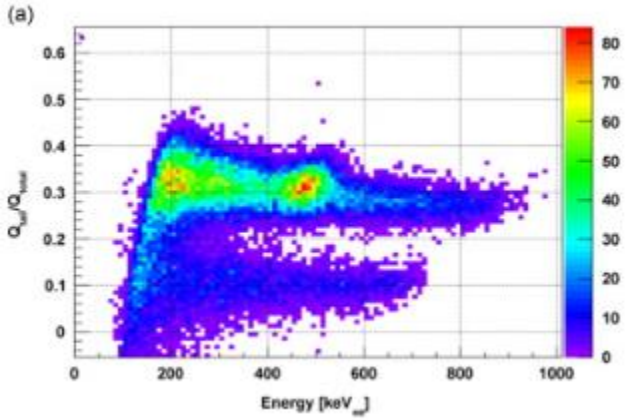

Figure 10. Li-3-PSA liquid scintillator PSD plot for ^{252}Cf **[20]**

The Li-3-PSA crystal was the top performing medium of this study. It yielded a FOM of 4.37 for thermal neutron separation from gamma rays and a FOM of 2.99 for fast neutron separation from gamma rays [20]. The respective PSD plot is shown in Figure 11. Three distinct "clouds" are discernable in this figure. The top "cloud" is formed from thermal neutrons. The middle "cloud" is from fast neutrons. The bottom "cloud" is from gamma rays.

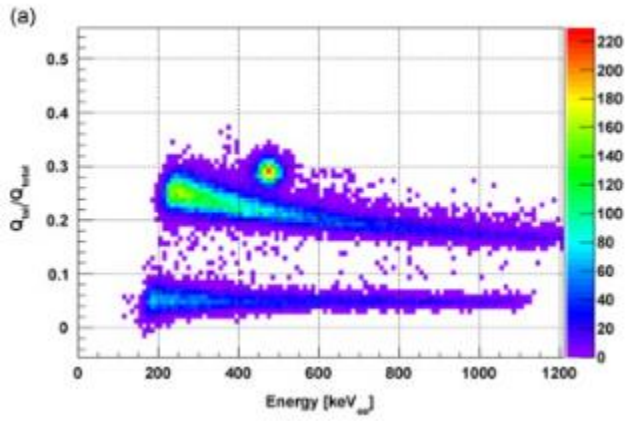

Figure 11. Li-3-PSA crystal PSD plot for ^{252}Cf **[20]**

Advantages of the Li-3-PSA-based organic scintillators include their increased efficiency for the ^{6}Li/thermal neutron capture for larger scintillators (approximately 95% for scintillators greater than 3 centimeters (cm) in thickness) [20]. In addition, and unlike CLYC, Li-3-PSA-based organic scintillators are not hygroscopic which enables easier and more affordable manufacturing [20].

The elpasolite CLYC has been thoroughly studied for purposes of gamma-ray spectroscopy, thermal neutron detection, and gamma-ray/thermal neutron discrimination. Most recently, CLYC has been investigated for the purposes of fast neutron spectroscopy and the discrimination of gamma rays, thermal neutrons, and fast neutrons.

The detection of fast neutrons by the means of interaction with ^{6}Li is possible, but less probable due to the low cross-section for fast neutrons [6]. The resolution of fast neutron/^{6}Li reaction peaks is very poor (approximately 15%) appearing more like a continuum and is often overpowered by the higher amplitude and better resolution of the thermal neutron/^{6}Li reaction peak [6]. A study conducted by D'Olympia, et al, investigates a 95% ^{6}Li-enriched CLYC scintillator in which the continuum created by fast neutrons interacting with ^{6}Li is observed [21]. This phenomenon is presented in Figure 12 and Figure 13.

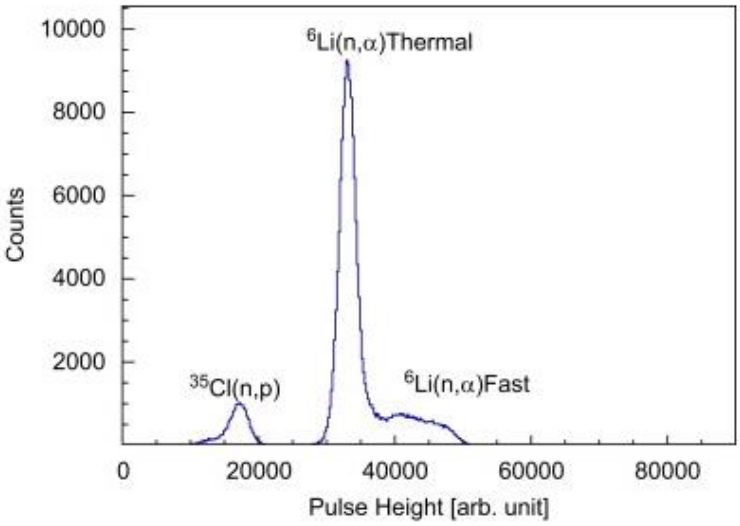

Figure 12. Energy spectra for incident 1.3 MeV neutrons on CLYC **[11]**

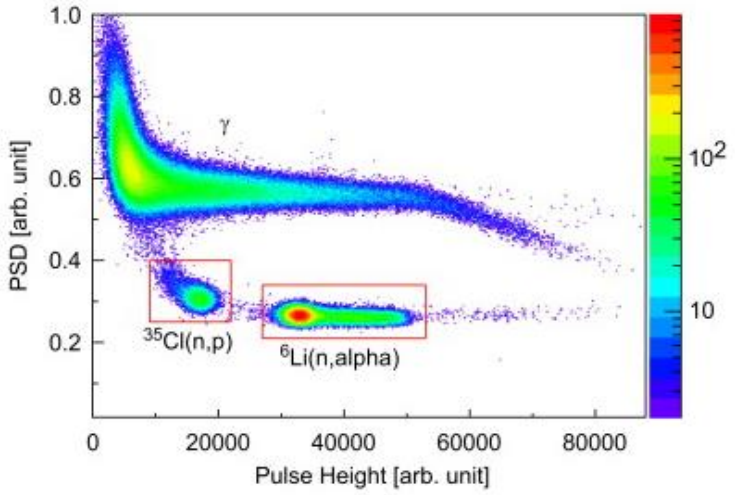

Figure 13. PSD plot for 1.3 MeV neutrons incident on CLYC **[11]**

A third peak is observed in the neutron energy spectrum. This peak is due to fast neutrons interacting with ^{35}Cl in CLYC. This reaction has a Q-value of 600 keV which is much different than that for the ^{6}Li(n, α)^{3}H reaction [22]. A second possible fast neutron reaction of ^{35}Cl results in the creation of an α-particle and phosphorus-32 (^{32}P) [22]. The Q-value for this reaction is 0.937 MeV [10]. The advantage of these two ^{35}Cl reactions is that the outgoing proton or alpha particle

has an energy proportional to that of the incident fast neutrons [10]. Furthermore, the resolution of the resultant fast neutron peaks have been reported to be as good as 7.8% at approximately 2.5 MeV [23].

By increasing the ^{7}Li content and reducing the ^{6}Li in CLYC, its fast neutron spectroscopy capability can be optimized. The ^{6}Li-depleted CLYC, herein referred to as CLYC-7 (versus ^{6}Li-enriched CLYC herein referred to as CLYC-6), suppresses sensitivity to thermal neutrons and this, enhances the ability to observe fast neutrons [10]. This phenomenon can be observed by comparing Figure 14 and Figure 15 [22]. These PSD plots were created from the measurement of an AmBe source by a 95% ^{6}Li-enriched CLYC and a 99% ^{7}Li-enriched CLYC. In Figure 14, there is a distinct thermal neutron "cloud." In Figure 15, there is no thermal neutron "cloud."

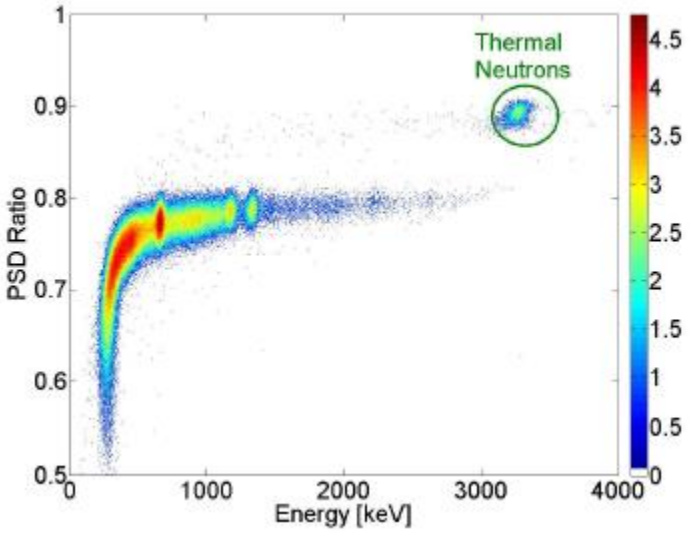

Figure 14. PSD plot of CLYC-6 response to AmBe **[22]**

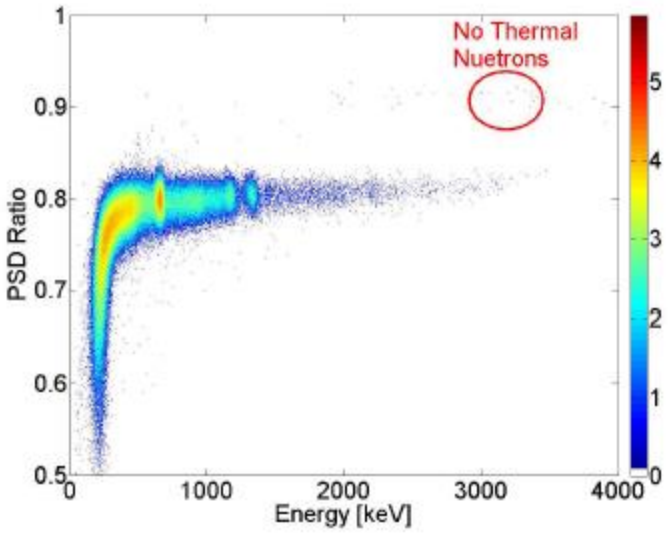

Figure 15. PSD plot of CLYC-7 response to AmBe **[22]**

A study conducted by Giaz, et al, investigates fast neutron spectroscopy and PSD capabilities with a 1-inch-by-1-inch CLYC-7 scintillator [23]. Fast neutron spectroscopy was successfully performed measuring mono-energetic neutrons between 1.9 MeV and 3.8 MeV utilizing a pulse accelerator beam. The resulting fast neutron spectra are presented in Figure 16. It is observed in this figure that a distinct peak appears at 1.9 MeV, 2.23 MeV, 2.7 MeV, 2.8 MeV, 3.3 MeV, and 3.8 MeV. It is also observed that the peak moves to the right with increasing incident neutron energy.

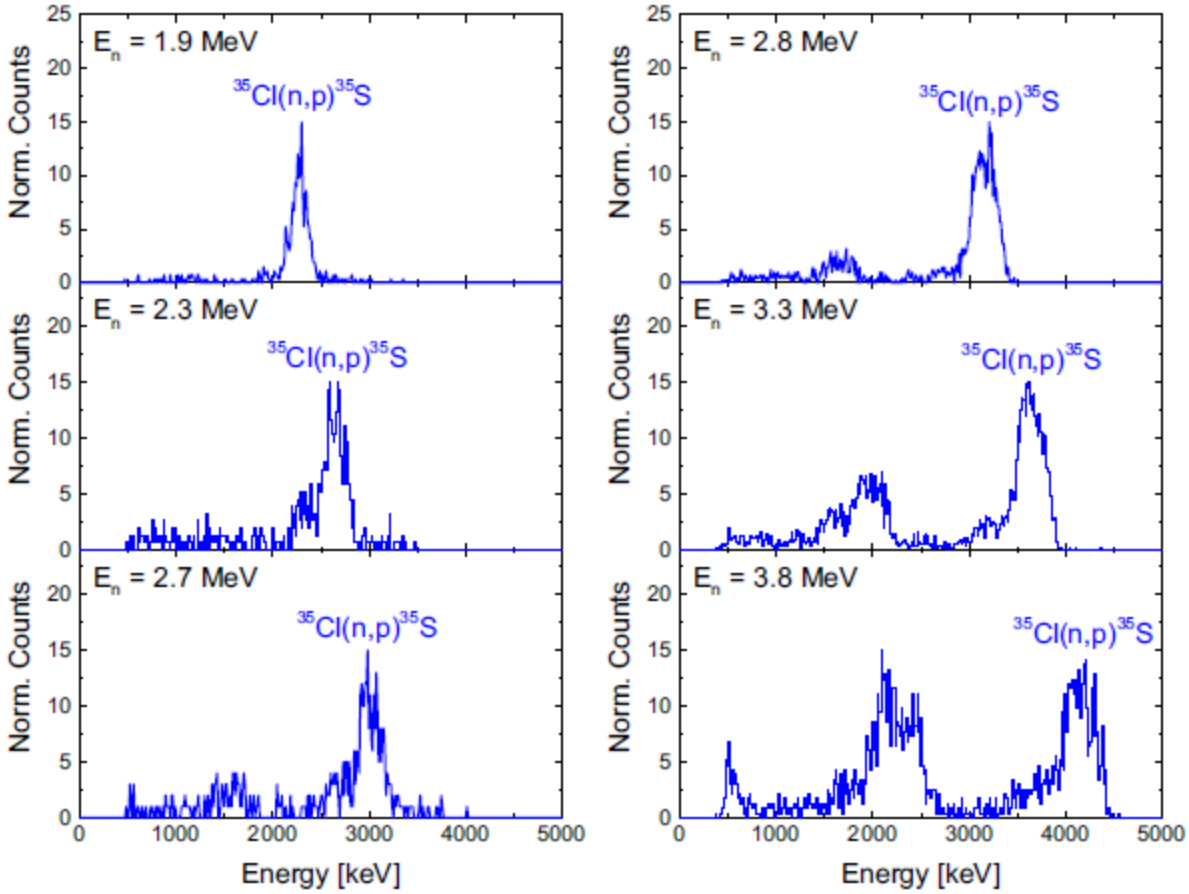

Figure 16. CLYC-7 fast neutron energy spectrum for 1.9 – 3.8 MeV mono-energetic neutrons **[23]**

For CLYC-6, fast neutron spectroscopy is not possible between 3.0 and 3.5 MeVee since this is where the thermal neutron peak appears [23]. This feature is observed in Figure 17 where the fast neutrons continue to move to the right with increased incident neutron energy until it merges with the thermal neutron peak. The amplitude of the thermal neutron peak overpowers any fast neutron peaks. In CLYC-7, the thermal neutron peak does not appear and fast neutron spectroscopy between 3.0 and 3.5 MeVee is possible.

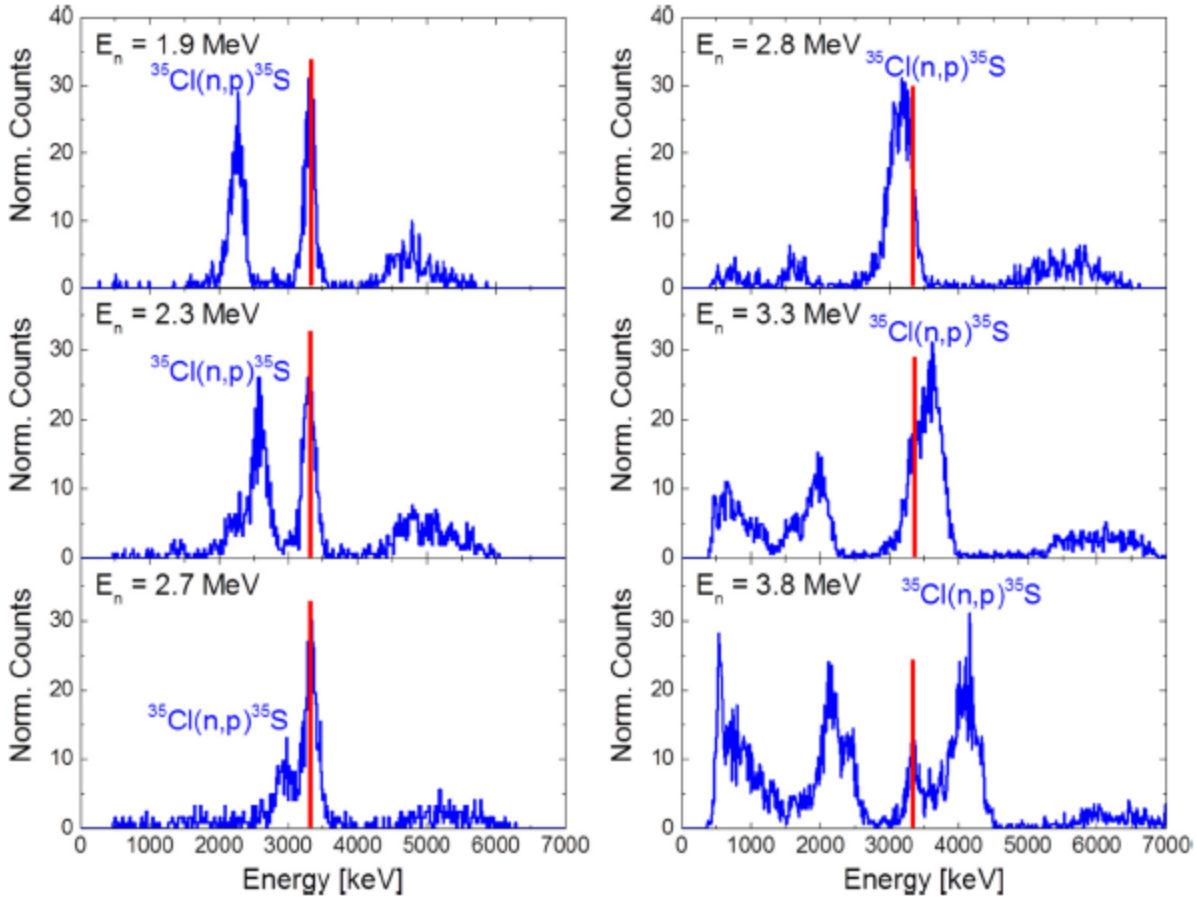

Figure 17. CLYC-6 fast neutron energy spectrum for 1.9 – 3.8 MeV mono-energetic neutrons **[23]**

At higher energies, the incident fast neutron energy is not as easily obtained. Spectral unfolding or time-of-flight measurements are required to determine the incident fast neutron's energy [21]. This is due to the excited stated of ^{35}S (a product of the fast neutron/^{35}Cl reaction) and the $^{35}Cl(n,\alpha)^{32}P$ reaction. These higher energy fast neutron spectra were measured by D'Olympia, et al, with two 1-inch-by-1-inch CLYC-7 scintillators utilizing a particle accelerator [21]. Fast neutrons between 0.5 MeV and 20 MeV were measured. Both PSD and fast neutrons spectroscopy measurements were acquired. The resultant PSD plots are presented in Figure 18. Up to 4 MeV, the FOM for fast neutron and gamma-ray discrimination was 4.02 [21]. The resultant fast neutron

spectra are shown in Figure 19. The same phenomenon of the $^{35}Cl(n, p)^{35}S$ appearing at energies proportional to that of the incident fast neutrons is observed. A second peak appears at 1.80 MeV: this is the peak resultant of the $^{35}Cl(n, \alpha)^{32}P$ reaction. This peak continues to grow until a growing continuum overtakes that peak at 13.5 MeV.

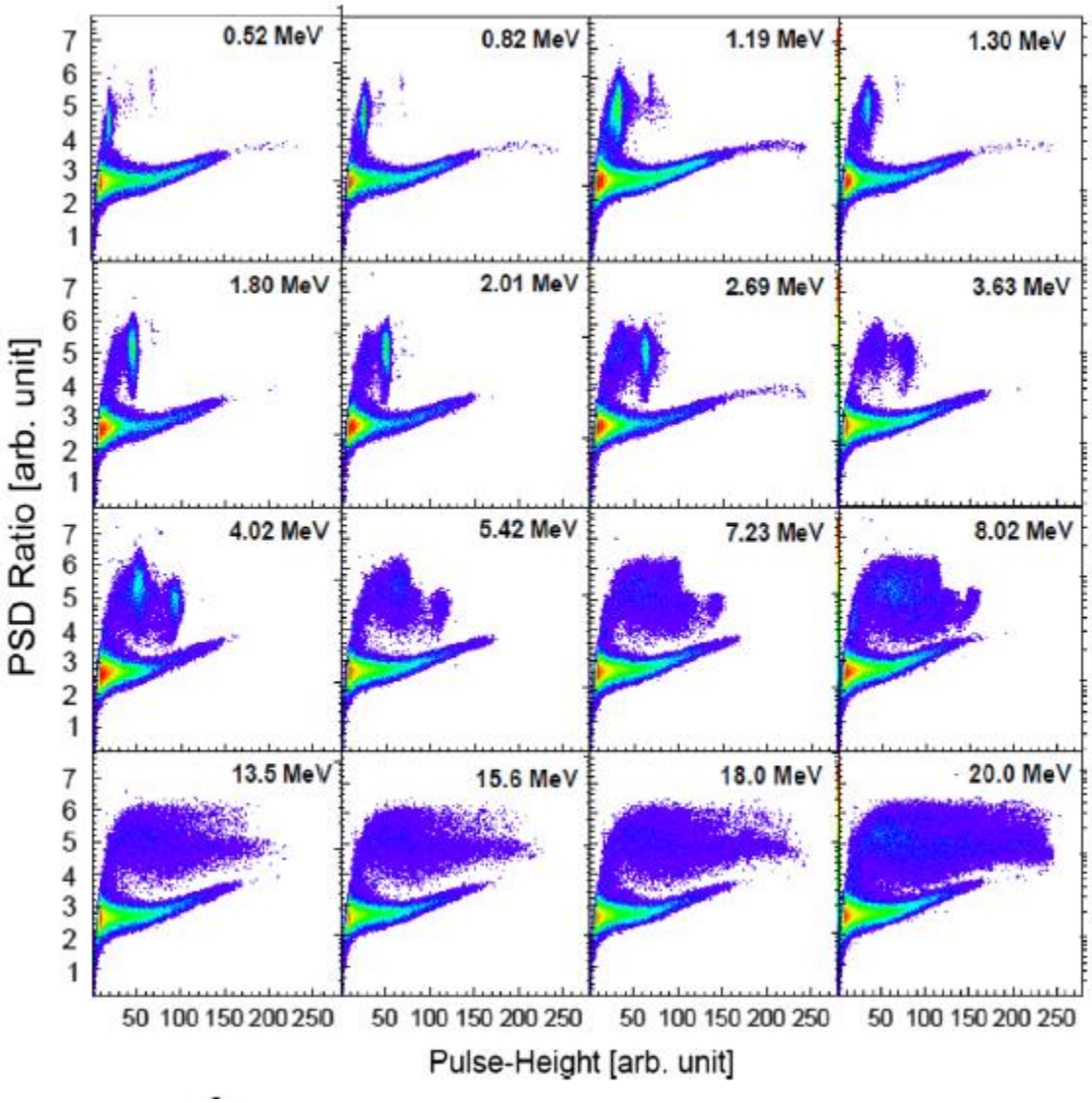

Figure 18. PSD plots for CLYC-7 response to 0.52 – 20 MeV neutrons **[21]**

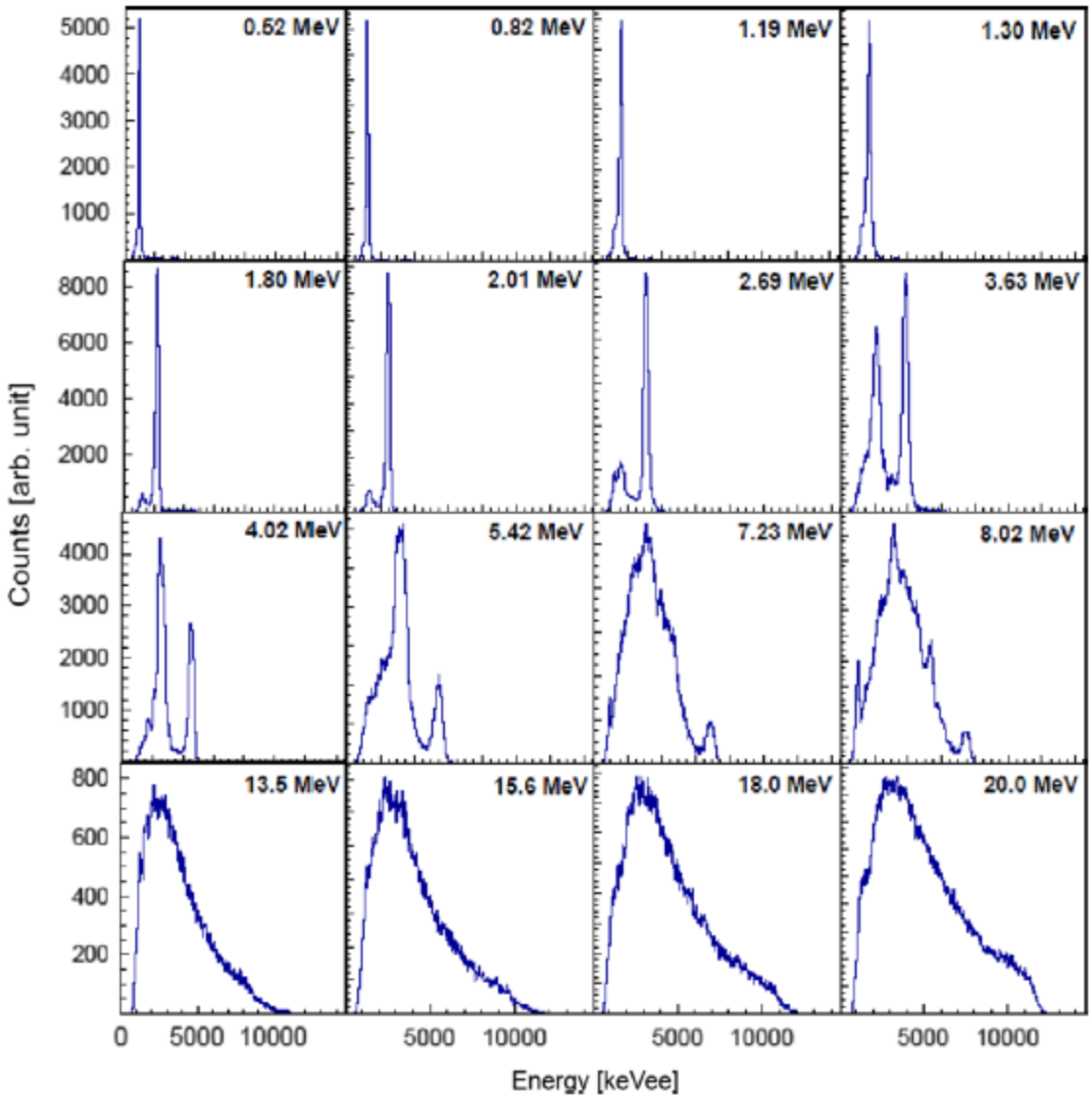

Figure 19. Fast neutron spectrum for CLYC-7 response to 0.52 – 20 MeV neutrons **[21]**

Advantages of CLYC-7 include that ability to perform fast neutron spectroscopy. At higher energies, fast neutron spectroscopy is still possible, but requires spectral unfolding or time of flight measurements. PSD between fast neutrons and gamma rays is superb. Further work must be done to unfold higher energy fast neutron spectra, confirm discrimination of fast neutrons from thermal neutrons and the both from gamma rays. It is hypothesized that an optimal mixture of ^{6}Li and ^{7}Li

can enable gamma-ray and fast neutron spectroscopy, thermal neutron detection, and thermal neutron, fast neutron, and gamma-ray PSD in a single detector.

2.4 Handheld Radiation Detectors

Most neutron/gamma-ray detectors currently manufactured and deployed for in-the-field use consist of two detection mediums: one for gamma rays and the other for neutrons. Typically these systems consist of a NaI:Tl scintillator and a ^{3}He gas proportional counter. The NaI:Tl scintillator is limited to gamma-ray spectroscopy whereas, the ^{3}He gas proportional counter is limited to thermal neutron detection.

One such NaI:Tl and ^{3}He gas proportional counter-based system is the Canberra InSpector ™ 1000 Digital Handheld Multichannel Analyzer [24]. The InSpector ™ 1000 utilizes an internal Geiger-Mueller counter for basic count rate and dose measurement. An optional NaI:Tl gamma-ray scintillator probe and ^{3}He gas proportional counter probe are utilized to increase the capabilities of the system. The InSpector ™ 1000 with the gamma-ray probe only and with both probes is presented in Figure 20.

The InSpector ™ 1000 is widely used in the applications of homeland security, border control, nonproliferation, health physics, treaty verification, and in scientific/engineering experiments [24]. It is rugged, easy to carry and manipulate, and is very user friendly. This system is capable of source localization, isotope identification, dose rate measurement, and gamma-ray spectroscopy. Screenshots of the InSpector ™ 1000's various operating modes are presented in Figure 21. The InSpector ™ 1000 is not capable of fast neutron spectroscopy. Other disadvantages of this system include its larger size and required probes for additional capabilities. However, it does utilize proven technologies in gamma-ray spectroscopy and thermal neutron detection packaged within a commercially manufactured and widely used product.

Figure 20. The Canberra InSpectorTM 1000 Digital Handheld Multichannel Analyzer with optional NaI:Tl gamma-ray probe (left) and with optional neutron probe (right) **[24]**

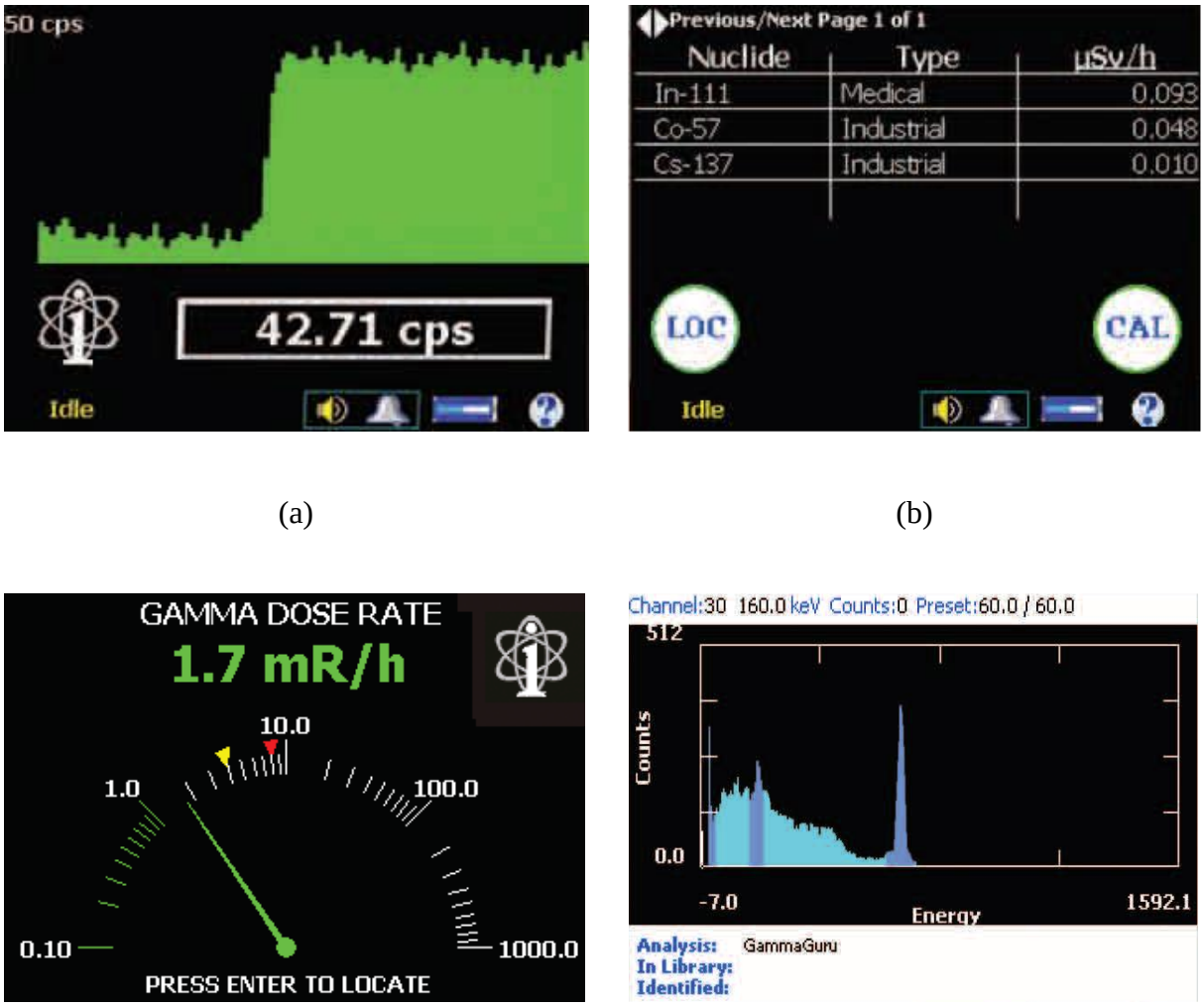

(a) (b)

(c) (d)

Figure 21. Capabilities of the InSpectorTM 1000 (a) source localization, (b) isotope identification, (c) dose rate measurement, and (d) gamma-ray spectroscopy **[24]**

The first CLYC-based handheld detector is the Advanced Radiation Monitoring Device (ARMD) [3]. ARMD was created as a result of collaboration between SCI Technology, Inc., Bubble Technology Industries, LANL, Saint Gobain Crystals, and Radiation Monitoring Devices, Inc. The ARMD handheld detector is presented in Figure 22. ARMD consists of four 1-inch by 1-inch CLYC-6 scintillators optically coupled to four Hamamatsu 1-inch square super bi-alkali

PMTs, batteries, and subsequent electronics enclosed in a handheld device with display screen and keypad.

ARMD is capable of gamma-ray spectroscopy and thermal neutron detection [3]. As observed in Figure 23, the gamma-ray spectrum is separated from the thermal neutron peak by means of PSD software on-board ARMD. The ARMD can also transmit measurement information via Bluetooth to a tablet for further analysis including isotope identification and source localization.

Figure 22. The ARMD handheld detector **[3]**

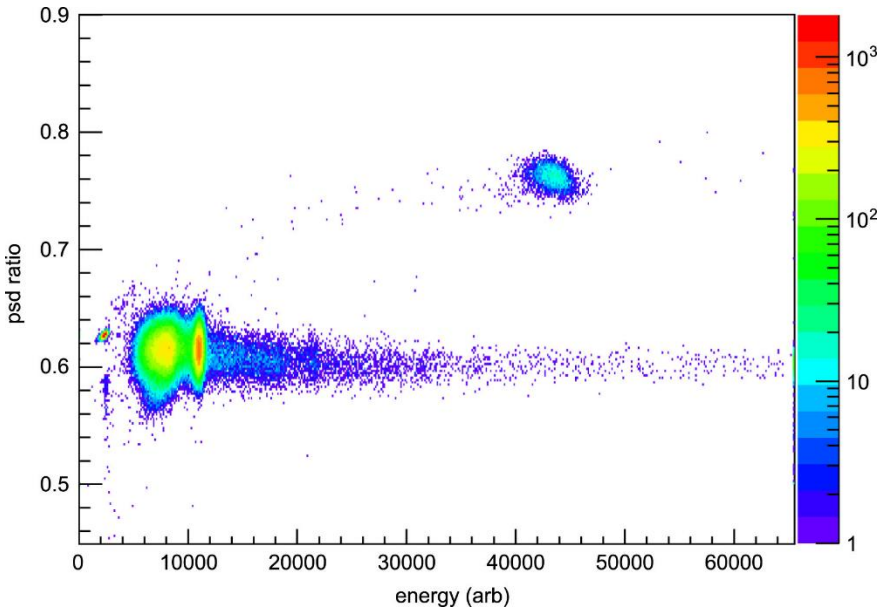

Figure 23. PSD with ARMD **[3]**

A second CLYC-based wearable scintillator is the Low-Profile Sensor (LPS) developed by PNNL [25]. The LPS consists of two CLYC-6 scintillators optically coupled to two Hamamatsu ultra bi-alkali PMTs, and internal calibration source, custom PMT base, batteries, and subsequent electronics enclosed in a housing with display screen and keypad. The LPS is carried in a pouch for convenience. Figure 24 presents the LPS and the wearable pouch which holds the LPS. The LPS has additional features of a USB port and WiFi capabilities.

The LPS utilizes the same software and algorithm as the Lynx system to identify measured isotopes [25]. The measure gamma rays and thermal neutrons are compared to known background or benign radiation sources in order to identify the measured isotope(s). Instead of utilizing two different detection mediums for gamma rays and neutrons separately, the LPS uses gamma-ray and thermal neutron signals detected from the single CLYC scintillator discriminated with PSD as input to the algorithm. An additional algorithm is utilized to identify anomalous spectra. A PSD plot for measurements of a ^{137}Cs and ^{252}Cf source with the LPS is shown in Figure 25.

Figure 24. LPS and a wearable pouch **[25]**

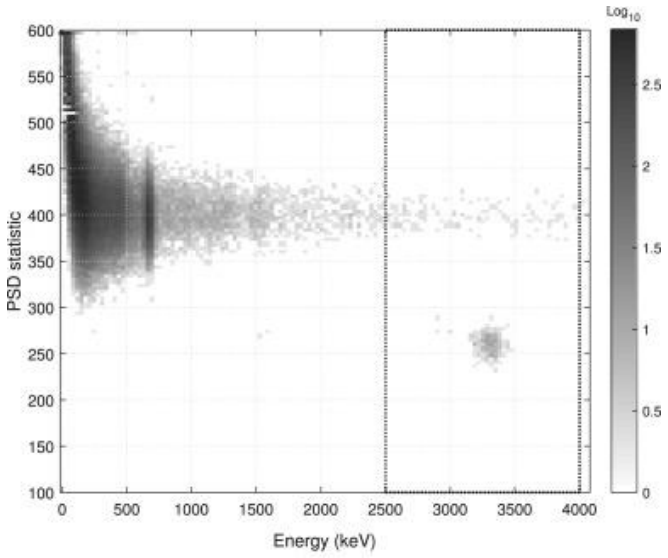

Figure 25. PSD with LPS **[25]**

Two other CLYC-based handheld detectors are available commercially. These detectors include the Thermo Scientific RIIDEye^{TM} X Series (Figure 26) and the Target Systemelektronik F500 (Figure 27). The RIIDEye^{TM} X Series uses a NaI or LaBr scintillator for gamma-ray detection and a CLYC scintillator for neutron detection alone. The F500 is similar to the RIIDEye^{TM} X Series in that it has a NaI:Tl scintillator for gamma-ray detection and an optional CLYC scintillator for gamma-ray/neutron detection [26].

Both of these handheld systems have similar capabilities to the ARMD and LPS systems, but rely on two different detection mediums for the detection of gamma rays and thermal neutrons separately. The capability to perform multi-mode detection, spectroscopy, and PSD utilizing CLYC has yet to be developed or commercialized. Development of such a handheld sensor would enable a more straightforward and detailed analysis and identification of measured isotopes given the capabilities afforded by fast neutron spectroscopy.

Figure 26. RIIDEyeTM X Series handheld radiation detector **[27]**

Figure 27. F500 handheld radiation detector **[26]**

2.5 Directional Detection Systems

Several directional detection systems of interest have been developed recently. The first of these systems is a wireless radiation sensor network (WRSN) which utilizes an array of Bubble Technology Industries RadCompass ^{TM} detectors [28]. These detectors consist of Geiger-Muller tubes capable of detecting incident gamma rays. A rendering of the WRSN is presented in Figure 28.

The WRSN utilizes both a point-of-closest-approach and a maximum logarithm-likelihood algorithm to determine the distance to the source and the source position [28]. These algorithms coupled with network communication enable the source localization. Figure 29 shows the results of one such source localization simulation. This simulation passes a ^{60}Co source through the WRSN consisting of twelve RadCompass^{TM} detectors in an array. It is observed from the results plotted in Figure 29 that the estimate of the source position stabilizes and is more accurate the closer the source gets to the center of the array.

The WRSN is not capable of gamma-ray or fast neutron spectroscopy. Additionally, the WRSN is not capable of thermal neutron detection. It is limited to the detection of gamma rays. It is further limited by its size and portability since a large array of detectors is required for source localization.

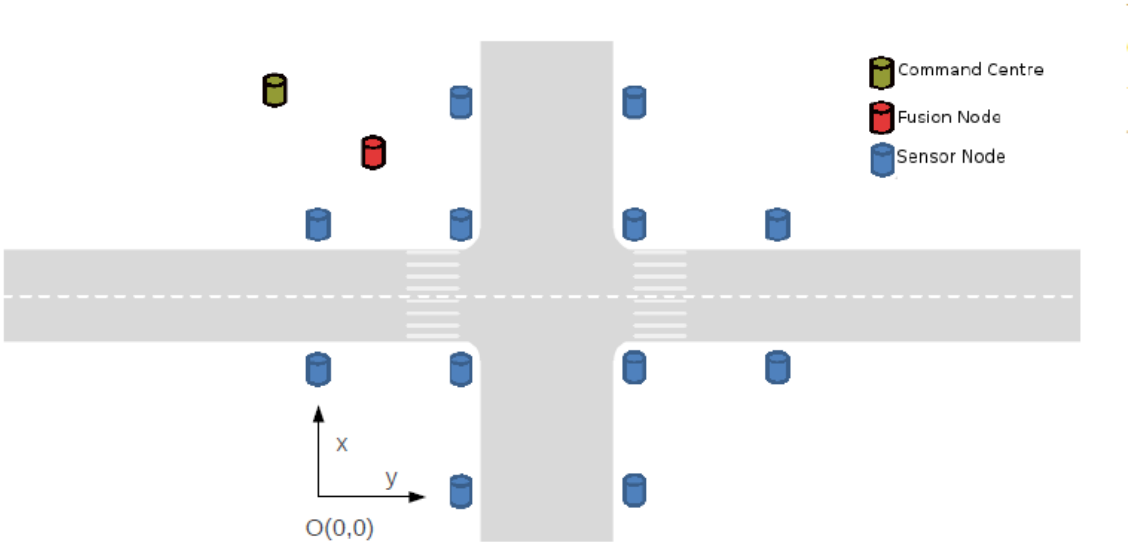

Figure 28. WRSN rendering with twelve RadCompassTM detectors **[28]**

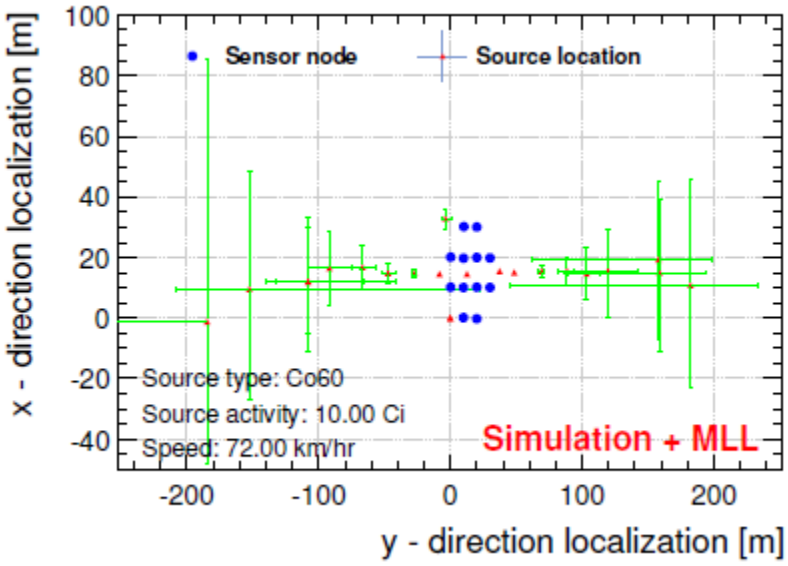

Figure 29. Results of source localization with WRSN detectors **[28]**

A more versatile and compact system is the dual neutron/gamma-ray directional detector [29]. This directional detection system utilizes only three CLYC scintillators. The scintillators are optically coupled to Hamamatsu PMTs connected to high-voltage (HV) bases. The HV bases are connected to a Bridgeport Instruments, Inc., qMorpho multi-channel analyzer (MCA) and digitzer.

The qMorpho can be connected to a computer via USB where the Igor Pro-based Wavemetrics software is used to perform on-the-fly analysis of measurements. The dual neutron/gamma-ray directional detector is presented in Figure 30.

The dual neutron/gamma-ray directional detector utilizes the maximum likelihood estimation algorithm (MLEA) to predict the location of the measured source [29]. The system rotates 360° around a vertical axis. An energy spectrum is collected at every 10° rotation of the system. Counts collected under the characteristic peaks of the measured source are used as input to the MLEA.

Results of source localization measurements are presented in Figure 31. The localization of a ^{137}Cs gamma-ray source and a plutonium beryllium (PuBe) neutron source was predicted within ±11% of the actual source location.

One advantage of this system is that it is compact. It is also capable of source localization based on both gamma-ray and thermal neutron signals. However, this system is only a prototype. Furthermore, it is not capable of fast neutron spectroscopy or isotope identification without end-user interpretation of the resultant spectra.

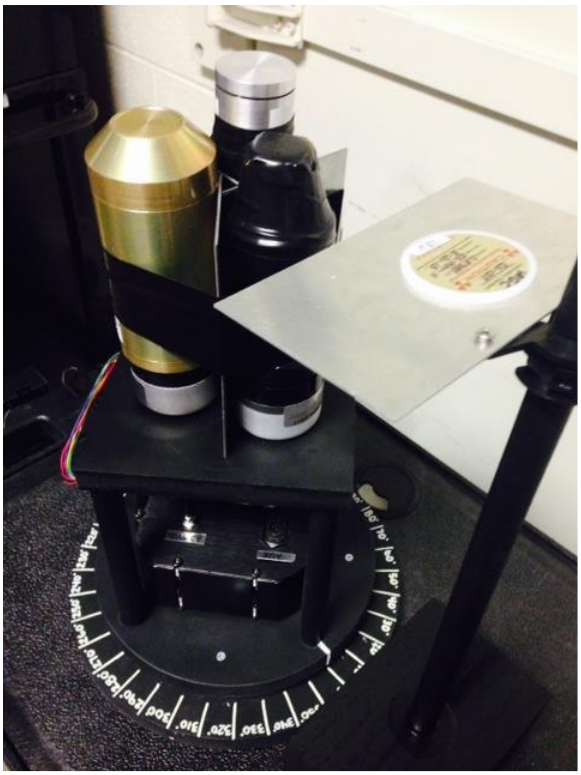

Figure 30. Dual neutron/gamma-ray directional detector **[29]**

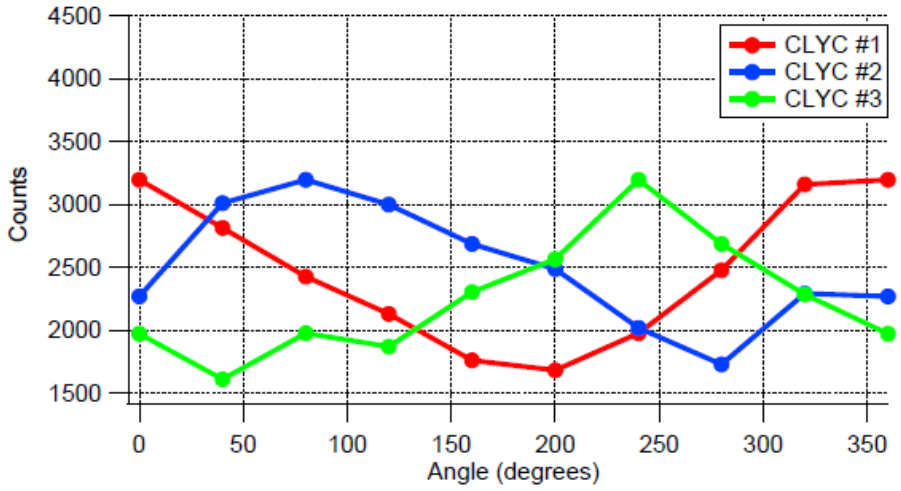

(a)

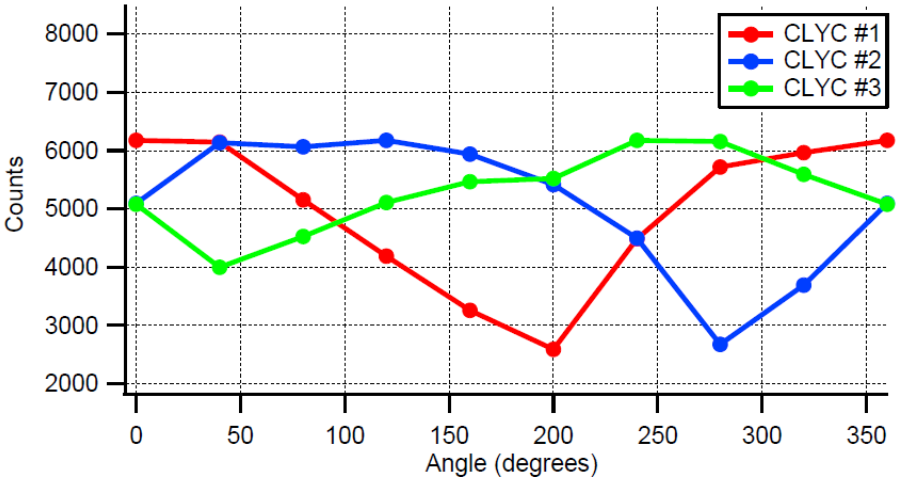

(b)

Figure 31. Directional detection of (a) ^{137}Cs and (b) PuBe sources **[29]**

A more novel directional detection system enables source localization with only two scintillators and a high-density polyethylene (HDPE) collimator. This system utilizes the technique of time-encoded imaging (TEI) for directional fast neutron and gamma-ray detection [30]. A HDPE time-modulated collimator rotates 360° around two 1inch-by-1inch EJ-309 liquid scintillator cells. The use of two scintillators instead of one, increases the volume in which neutrons can be detected and thus, increases the number of neutrons detected and improves the quality of

the results. Two PMTs and subsequent electronics connect the detection system to a computer for on-the-fly analysis. The TEI detection system is shown in Figure 32.

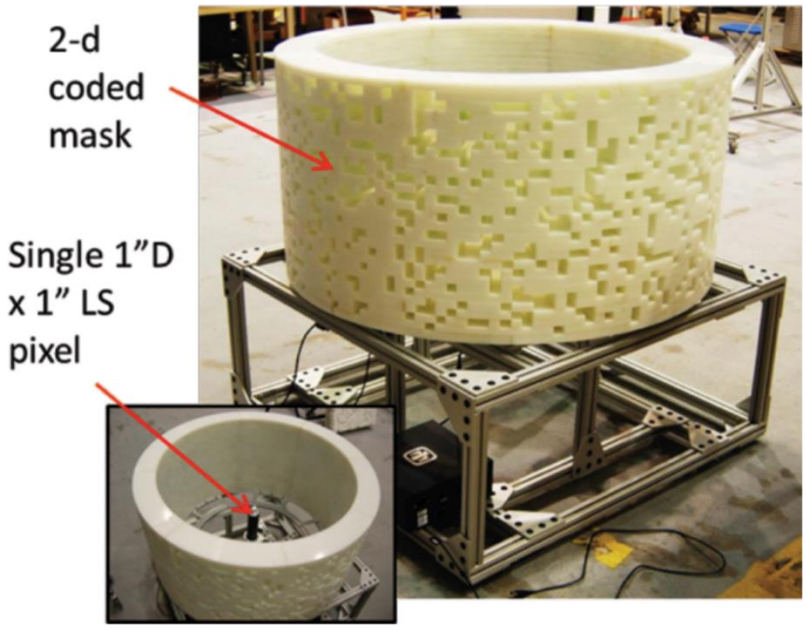

Figure 32. TEI directional detection system **[30]**

The random pattern of openings on the collimator enables time modulation [30]. Each opening has a designated position on the collimator and associated angle of incidence and time stamp. All gamma-ray and fast neutron signals passing through these openings are assigned a time stamp and thus, an angle of incidence. PSD is then applied to the gamma-ray and fast neutron signals to separate them. A maximum likelihood expectation maximization (MLEM) algorithm is then utilized to create an image of the measured source or to locate it in two dimensions.

The time-encoded measurements for a ^{252}Cf source is presented in Figure 33. The data processed by the MLEM algorithm results in the two-dimensional image and position presented in Figure 34.

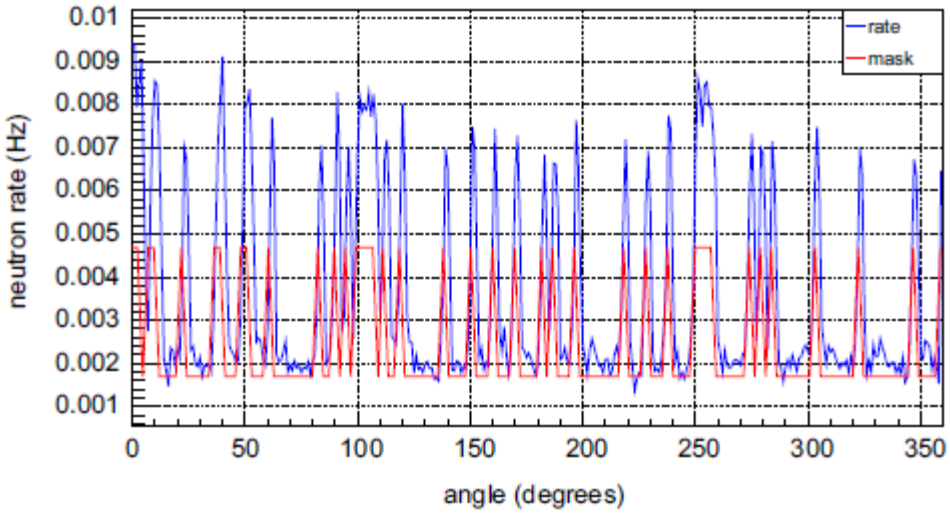

Figure 33. Time-encoded measurements of ^{252}Cf with collimated detector **[30]**

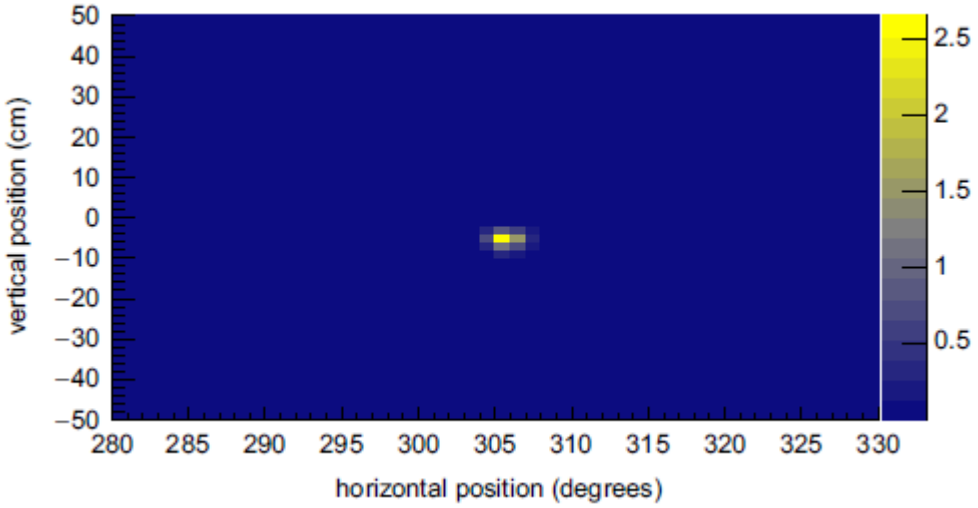

Figure 34. Imaging results of ^{252}Cf with collimated detector **[30]**

CHAPTER 3

COMPUTATIONAL STUDY

3.1 Parametric Study of ^{6}Li versus ^{7}Li in CLYC

To determine the feasibility of detecting photons, thermal neutrons, and fast neutrons within a single CLYC scintillator cell, it is of interest to determine an optimum enrichment of ^{6}Li and ^{7}Li in CLYC. The isotope of ^{6}Li enables thermal neutron detection by means of the reaction $^{6}Li(n,\alpha)^{3}H$. Whereas, the ^{7}Li isotope suppresses the thermal neutron signature thus improving the fast neutron spectroscopy capability. The difficulty of being able to detect thermal neutrons and perform fast neutron spectroscopy simultaneously is due to the thermal neutron peak appearing at 3.2 MeV GEE overwhelming any fast neutron peaks in proximity to thermal neutron peak.

The Monte Carlo N-Particle 6 (MCNP6) code developed by Los Alamos National Laboratory code was used to perform this parametric study [31]. The isotopic enrichment of ^{6}Li and ^{7}Li was varied from 0% to 100% for both isotopes. The same model from the CLYC-7 characterization scenarios was used. An isotropic point source with two different energies was used: 0.0253 eV and 2.5 MeV. These energies were selected since the signature peaks in the neutron spectra overlap. Another scenario was simulated with an isotropic point source with a different combination of energies: 0.0253 eV and 3.5 MeV. These energies result in signature peaks that are in very close proximity to one another. The sources were placed 20 cm from the front face of the scintillator. The 2-D model of this configuration is presented in Figure 35.

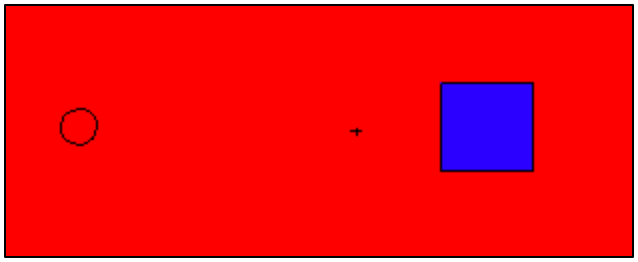

Figure 35. MCNP model of 2 inch-by-2 inch CLYC-7 scintillator with source; the blue square is a CLYC scintillator, the red circle and square surrounding CLYC is air, the red-filled circle contains 0.0253 eV or 3.5 MeV point source.

Determining an optimal enrichment of ^{6}Li and ^{7}Li would enable the creation of a scintillator capable of photon, thermal neutron, and fast neutron detection within a single medium. This would reduce the number of radiation detection devices needed to perform measurements in the field or reduce the size of radiation detection devices capable of multimode detection.

3.2 CLYC Characterization and Modeling of Handheld Multimode Radiation Sensor

The MCNP6 code was utilized to simulate the response of a 2 in-by-2 in CLYC-7 scintillator to various gamma-ray and neutron sources. Due to its simplistic construction and its use of a 2 in-by-2 in CLYC-7 scintillator, the Handheld Multimode Radiation Sensor is also well represented by this set of simulations.

The results of this simulation will provide a prediction of the response of CLYC-7 to various gamma-ray and neutron sources. These responses are confirmed by the experimental characterization of CLYC-7. Once these responses are confirmed, they can be added to a response function library to enable source identification in the two applications of the CLYC-7 scintillator discussed herein. These results also indicate the predicted performance and response of the Handheld Multimode Radiation Sensor to gamma-ray and neutron radiations from various sources.

The gamma-ray sources investigated include ^{137}Cs and ^{60}Co. The neutron sources investigated include PuBe, ^{252}Cf, and mono-energetic fast neutrons ranging from approximately 0.2 MeV to 20 MeV. Other nuclear materials that could be encountered in-the-field were also investigated including weapons-grade Pu (WGPu), reactor-grade Pu, (RGPu), depleted uranium (DU), natural uranium (NU), low-enriched uranium (LEU), and highly-enriched uranium (HEU).

Each source is placed 20 cm out from the face of the scintillator. The 2-D model of this simulation is the same as presented in Figure 35.

The F8 Pulse Height Tally of MCNP6 was used to determine the total number of photon and neutron interactions with the CLYC-7 scintillator. The F8:p (for photons) tally was used to determine the total number of photon interactions. Since the F8:n (for neutrons) tally is unreliable [76], the F8:h (for protons), F8:a (for alpha particles), and F8:d (for deuterons) tallies were used to determine the total number of neutron interactions. Neutron interactions within CLYC-7 result in the production of protons, alpha particles, or deuterons. Thus, the tallying of these product particles enables evaluating the neutron interactions.

3.3 Modeling of Collimated Directional Radiation Detection System

MCNP6 was utilized two-fold for the simulation of the Collimated Directional Radiation Detection System (CDRDS). The first simulation was performed to determine the optimal thickness of both the neutron collimator and the photon collimator in order to shield the CLYC-7 scintillator adequately from both radiations. The neutron collimator is made up of HDPE whereas the photon collimator is made up of lead.

Each collimator was varied from 0 inch to 5 inch thickness with increments of 0.5 inch (or from 1.27 cm to 12.7 cm in increments of 1.27 cm). The neutron and photon masks were omitted

since it is the total thickness of the collimators which are of interest for shielding purposes. The voids of each mask are intended to let each respective particle through. The 4 MeV isotropic neutron point source was utilized for the neutron collimator thickness study. The 4 MeV isotropic photon source was utilized for the photon collimator thickness study. The point sources were placed 1 m from the outer face of the Collimated Directional Radiation Detection System. The 2-D model for both the neutron and photon collimator simulation is presented in Figure 36.

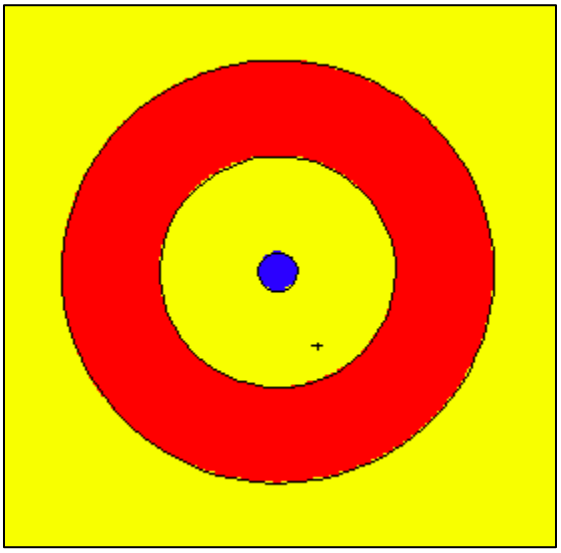

Figure 36. MCNP6 model of the neutron/photon collimator thickness study; the blue circle is the CLYC scintillator, the red hollow circle is the lead or HDPE collimator, the yellow surrounding the CLYC scintillator and collimator is air

The second simulation with the Collimated Directional Radiation Detection System was used to evaluate the response of the system, with the selected collimator thickness from the previous study, to radioactive sources and/or nuclear materials that it could be used to image and locate. The results of this simulation would indicate the feasibility of the selected design for the

Collimated Directional Radiation Detection System and its level of performance in regards to imaging and locating gamma-ray and neutron sources.

This model included both the neutron and photons masks on the collimators. Both collimators are heterogeneously combined to form a single collimator assembly with two different constituents and thus, two different masks. The voids of the neutron mask are where the photon mask is inlaid. The neutron mask was modeled as high-density polyethylene (HDPE). The photon mask was modeled as lead.

A modified uniformly redundant array (MURA) of 58 by 58 elements was selected for the neutron and photon masks. This type of coded aperture was selected based on previous success in imaging both neutron and photons with good resolution when used in the plane geometry (i.e., a flat coded aperture) [31]. This MURA is shown in Figure 37.

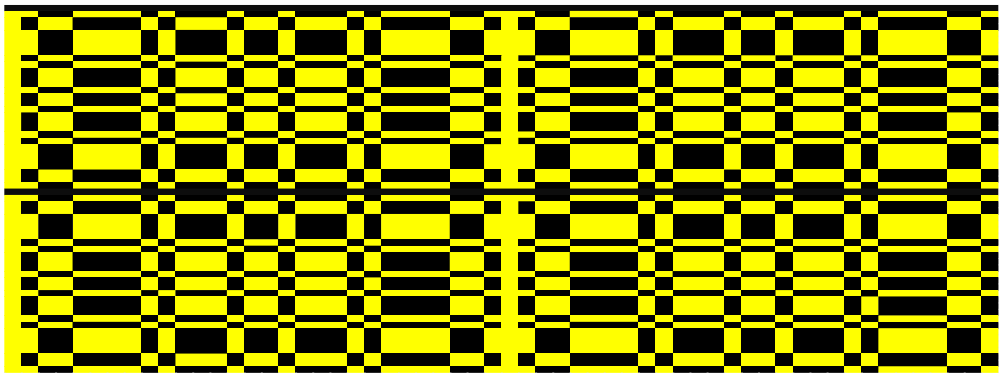

Figure 37. 2-D 58-by-58 MURA used for the Collimated Directional Radiation Detection System; the yellow units represent polyethylene and the black units represent lead

HEU was placed 2 m from the face of the collimator, Figure 38 provides the 2-D model of the Collimated Directional Radiation Detection System. The system was modeled with a

rectangular collimator with extra material instead of a cylinder so to simplify the geometry in MCNP6.

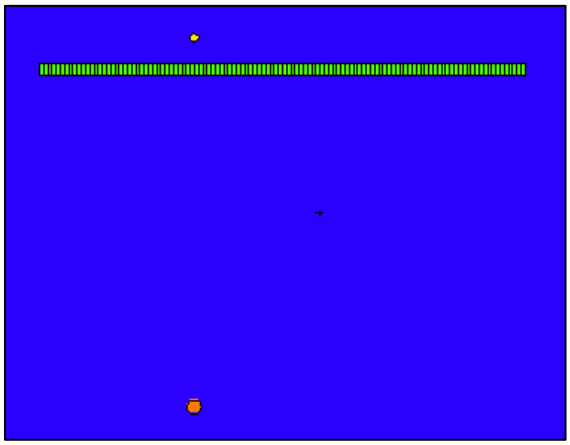

(a)

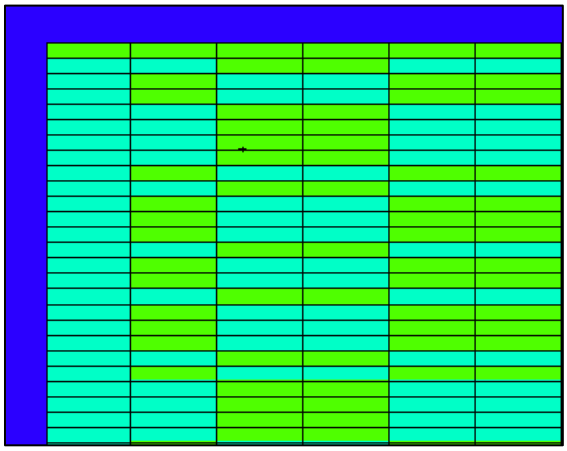

(b)

Figure 38. MCNP6 model of the Collimated Directional Radiation Detection System (a) top view and (b) zoomed-in front view; yellow circle is CLYC scintillator, orange circle is HEU, lime-green is lead, aquamarine is HDPE, blue is air

3.4 Decoding of CDRDS Measurement Data

The Maximum Likelihood Expectation Maximization (MLEM) algorithm was utilized to reconstruct the image of both photon and neutron sources from data obtained with the CDRDS computationally and experimentally. The MLEM algorithm used in this study is based on that proposed by L. A. Shepp and Y. Vardi [32]. This algorithm is tailored to the time-encoded approach to imaging as follows:

$$\hat{\lambda}^{new}(s) = \hat{\lambda}^{old}(s) \sum_{t=1}^{T} \frac{n^*(t) \cdot p(s,t)}{\sum_{s'=1}^{S} \hat{\lambda}^{old}(s') \cdot p(s',t)} \qquad s \; and \; s' = 1, 2, 3, \ldots S \qquad \textbf{Equation 8}$$

where s is the projected source pixel, s' is a dummy variable also indicating the projected source pixel, t is the time, $\hat{\lambda}^{new}(s)$ is the current estimate for the source rate in Hertz (Hz) for projected source pixel s, $\hat{\lambda}^{old}(s)$ is the previous estimate for the source rate in Hz for projected source pixel s, $n^*(t)$ is the total counts in the detector at time t, and $p(s,t)$ is the detector response matrix. This equation is iterated until the value of $\hat{\lambda}^{new}(s)$ has converged upon an answer.

The detector response matrix is formed by considering two factors. The first factor is the attenuation of the incident radiation by the collimator (either by HDPE or lead). The second factor is position of the collimator at time t. These two factors take form in the following equation:

$$p(s,t) = \frac{\frac{I}{I_0} \cdot \cos(\alpha(t))}{L(s)} \sqrt{\left[1 - \left(\frac{D}{d}\right)^2\right]^{-1}} \qquad \textbf{Equation 9}$$

where $\frac{I}{I_0}$ is the fraction of radiation that is absorbed by the collimator, $\alpha(t)$ is the angle corresponding to the time stamp, $L(s)$ is the estimated distance between the detector and the possible source position s, D is the outer diameter of the collimator, and d is the diameter of the detector. It should be noted that $\frac{I}{I_0}$ is calculated differently for photons and neutrons. For photons:

$$\frac{I}{I_0} = \exp\left(-\left(\frac{\mu}{\rho}\right)\rho h\right) \qquad \textbf{Equation 10}$$

where $\frac{\mu}{\rho}$ is the attenuation coefficient of lead given the incident photon energy, ρ is the density of lead, and h is the thickness of the lead collimator [33]. For neutrons:

$$\frac{I}{I_0} = \exp(-\sigma n h) \qquad \textbf{Equation 11}$$

where σ is the microscopic absorption cross-section of HDPE given the incident neutron energy, n is the number density of HDPE, and h is the thickness of the HDPE collimator [33]. Attenuation through both Pb and HDPE are considered for the calculation of the detector response matrix for the neutron and photon case.

The MLEM algorithm described is implemented in the form of a Matlab code to process all of the computational and experimental CDRDS data. The example of the Matlab code for the neutron case is presented in Appendix B.

There exists a known instability in the MLEM algorithm [34]. Since the MLEM algorithm assumes a Poisson likelihood of the estimate that converges to the actual source position, therein lies Poisson noise which induces a high frequency instability. This instability materializes as an incorrect estimate of the source location at certain iterations of the MLEM algorithm. There are various methods for avoiding this instability [34]. One such method is to stop the algorithm at a selected iteration at which the estimate is both converged and agrees with the actual source position. This approach is used in the application of the MLEM algorithm to the CDRDS study. The number of iterations selected that yielded a converged and agreeable estimate was 200 for each computational and experimental case.

CHAPTER 4

EXPERIMENTAL STUDY

4.1 CLYC-7 Detector Characterization

A Radiation Monitoring Devices, Inc., (RMD) 2inch-by-2inch CLYC-7 scintillator mounted to a PMT and sealed within housing was characterized in terms of its response to gamma rays and neutrons. This unit is presented in Figure 39.

Figure 39. RMD 2inch-by-2inch CLYC-7 detector

The results of this study indicate the level of performance of CLYC-7 as applied to photon and fast neutron spectroscopy. The results also confirm the capability of CLYC-7 to be used in the Handheld Multimode Radiation Sensor and the Collimated Directional Radiation Detection System.

The first set of measurements was performed at the University of Kentucky Van de Graaff Accelerator Laboratory. By changing the types of particles accelerated (i.e, protons or deuterons), the type of target (i.e, tritium or deuterium gas), and the angular position of the CLYC-7 scintillator

with respect to the accelerator beamline (0° being in-line with the beamline), a wide range of fast neutron energies can be set for experiments [35]. Three nuclear reactions were used: T(p, n)^{3}He, T(d, n)^{4}He, and D(d, n)^{3}He. The CLYC-7 scintillator was placed at various angles from 0° to 150° with respect to the accelerator beamline. The combinations of reaction type and CLYC-7 angular position that were used and the resulting fast neutron energies are presented in Table 2.

Table 2. Fast neutron energies studied with CLYC-7 using the UKy Van de Graaff Accelerator

Reaction Type	Angular Position	Neutron Energy (MeV)
T(p, n)^{3}He; p = 4.5 MeV	0°	4.22
T(p, n)^{3}He; p = 4.5 MeV	30°	3.82
T(p, n)^{3}He; p = 4.5 MeV	40°	3.53
T(p, n)^{3}He; p = 4.5 MeV	50°	3.21
T(p, n)^{3}He; p = 4.5 MeV	60°	2.87
T(p, n)^{3}He; p = 4.5 MeV	65°	2.70
T(p, n)^{3}He; p = 4.5 MeV	75°	2.37
T(p, n)^{3}He; p = 4.5 MeV	85°	2.06
T(p, n)^{3}He; p = 4.5 MeV	95°	1.79
T(p, n)^{3}He; p = 4.5 MeV	105°	1.56
T(p, n)^{3}He; p = 4.5 MeV	110°	1.46
T(p, n)^{3}He; p = 2.1 MeV	0°	1.30
T(p, n)^{3}He; p = 2.1 MeV	30°	1.15
T(p, n)^{3}He; p = 2.1 MeV	55°	0.86

Reaction Type	Angular Position	Neutron Energy (MeV)
T(p, n)^{3}He; p = 2.1 MeV	75°	0.62
T(p, n)^{3}He; p = 2.1 MeV	90°	0.47
T(p, n)^{3}He; p = 2.1 MeV	120°	0.28
T(p, n)^{3}He; p = 2.1 MeV	145°	0.21
T(d, n)^{4}He; d = 3.5 MeV	0°	20.2
T(d, n)^{4}He; d = 3.5 MeV	30°	19.5
T(d, n)^{4}He; d = 3.5 MeV	55°	18.0
T(d, n)^{4}He; d = 3.5 MeV	75°	16.5
T(d, n)^{4}He; d = 3.5 MeV	95°	15.1
T(d, n)^{4}He; d = 3.5 MeV	110°	14.1
T(d, n)^{4}He; d = 3.5 MeV	115°	13.7
T(d, n)^{4}He; d = 3.5 MeV	120°	13.5
T(d, n)^{4}He; d = 3.5 MeV	130°	13.0
T(d, n)^{4}He; d = 3.5 MeV	140°	12.5
T(d, n)^{4}He; d = 3.5 MeV	150°	12.2
D(d, n)^{3}He; d = 5.5 MeV	0°	8.73
D(d, n)^{3}He; d = 5.5 MeV	10°	8.62
D(d, n)^{3}He; d = 5.5 MeV	15°	8.50
D(d, n)^{3}He; d = 5.5 MeV	25°	8.10
D(d, n)^{3}He; d = 5.5 MeV	30°	7.85

Reaction Type	Angular Position	Neutron Energy (MeV)
D(d, n)^{3}He; d = 5.5 MeV	35°	7.56
D(d, n)^{3}He; d = 5.5 MeV	40°	7.24
D(d, n)^{3}He; d = 5.5 MeV	45°	6.90
D(d, n)^{3}He; d = 5.5 MeV	50°	6.55
D(d, n)^{3}He; d = 5.5 MeV	55°	6.18
D(d, n)^{3}He; d = 5.5 MeV	60°	5.82
D(d, n)^{3}He; d = 5.5 MeV	65°	5.45
D(d, n)^{3}He; d = 5.5 MeV	70°	5.10
D(d, n)^{3}He; d = 5.5 MeV	75°	4.75
D(d, n)^{3}He; d = 5.5 MeV	80°	4.42

The initial measurement time was 15 minutes for each incident neutron energy. This collection time was either decreased/or increased to achieve a count rate of 10,000 counts per second (cps). The CLYC-7 scintillator was mounted to a large lever arm at the end of the accelerator beamline. This configuration is shown in Figure 40 and Figure 41. The CLYC-7 scintillator was initially placed 91.5 cm from the end of the accelerator beamline. This distance was decreased as the angular position was increased so to also achieve a count rate of 10,000 cps.

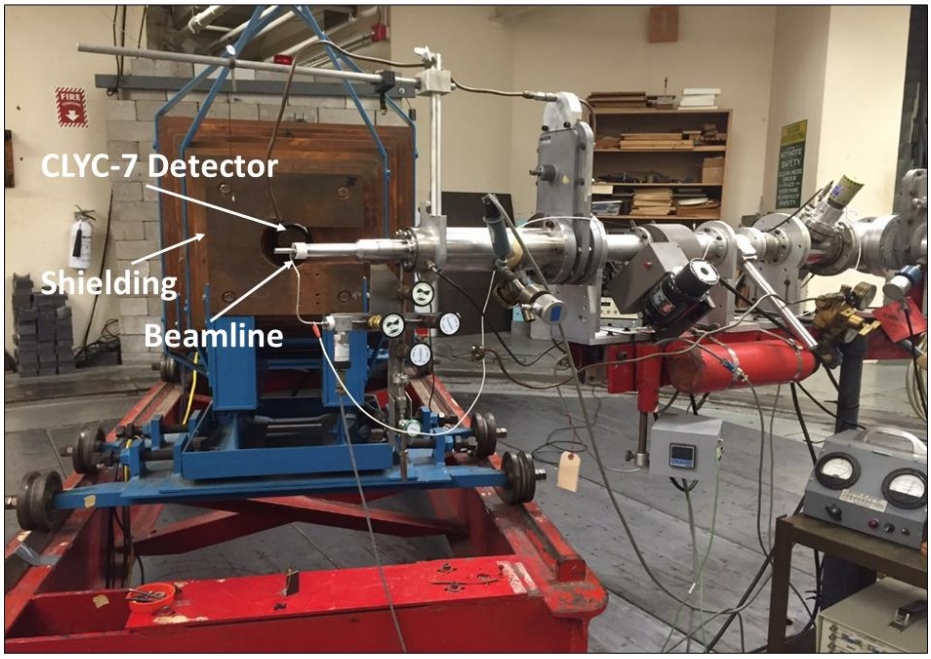

Figure 40. Front view of CLYC-7 scintillator configuration with UKy Van de Graaff accelerator

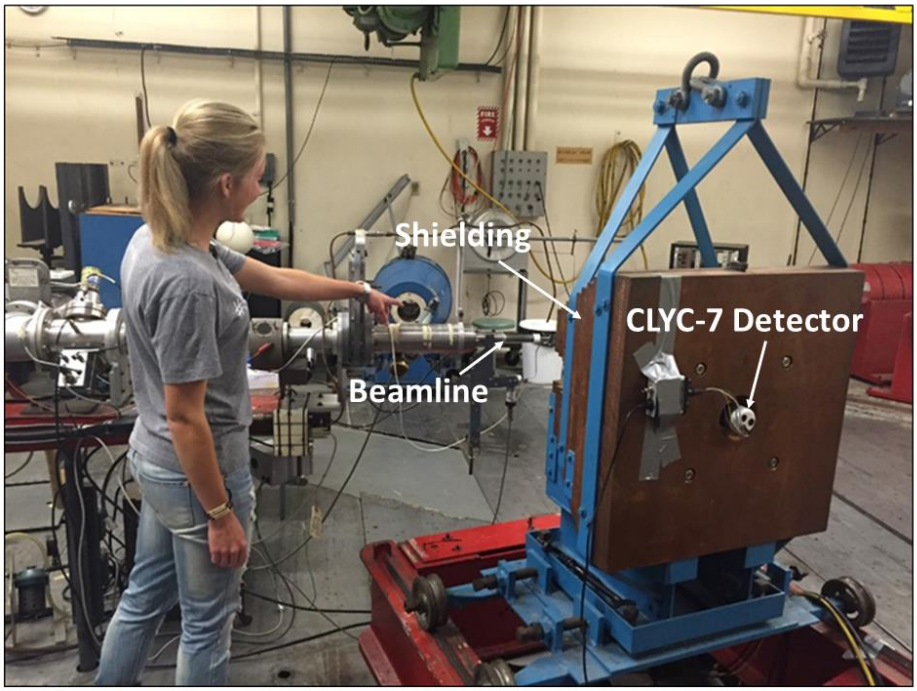

Figure 41. Back view of CLYC-7 scintillator configuration with UKy Van de Graaff accelerator

The second set of characterization measurements was performed at the University of Nevada, Las Vegas Nuclear Engineering Laboratory. The CLYC-7 response to gamma-rays was investigated for ^{137}Cs, ^{60}Co, and ^{133}Ba sources. Its response to poly-energetic neutron flux was investigated using ^{252}Cf and PuBe sources.

The measurement configuration for the photon sources and the ^{252}Cf neutron source is presented in Figure 42. The CLYC-7 scintillator was placed in 10 cm from each source. The measurement configuration for the PuBe neutron source is presented in Figure 43. The front face of the detector was placed in-line with and 10 cm from the port on the 55-gallon drum containing the PuBe source. All photon measurements were carried out for 5 minutes for each source. All neutron measurements were carried out for 15 minutes.

The energy spectra, energy resolution of the characteristic peaks, and total counts for the characteristic peaks were measured for each photon source. In addition to the detector responses for the neutron sources, PSD information was also recorded. Collectively, this information enables the characterization of the 2-inch-by-2-inch CLYC-7 scintillator, the comparison of experimental data to the computational date, the determination of how well the scintillator responds to various photon and neutron sources, and the beginnings of a spectral library of which can be used for radioactive source identification.

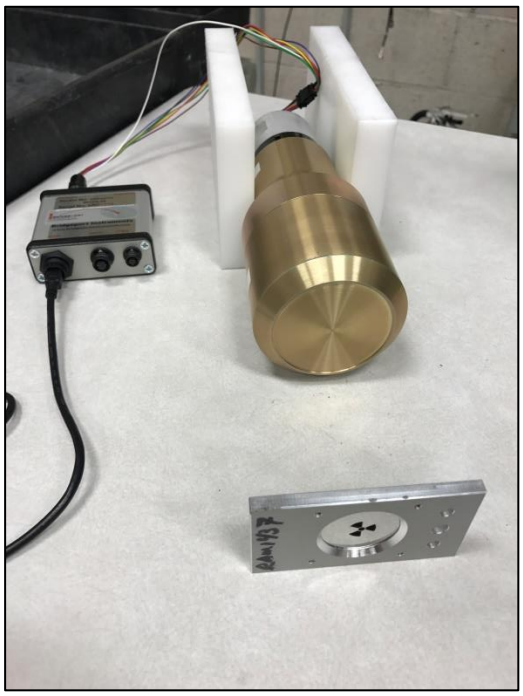

Figure 42. Measurement configuration of CLYC-7 scintillator with the ^{137}Cs photon source at the UNLV Nuclear Engineering Laboratory

Figure 43. Measurement configuration of CLYC-7 scintillator with a PuBe source at the UNLV Nuclear Engineering Laboratory

4.2 CLYC Handheld Multimode Radiation Sensor

4.2.1 Design

The HMRS utilizes a single 2-inch-diameter-by-2inch height CLYC-7 scintillator as the detection medium. However, the scintillator can be changed out to any scintillator up to 2-inch diameter by 2-inch height. The scintillator detector is connected to a Bridgeport Instruments (BPI) eMorpho MCA and digitizer using a high voltage (HV)-base. The eMorpho is connected to a Raspberry Pi 3 Model B+ computer. The Raspberry Pi is approximately 3.5-inch-long, 2.5-inch-wide, and ¾-inch-tall. The Raspberry Pi has 1 gigabyte (GB) of random access memory (RAM), a Quad Core Broadcom BCM2837 64-bit ARMv8 processor, BCM43143 WiFi chip, and 4 USB

ports [36]. The Raspberry Pi powers the eMorpho and communicates with it. The Raspberry Pi is powered by a 5 V battery. A PiTFT Plus touchscreen connects directly to the top of the Raspberry Pi providing a 3.5-inch-long, 2.5-inch-wide display for the user [37]. All of the aforementioned components are housed in a 3D-printed PLA housing with handles for ease of carrying and manipulation. The CAD rendering and the actual build of the HMRS are presented in Figure 44 and Figure 45, respectively.

Several software applications were installed and configured on the Raspberry Pi to enable communication with the eMorpho. BPI's Morpho Data Server (MDS) was installed on the Raspberry Pi. This software performs the actual communication between the Raspberry Pi and the eMorpho [38]. This communication is performed with the deployment of a web application. To run a web application, Apache 2.4, PHP, SVGraph, and ZMQ were all installed and configured on the Raspberry Pi. Together with the MDS, these software applications provide real-time energy spectra, traces, and count rates on the HMRS. Data can also be stored on the Raspberry Pi and transferred to another computer (i.e., a desktop or laptop) via the ZMQ protocol for post processing.

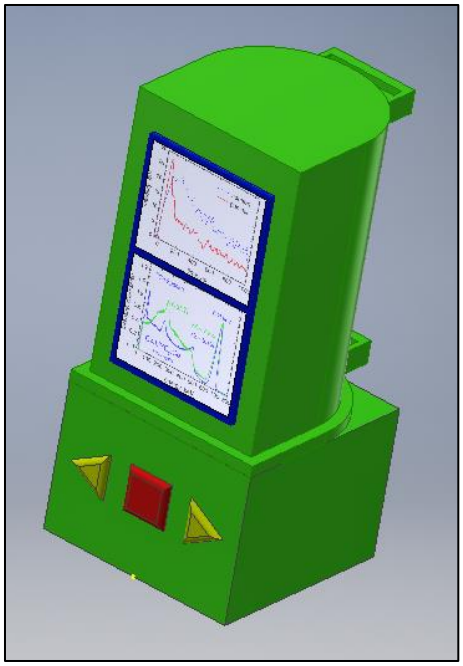

Figure 44. CAD rendering of Handheld Multimode Radiation Sensor

Figure 45. The assembled HMRS unit

4.2.2 Laboratory Measurements

All of the measurements performed as described in Section 4.1 and their results as discussed in Section 5.3.1 would be the same for the measurements performed with the HMRS. The only differences between the CLYC-7 characterization measurements and the HMRS measurements would be the insertion of the CLYC-7 detector assembly (the CLYC-7 scintillator, HV base, and eMorpho) into the HMRS housing, the use of the Raspberry Pi and touchscreen to monitor and analyze results, and the addition of a battery pack to provide power to the eMorpho and Raspberry Pi. None of these additions would yield different results from those presented in Section 5.3.1.

Therefore, the measurements taken with the HMRS were limited to ensuring the functionality of the HMRS and the MDS used to monitor and analyze the results. The spectra, traces, and count rates using ^{137}Cs, ^{60}Co, ^{252}Cf, and PuBe sources were recorded with the HMRS.

4.3 CLYC Collimated Directional Radiation Detection System

4.3.1 Design

The CDRDS consists of only one detection medium: a single 2-inch-diameter-by-2inch-height CLYC-7 scintillator. The scintillator is interchangeable, so that any type of scintillator of similar dimensions may be used with this system. The CLYC-7 scintillator is connected to a BPI's eMorpho MCA and digitizer by means of a HV-base. The eMorpho is connected to a computer for on-the-fly analysis with a USB cable. The USB cable also provides power to the eMorpho. The eMorpho can also be configured to transfer data wirelessly by utilizing a WiFi adapter and a battery power supply.

A hollow 18-inch-diameter by 10-inch-height cylindrical collimator consisting of a heterogeneous combination of water jet-cut HDPE and lead (Pb) surrounds the CLYC-7

scintillator. The placement of the HDPE and Pb in the collimator creates two coded apertures (simultaneously in the single design). The HDPE makes-up a rank-29 modified uniformly redundant array (MURA) coded aperture. The voids within this MURA are filled with the Pb and make-up the second coded aperture. The collimator is rotated 360° in the horizontal plane by a Lazy Susan bearing in contact with two Pololu High-Traction Sticky Tires that are rotated by two NEMA 23 stepper motors. The stepper motors are driven by a two Geckodriver G251X stepper motor drivers and an Arduino Uno. The Arduino Uno is powered by a 5 volt (V) battery. The stepper motors and drivers are powered by a 24 V 4 ampere (A) switching power supply.

The collimator, Lazy Susan bearing, detector, and subsequent electronics are secured to a 20-inch by 20-inch by 8-inch base. This base consists of 1 in-by-1 in slotted aluminum extrusions that are secured by L-plates and M4 screws and T-nuts.

Measurements were carried out at discrete time steps, corresponding to specific angles of rotation, as the collimator is rotated 360° in the horizontal plane. These measurements are consolidated for post-processing. Utilizing the recorded measurements, the known coded aperture patterns, and the convolution theorem, an image of the measured radioactive source can be reconstructed in two-dimensions enabling source localization.

The CAD model of the Collimated Directional Radiation Detection System is presented in Figure 46. This model was used as the basis for constructing the system. The assembled Collimated Directional Radiation Detection System is shown in Figure 47.

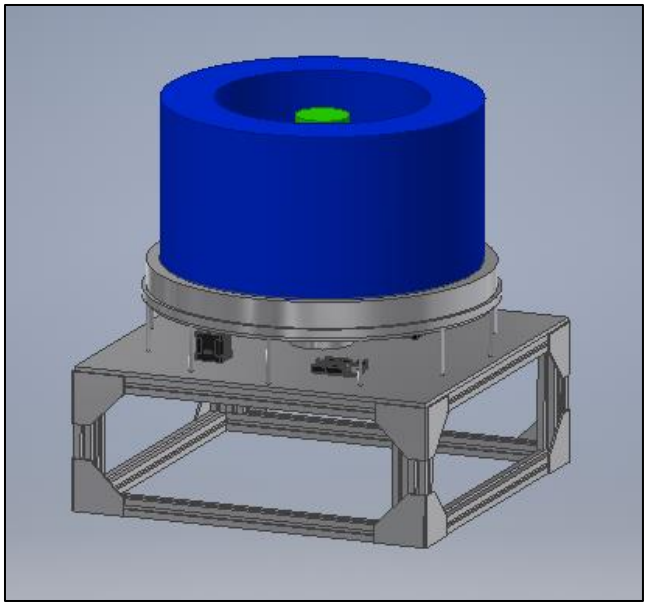

Figure 46. CAD-rendering of Collimated Directional Radiation Detection System

Figure 47. The assembled CDRDS unit

4.3.2 Laboratory Directional Measurements

The time-encoded images of ^{252}Cf, PuBe, ^{137}Cs, and ^{60}Co sources in five different configurations were measured with the CDRDS at the UNLV Nuclear Engineering Laboratory. Each configuration is assigned a number, #1 through #6, and is discussed in detail in the following paragraphs.

Configuration #1 measured the ^{252}Cf source with the CDRDS with the HDPE collimator only as shown in Figure 48. The ^{252}Cf source was aligned with the 0° mark on the CDRDS. It was placed 10 cm from the collimator face and 18 cm above the collimator base. Measurements were collected at 58 different angles corresponding to the 58 MURA coded aperture columns on the CDRDS for five minutes at each angle.

Figure 48. Configuration #1 of CDRDS measurements

The Configuration #2 measured both the ^{137}Cs and ^{60}Co sources simultaneously with the CDRDS with the HDPE collimator only as shown in Figure 49. The ^{137}Cs source was placed at 30° in reference to the 0° mark on the CDRDS. The ^{60}Co source was placed at 60° in reference to

the 0° mark on the CDRDS. Both sources were placed 10 cm out from the collimator face and 18 cm above the collimator base. Measurements were collected at 58 different angles corresponding to the 58 MURA coded aperture columns on the CDRDS for three minutes at each angle.

Figure 49. Configuration #2 of CDRDS measurements

Configuration #3 measured both the ^{137}Cs and ^{60}Co sources simultaneously with the CDRDS with the both the HDPE and Pb collimator as shown in Figure 50. The ^{137}Cs source was placed at 30° in reference to the 0° mark on the CDRDS. The ^{60}Co source was placed at 60° in reference to the 0° mark on the CDRDS. Both sources were placed 29 cm out from the collimator face. The ^{137}Cs source was positioned at a height of 31 cm above the floor. The ^{60}Co source was positioned at a height of 46 cm above the floor. Measurements were collected at 58 different angles corresponding to the 58 MURA coded aperture columns on the CDRDS for three minutes at each angle. Measurements were then repeated with both sources at 1m from the collimator face so to compare effects of distance from the collimator to the source on the reconstructed image.

Figure 50. Configuration #3 of CDRDS measurements at 29 cm from collimator face

Configuration #4 measured the ^{252}Cf source with the CDRDS with both the HDPE and Pb collimator as shown in Figure 51.

The ^{252}Cf source was placed at the 0° mark on the CDRDS. The source was placed 10 cm out from the collimator face and 18 cm above the collimator base. Measurements were carried out at 58 different angles corresponding to the 58 MURA coded aperture columns on the CDRDS for five minutes at each angle.

Figure 51. Configuration #4 of CDRDS measurements

Configuration #6 measured the PuBe source with the CDRDS with both the HDPE and Pb components in the collimator as shown in Figure 52. The PuBe source was removed from its 55-gallon drum and placed at 180° in reference to the 0° mark on the CDRDS. The source was placed 50 cm out from the collimator face and 40 cm above the ground. Measurements were performed at 58 different angles corresponding to the 58 MURA coded aperture columns on the CDRDS for four minutes at each angular position.

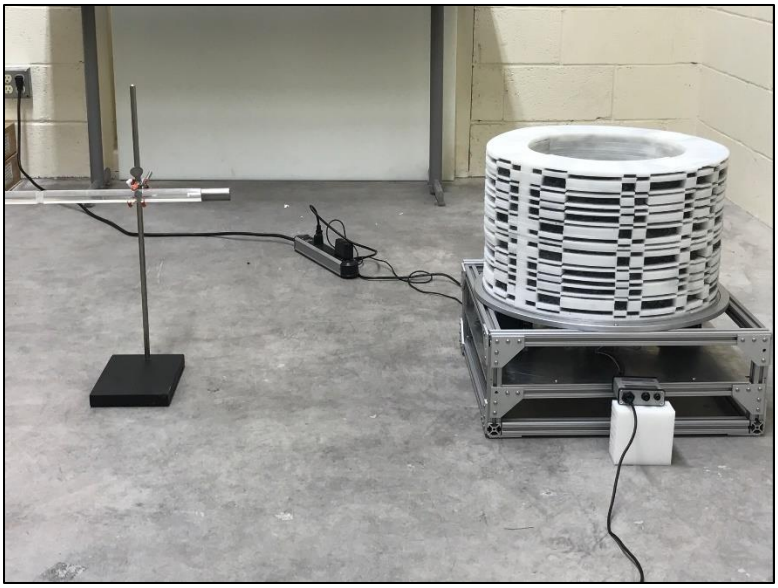

Figure 52. Configuration #5 of CDRDS measurements

CHAPTER 5

RESULTS AND DISCUSSION

5.1 Computational Study

5.1.1 Parametric Study of ^{6}Li versus ^{7}Li in CLYC

The isotopic enrichment of ^{6}Li and ^{7}Li in the CLYC scintillator MCNP6 model was varied from 0% to 100%, in increments of 5%, for each Li isotope. The CLYC response to thermal neutrons and 2.5 MeV fast neutrons at each enrichment combination was analyzed. The thermal neutron peak and the 2.5 MeV fast neutron peak both appear at approximately 3.2 MeV GEE. These peaks are captured in the energy spectrum presented in Figure 53. Any changes in the appearance of these peaks as the enrichment of ^{6}Li versus ^{7}Li in the CLYC scintillator is changed would be apparent by comparing the spectra for each ^{6}Li enrichment value. The 3.2 MeV GEE thermal neutron peak and the 2.5 MeV fast neutron peak are not readily discernable from one another at any combination of ^{6}Li and ^{7}Li by solely comparing the resultant energy spectra. A plausible alternative method to determine the optimal enrichment of ^{6}Li versus ^{7}Li would be PSD of the particles created in thermal neutron reactions (i.e., alpha particles) versus fast neutron reactions (i.e., protons).

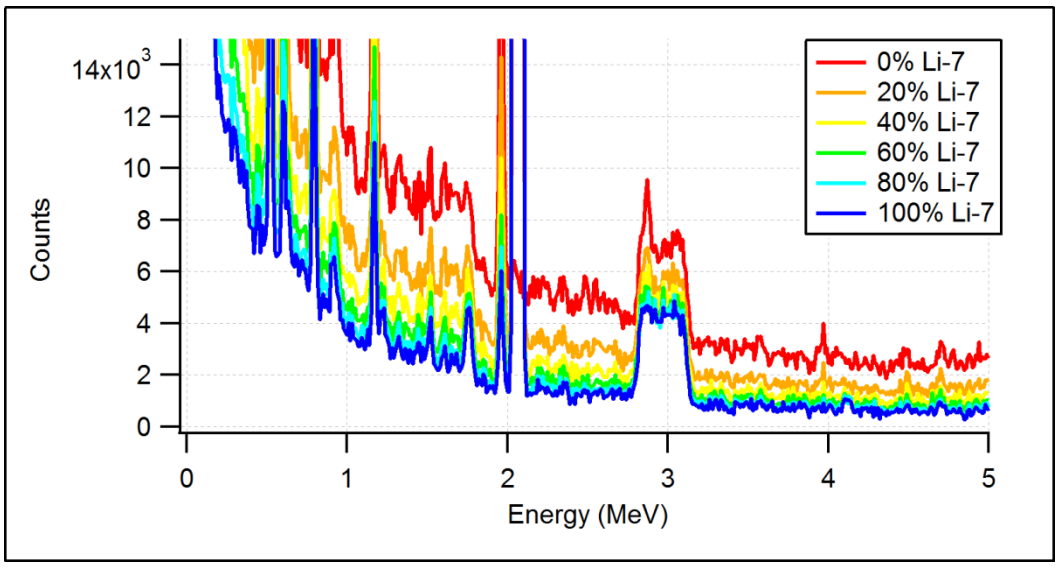

Figure 53. Parametric study of CLYC response to thermal neutrons and 2.5 MeV fast neutrons while varying ^{6}Li and ^{7}Li enrichment in CLYC

5.1.2 CLYC Characterization and Modeling of CLYC Handheld Multimode Radiation Sensor

5.1.2.1 Monoenergetic Source Detector Response

The response of the 2-inch-by-2-inch CLYC-7 scintillator to mono-energetic neutrons from 0.205 MeV to 20.02 MeV was analyzed in MCNP6. The fast neutron energies investigated were selected to reflect the fast neutron energies measured at the UKy Van de Graaff Accelerator Laboratory. The resultant detector responses are presented in Figure 54. Each different colored detector response in Figure 54 represents a different incident neutron energy. The dark blue detector response is from the lowest incident neutron energy and the light pink detector response is from the highest incident neutron energy.

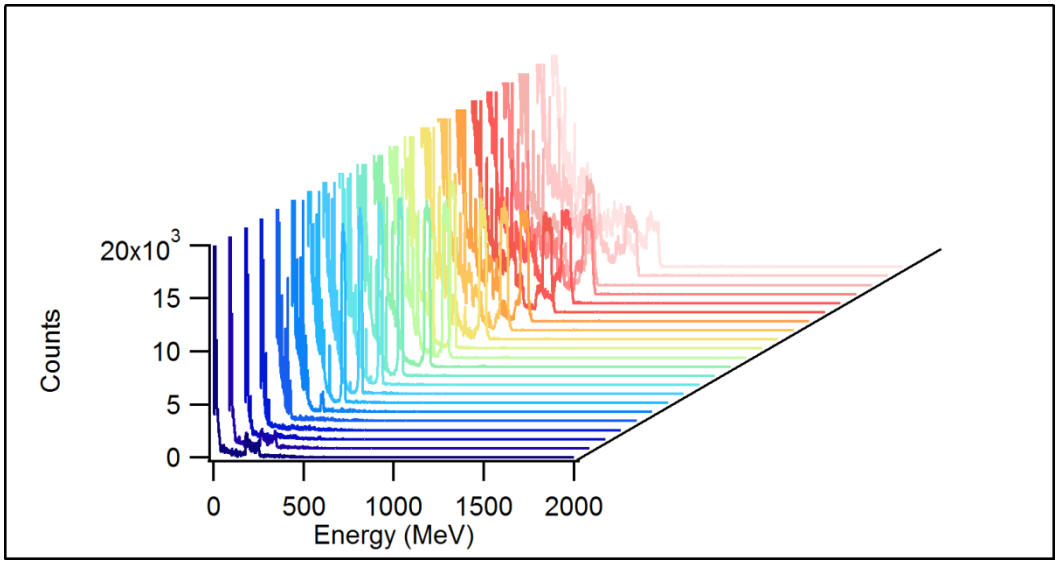

(a)

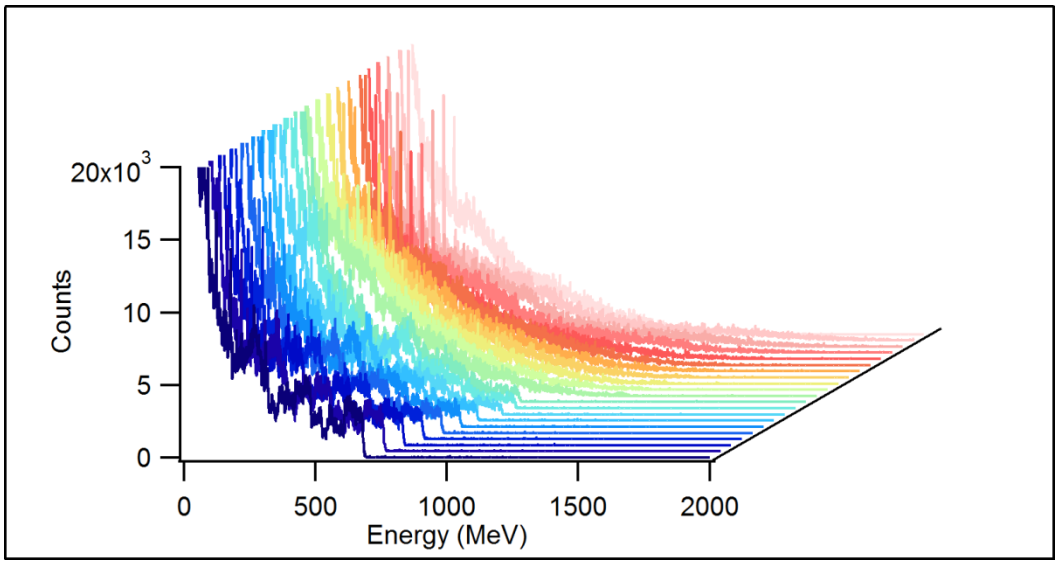

(b)

Figure 54. CLYC-7 response to mono-energetic fast neutrons from UKy Van de Graaff accelerator; from front to back (a) 0.205 to 5.10 MeV neutrons, (b) 5.82 to 20.2 MeV neutrons

For neutrons between 0.205 MeV and 0.861 MeV, the detector responses appear as distributions rather than single peaks. The distribution grows in width and decreases in magnitude as the neutron energy is increased from 0.205 to 0.861 MeV. At 1.15 MeV, the mono-energetic

neutrons begin to appear within a single peak albeit the peak is small in magnitude. This peak is very pronounced from 1.46 to 2.87 MeV. From 3.21 to 7.56 MeV, this peak gradually decreases in magnitude, but is still distinguishable from the background. The peaks that appear for neutrons from 1.15 to 7.56 MeV move to the right as incident neutron energy increases, i.e., the movement of the peaks is proportional to the incident neutron energy. This indicates that CLYC-7 can be used as a fast neutron spectrometer for mono-energetic neutrons from 1.15 to 7.56 MeV. From 7.85 to 8.495 MeV, the neutron spectra appear as distributions once again. However, the distributions continue to move to the right with increase in incident neutron energy. At 12.20 MeV, the distributions are over-whelmed by the background continuum. There is the movement of what appears to be the continuum distribution to the right as incident neutron energy increases.

This computational study indicates that CLYC-7 can be used as a fast neutron spectrometer. Although, incident mono-energetic neutrons between 1.15 and 7.56 MeV appear as peaks which is ideal for fast neutron spectroscopy; the spectrum unfolding can be utilized for other fast neutron energies with CLYC-7.

5.1.2.2 Radioactive Material Detector Response

The response of the 2-inch-by-2-inch CLYC-7 scintillator to various photon sources, neutron sources, and nuclear materials was also analyzed using MCNP6. The resultant responses are also indicative of the responses from the HMRS. This sensor utilizes a 2 in-by-2 in CLYC-7 scintillator and is very simplistic in design. Thus, it is well represented by the analyzed model.

Two photon sources were investigated: ^{60}Co and ^{137}Cs. The resultant spectra are presented in Figure 55 and Figure 56, respectively. The characteristic peak of ^{137}Cs can be observed in Figure 55 at 0.662 MeV. The characteristic peaks of ^{60}Co are also readily recognizable in Figure 56 at 1.17 MeV and 1.33 MeV. The 5% energy resolution built into the MCNP6 model was used as it

has been well-studied that CLYC-7 has a 0.662 MeV energy resolution of 5% or better. Without this input to the model, the peaks would have appeared as perfect lines.

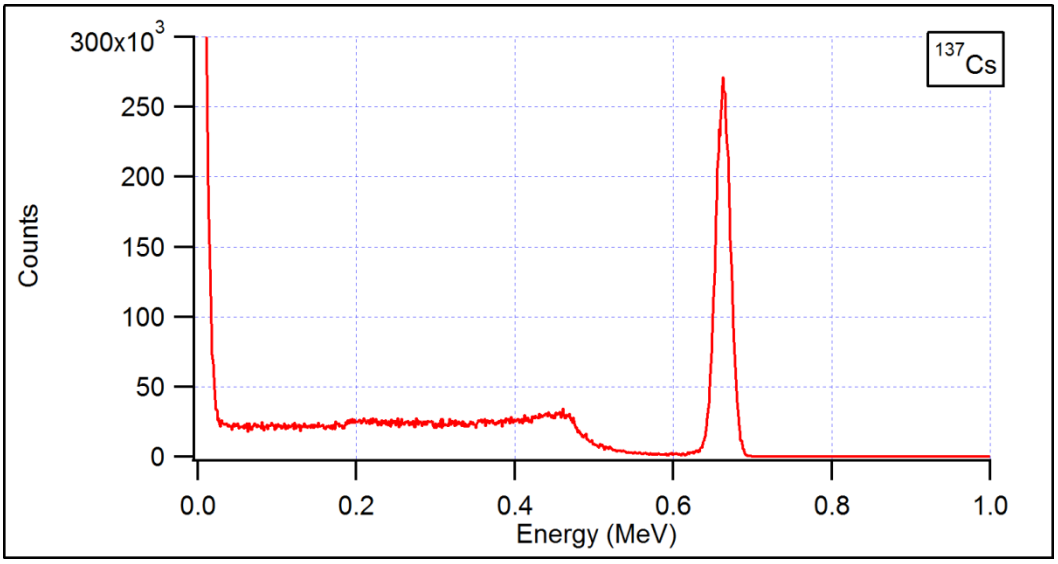

Figure 55. CLYC-7 response to ^{137}Cs photon source

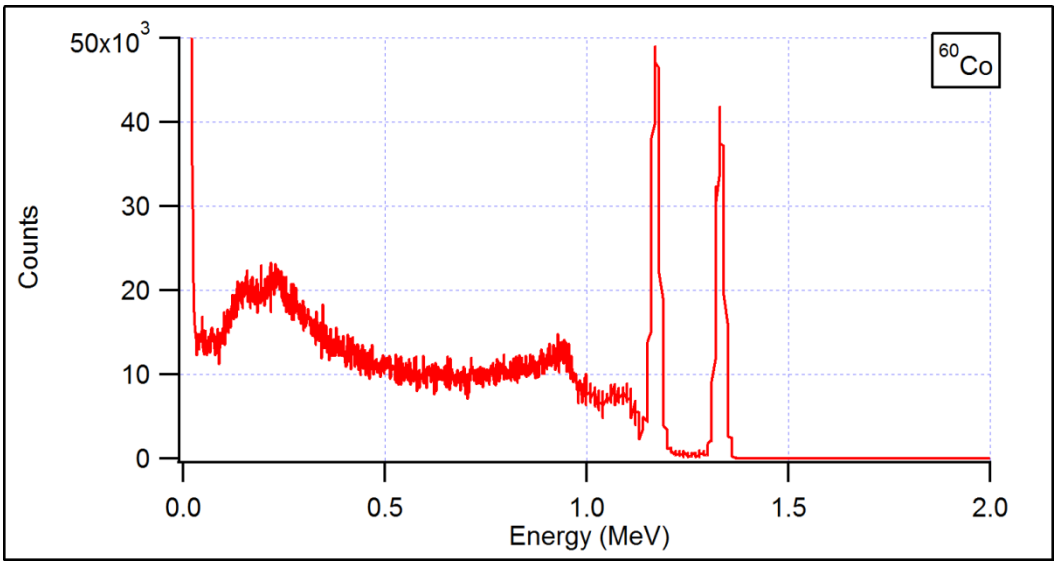

Figure 56. CLYC-7 response to ^{60}Co photon source

The response of the 2-inch-by-2-inch CLYC-7 scintillator to a PuBe and ^{252}Cf source was also analyzed in MCNP6. The resultant spectra are presented in Figure 57 and Figure 59, respectively.

Photons are created in secondary reactions within the PuBe. Photons are also created from neutron interactions with the surrounding environment with both the PuBe and ^{252}Cf sources. The spectrum created from the photons overwhelms the neutron energy spectrum of PuBe and ^{252}Cf. This is depicted in Figure 58 and Figure 60, respectively. With the ability of CLYC-7 to discriminate fast neutrons from photons, the photon spectrum can be removed revealing the fast neutron spectrum.

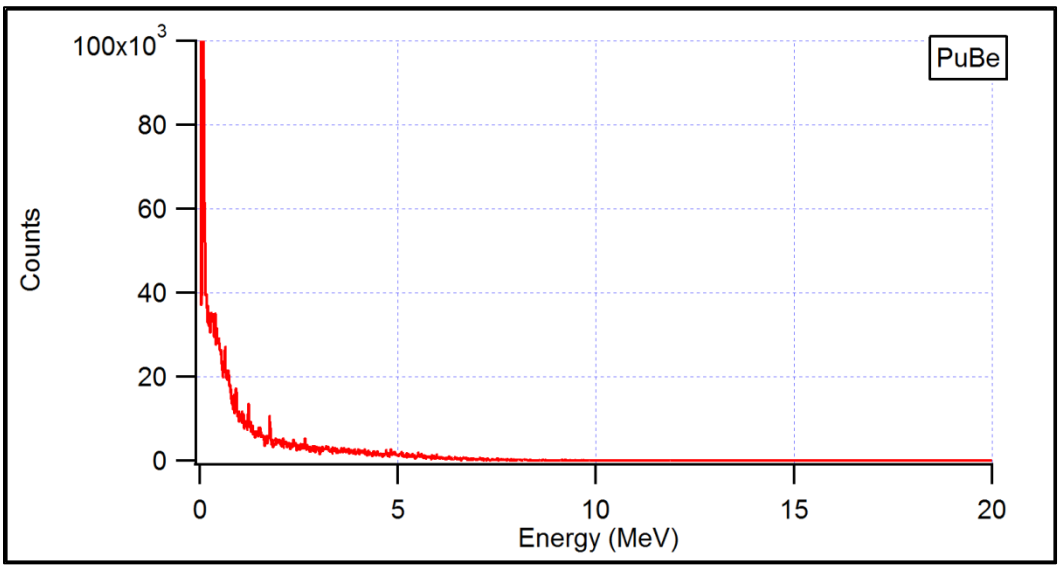

Figure 57. CLYC-7 response to PuBe source

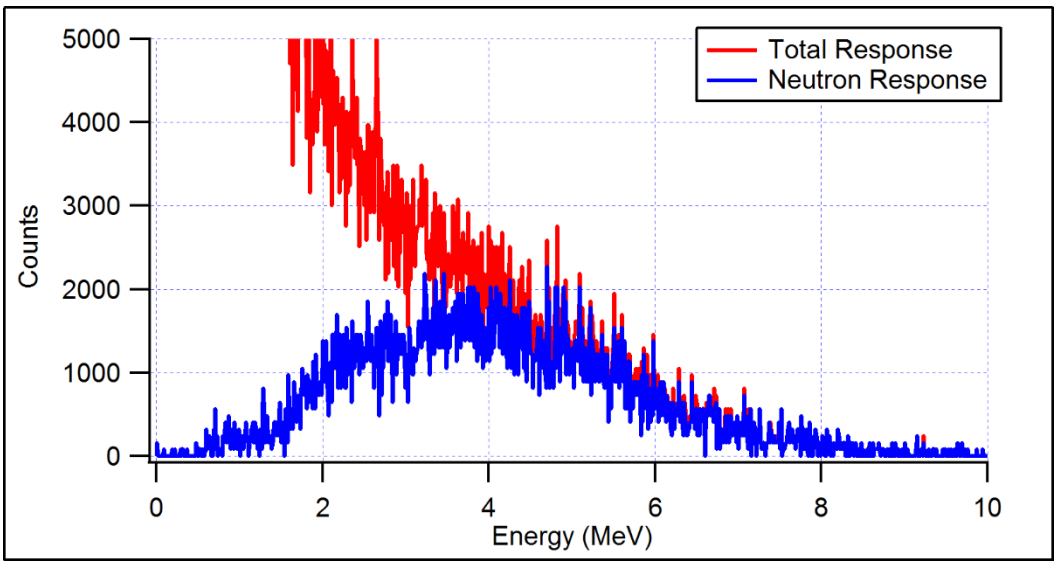

Figure 58. CLYC-7 response to PuBe source: photons and neutrons response versus fast neutrons response only

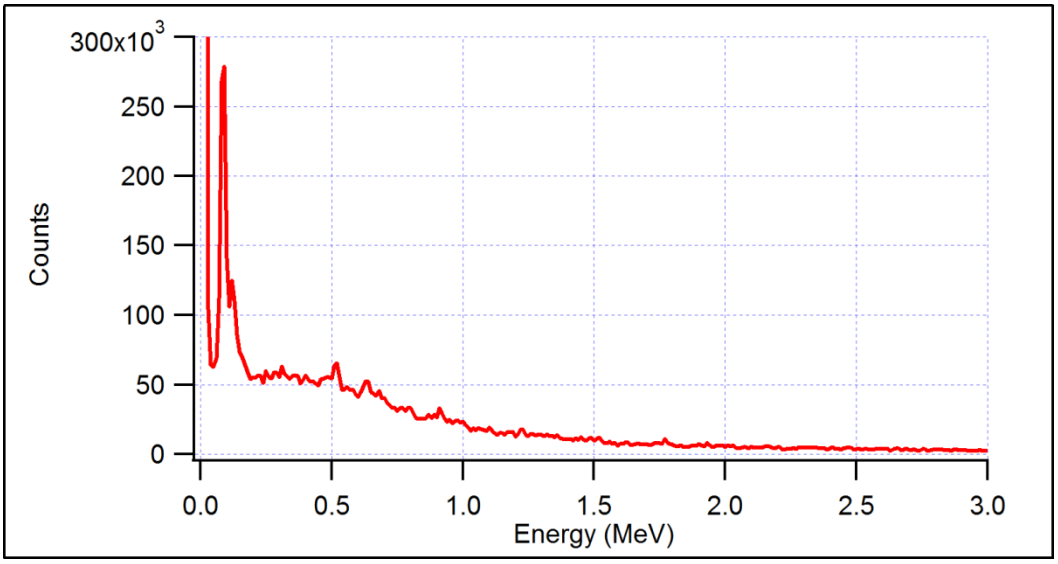

Figure 59. CLYC-7 response to ^{252}Cf source

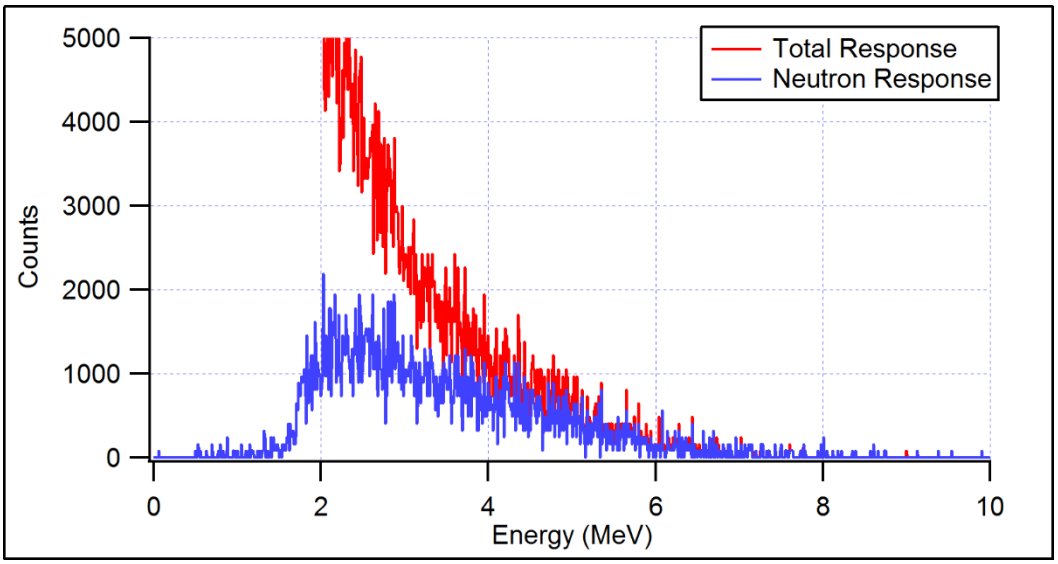

Figure 60. CLYC-7 response to ^{252}Cf source: neutron and photon response versus fast neutron response only

5.1.2.2 Nuclear Material Detector Response

The response of the 2 in-by-2 in CLYC-7 scintillator to various nuclear materials was also modeled in MCNP6. These materials included those which first responders may encounter in the field and are of interest to national security: RGPu, WGPu, NU, DU, LEU, and HEU. The resultant energy spectra for these materials are presented in Figure 61 and Figure 62. These spectra will be used in future research efforts for comparison to any field measurements of the same material with the 2 in-by-2 in CLYC-7 scintillator. These spectra will also contribute to the response library to enable future isotope identification.

The magnitude of both the RGPu and WGPu spectra are very similar. There are no characteristic photon peaks that appear in one spectrum and not the other. The fission neutron spectrum is lesser in magnitude than that of the photons and is difficult to observe.

In contrast to Pu, the varying enrichment of U does show a significant difference between spectra. It appears that as the enrichment of ^{235}U increases, the magnitude of the characteristic photon peaks decrease. This enables the identification of different enrichments of U. However, as with the Pu-based nuclear materials, the neutron spectra are lesser in magnitude than that of the photons and are difficult to observe in Figure 62.

There exist other means to identify the various enrichments of Pu and U discussed beyond the characteristic photon peaks that appear in the following figures. PSD enables the confirmation of the presence of neutrons. Also, the Pu and U sources modeled did not include daughter nuclides that would appear in both materials. Characteristic photon peaks from these daughter nuclides would also indicate the presence of Pu and U.

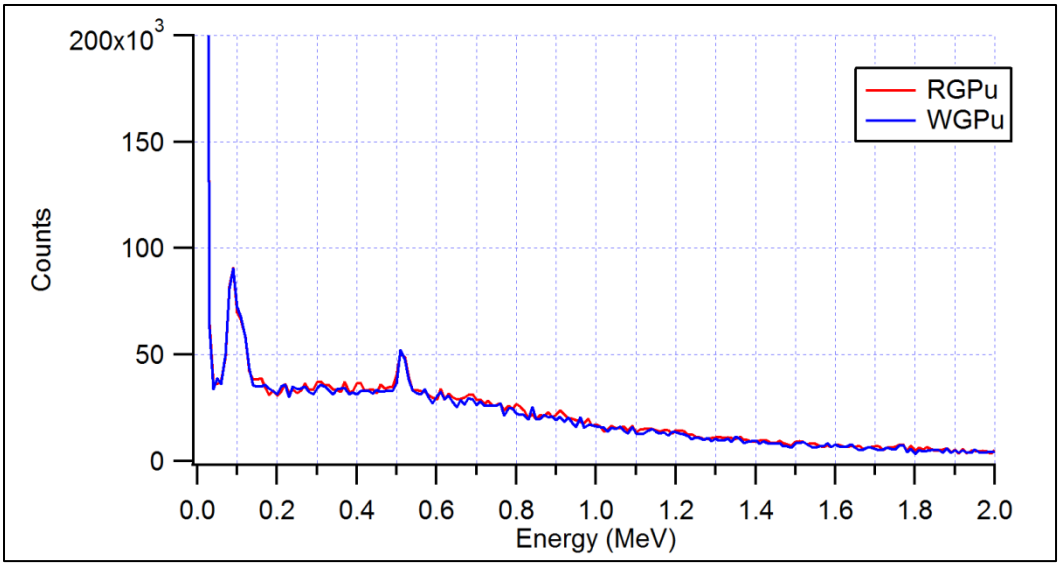

Figure 61. MCNP6-modeled CLYC-7 response to RGPu and WGPu

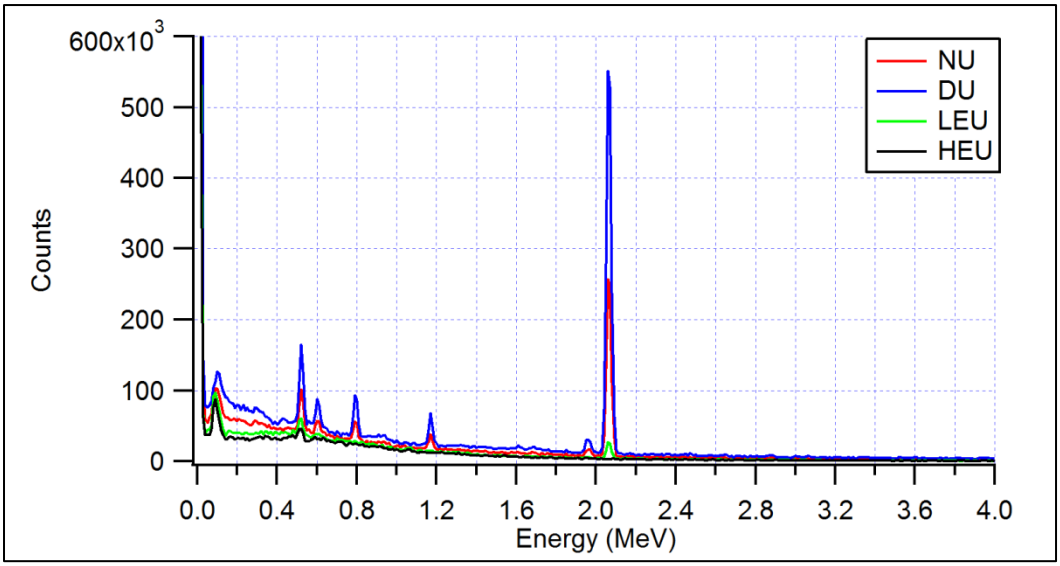

Figure 62. MCNP6-modeled CLYC-7 response to NU, DU, LEU, and HEU

5.2.1 Modeling of CLYC Collimated Detector

5.2.1.1 Collimator Optimization

Both the HDPE neutron collimator and the Pb photon collimator were modeled in MCNP6 to determine the optimal thickness to shield the CLYC-7 detector against neutrons and photons,

respectively. Both collimators were varied in thickness from 0 in to 5 in. A mono-energetic isotropic neutron source was placed 1 m away from the collimator face for the neutron case. A ^{137}Cs photon source was placed 1 m away from the collimator face for the photon case.

The results of the HDPE collimator study are presented in Figure 63. It is observed that as the thickness of the HDPE collimator increases, the neutron counts in the CLYC-7 scintillator decreases. The maximum shielding is achieved with a collimator thickness of 5 in. However, the neutron peak that appears in the energy spectrum for this case disappears into the background at approximately 3 in. So to minimize the size of the CDRDS while maintaining optimum shielding and therefore, image reconstruction, a HDPE collimator thickness of 3 in was selected for the design and development of the CDRDS.

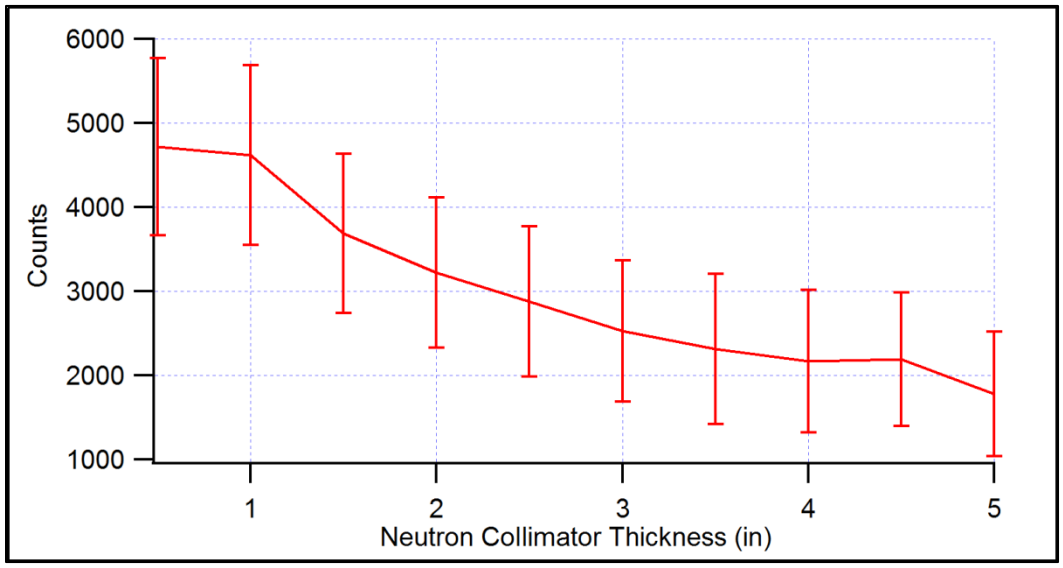

Figure 63. Neutron counts in CLYC-7 versus HDPE collimator thickness

The results of the Pb collimator study are presented in Figure 64. Similar to the neutron case, the photon counts in the CLYC-7 scintillator decrease with increasing Pb collimator thickness. The least amount of photon counts occur with a Pb collimator thickness of 5 in. However, and like the neutron case, the ^{137}Cs 662 keV energy peak disappears into the background of the energy

spectrum at approximately 3 in. Thus, a Pb collimator thickness of 3 in was selected for the design and development of the CDRDS so to minimize size while maintaining optimum shielding.

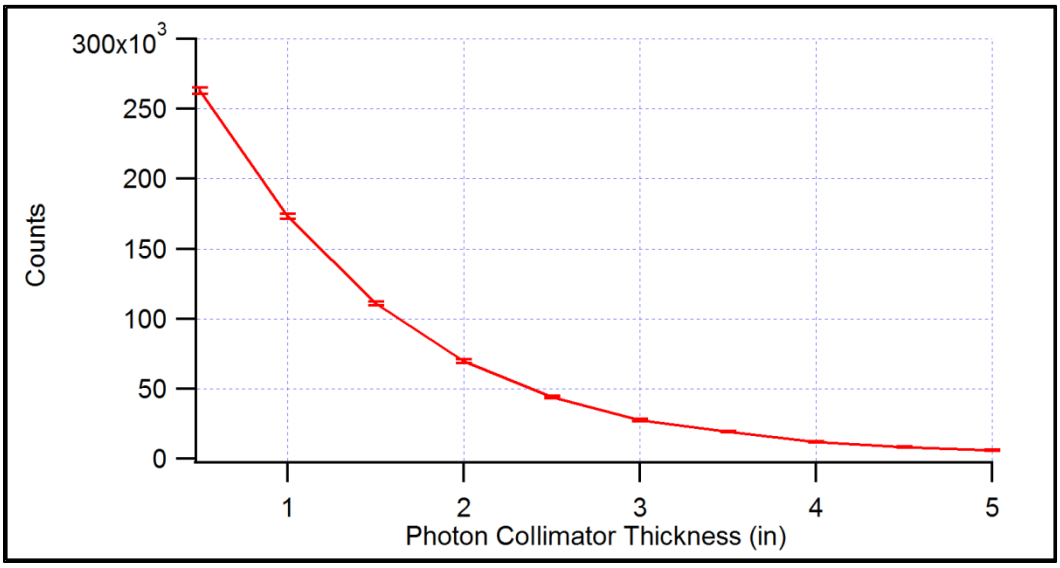

Figure 64. Photon counts in CLYC-7 versus Pb collimator thickness

5.2.1.2 Directional Response

The response of the CLYC-7 scintillator with both the HDPE and Pb collimators with coded aperture was studied in MCNP6 to determine the feasibility of the CDRDS collimator design and the functionality of the selected coded aperture. A HEU source was placed 2 m from the face of the collimator in-line with the center of the collimator. To simulate the rotation and the round shape of the collimator, the CLYC-7 scintillator and the HEU source were moved from one side of the model to the next in increments of 2.48 cm (the width of the aperture pixels).

The time-modulated (or angular) response of the CLYC-7 scintillator to the HEU source is presented in Figure 65. The higher-magnitude peaks are resultant of the sections of coded aperture in which there are more open pixels for neutrons or photons to travel through. These time-modulated results provide the time, or angle, at which a specific vertical column of pixels was closest to the measured source.

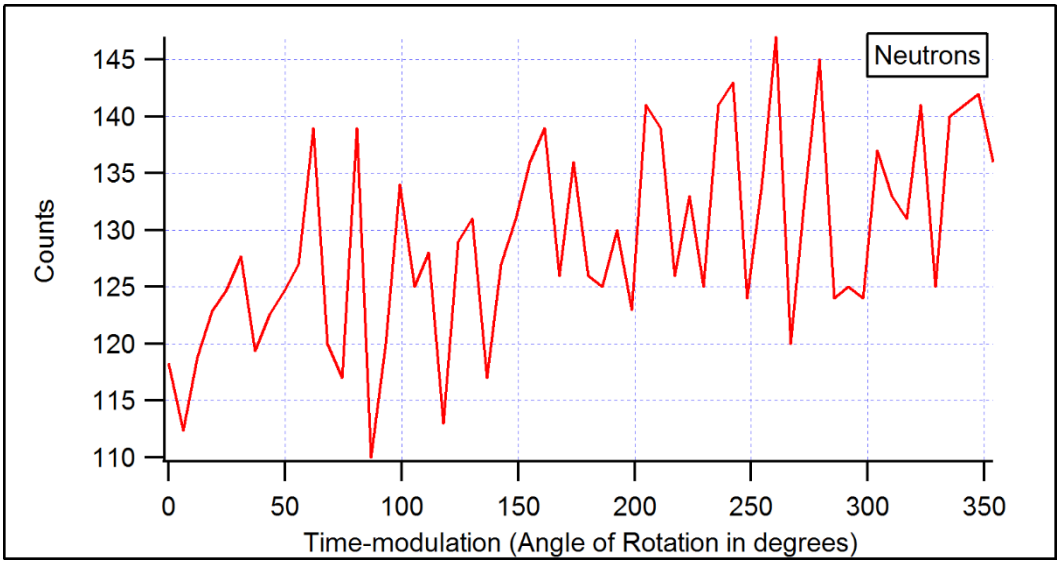

(a)

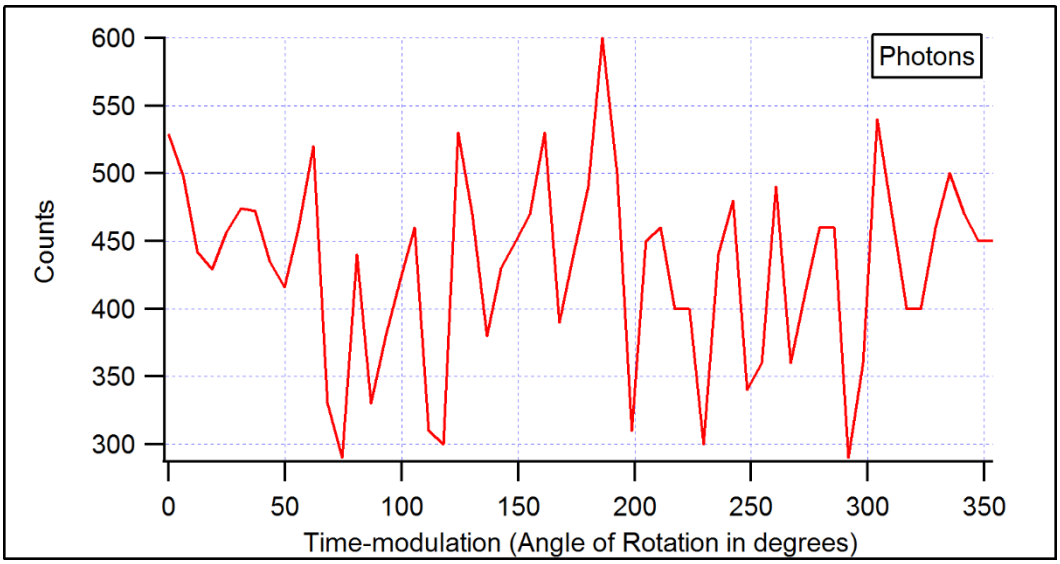

Figure 65. Time-modulated response of CLYC-7 to HEU source at x, y, z = (-70.6 m, -2.54 m, -203.81 m) for (a) neutrons (b) photons

After the time-modulated response was captured, the neutron and photon counts from each change in incremental rotation of the system were processed with the Matlab code to reconstruct the image of the measured source (see Appendix B). The resulting image is presented in Figure 66. The image of the HEU source appears at the far right side of the image which agrees with the

actual location of the source. The MLEM estimate for both the photon and neutron counts from the HEU appears only 1 cm higher and 3 cm to the right from where the actual source was located.

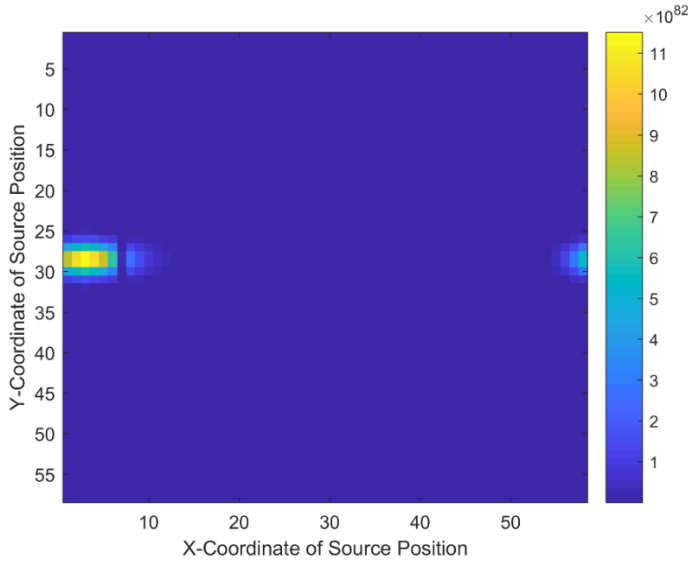

(a)

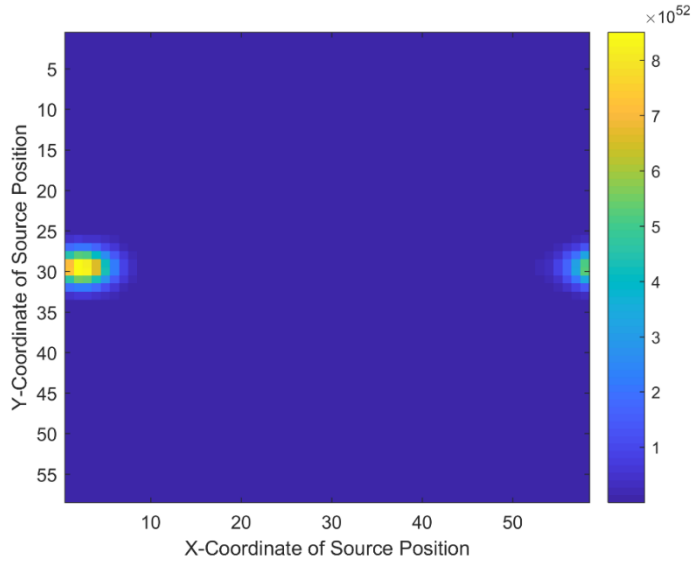

(b)

Figure 66. 2-D image of CLYC-7 response to directional measurement of HEU source at x, y, z = (-70.6 m, -2.54 m, -203.81 m) for (a) neutrons (b) photons

To determine if a correct image could be created for a source not in-line with the center of the collimator, the HEU source was moved upwards 10 cm, to the right 22.3 cm, and 179.8 cm closer to the collimator face. The respective MCNP6 neutron and photons counts were processed with the Matlab code and the image reconstruction was successful. The approximate 2-D location of the HEU source can be determined. The MLEM estimate for the HEU source location using both the photon and neutron estimates was only 3 coordinates higher and 5 coordinates further to the right than the actual position of the source. The resulting image is presented in Figure 67.

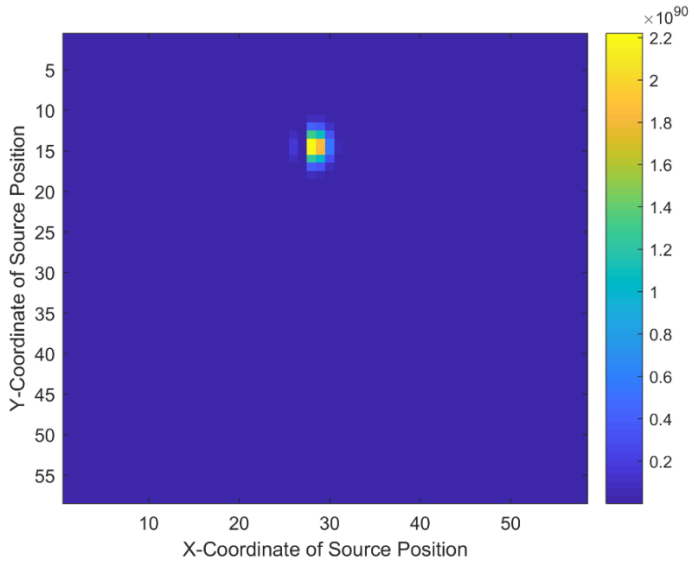

(a)

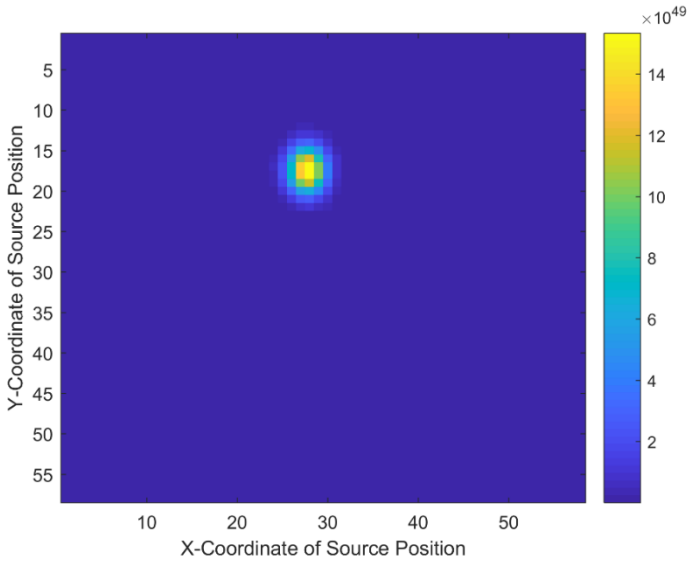

(b)

Figure 67. 2-D image of CLYC-7 response to directional measurement of HEU source at x, y, z = (-48.3 cm, 8.54 cm, -24 cm) for (a) neutrons (b) photons

5.3 Experimental Study

5.3.1 CLYC Characterization

5.3.1.1 Photon Measurements

Energy spectra were measured with the CLYC-7 scintillator for several photon sources at the UNLV Nuclear Engineering Laboratory. The energy resolutions of the respective characteristic photon peaks were determined by fitting each peak with a Gaussian. The counts under each peak (representing the total photon counts at that energy in the CLYC-7 scintillator) were also determined. The evaluated photon sources and measured data are presented in Table 3.

Table 3. Results of CLYC-7 photon measurements

Isotope	Activity	Characteristic Photon Energy	Energy Resolution	Total Counts under PhotoPeak
^{137}Cs	16 µCi	662 keV	6.440 %	230,027
^{60}Co	7 µCi	1.17 MeV	5.730 %	45,179
		1.33 MeV	4.968 %	34,073
^{133}Ba	14 µCi	81.0 keV	22.63 %	21,896
		303 keV	14.80 %	192,554
		356 keV	8.960 %	242,916

An energy resolution of 6.44 % was achieved with CLYC-7 for the ^{137}Cs characteristic photon peak at 662 keV. This energy resolution is better of that of NaI:Tl scintillators (approximately 7%) and is in agreement with those published for CLYC-7 [11]. However, the energy resolution of 4.968% was measured at the 1.33 MeV photon peak of ^{60}Co. Energy resolution improves with the increase in the incident photon energy as shown in Table 3.

The "Total Counts under Photopeak" values listed in Table 3 are utilized to determine the CLYC-7 intrinsic efficiency, ε_{int}, for detecting photons of various energies. The intrinsic efficiency detector provides a physical measure of how well the detector performs. The intrinsic efficiency is defined as follows:

$$\varepsilon_{int} = \frac{\#\ of\ photons\ in\ the\ photopeak}{\#\ of\ photons\ incident\ on\ the\ detector} \qquad \textbf{Equation 12}$$

The intrinsic efficiency is a function of the current source activity, the branching ratio of the emitted photon, the solid angle between the detector face and the source, and counts observed in the detector.

The intrinsic efficiency of the CLYC-7 photon response was calculated. The resultant efficiencies versus peak energy are shown in Figure 68. It is apparent that the detector efficiency decreases with increasing incident photon energy. At higher energies, photons are less likely to interact within the detector volume resulting in fewer registered counts. The resultant intrinsic efficiencies for the CLYC-7 response to photons are equal to if not better than NaI:Tl [39].

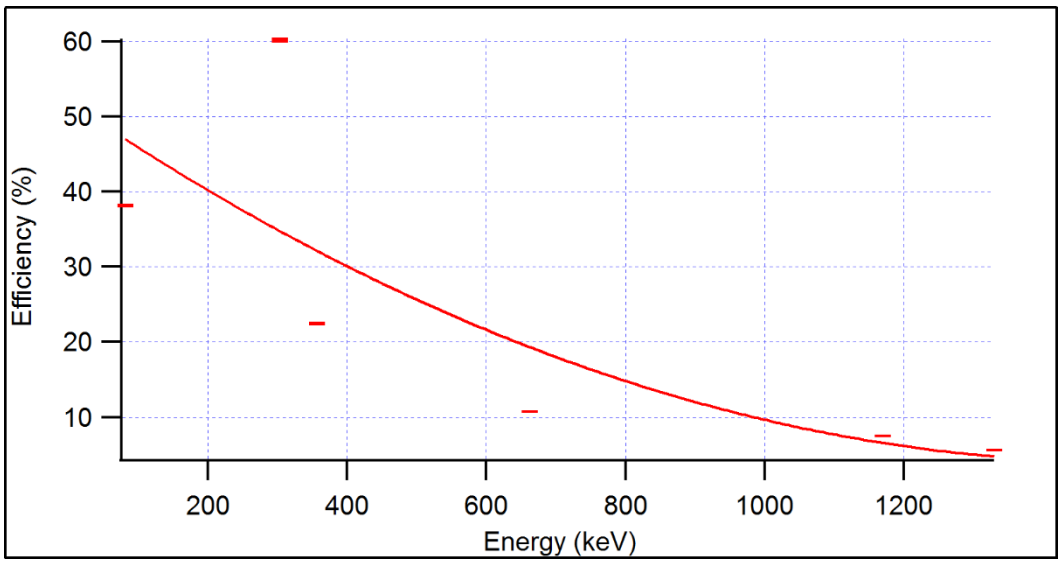

Figure 68. CLYC-7 intrinsic efficiency versus incident photon energy

5.3.1.2 Neutron Measurements

The response of the CLYC-7 scintillator to mono-energetic fast neutrons from UKy Van de Graaff Accelerator was investigated. Fast neutrons with incident energies from 0.205 MeV up to

20.2 MeV were measured. The measured detector responses over this range of energies are presented in Figure 69. Each different colored detector response in Figure 69 represents a different incident neutron energy. The dark blue detector response is from the lowest incident neutron energy and the light pink detector response is from the highest incident neutron energy. The resultant PSD plots at each incident neutron energy are shown in Figure 70.

Evaluating the resultant detector responses of Figure 69, a recognizable peak appears with an incident neutron energy of 0.474 MeV. This peak then continues to move to the right proportional to the incident neutron energy from 0.682 MeV to 2.869 MeV. At 3.211 MeV, a second peak begins to appear to the left of the first peak. This second peak also moves to the right proportional to the incident neutron energy from 3.211 MeV to 4.75 MeV. It is postulated that this second peak appears due to the occurrence of fast neutron interactions producing and alpha particle instead of a proton. At 5.095 MeV both peaks begin to fade into a continuum. However, the continuum continues to move to the right as the incident neutron energy increases up to 20.2 MeV.

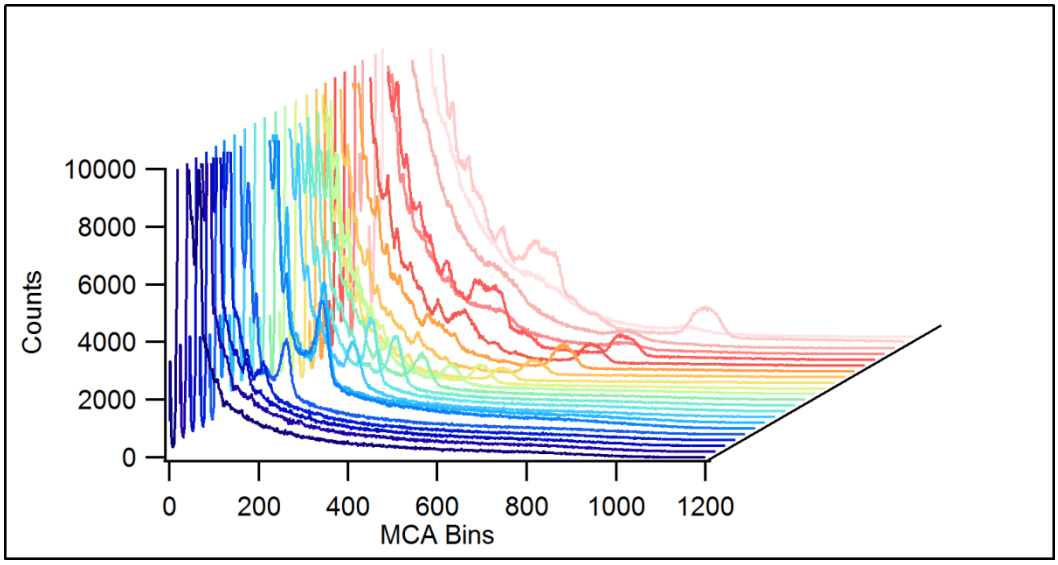

(a)

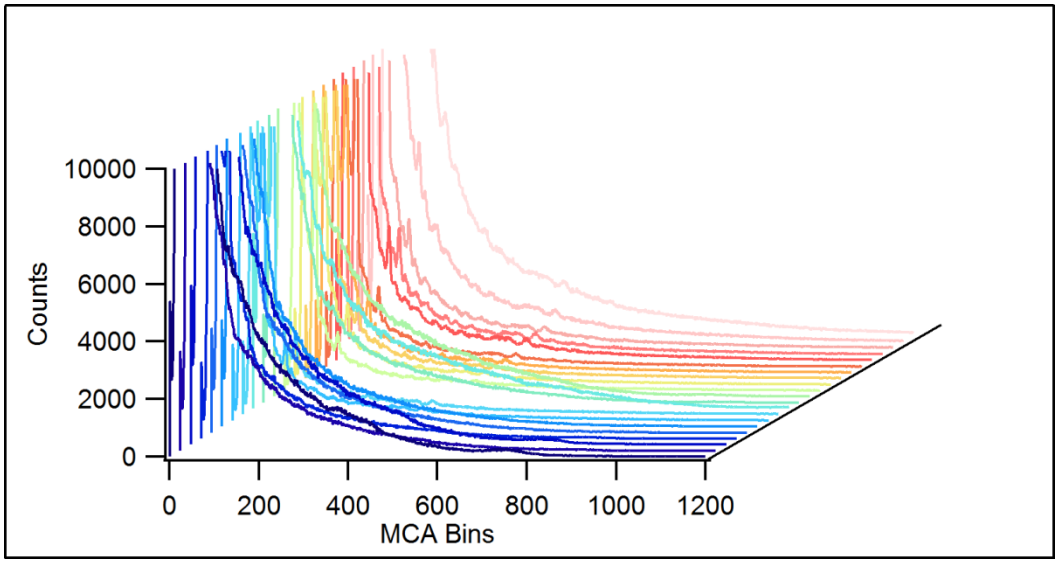

(b)

Figure 69. CLYC-7 responses for mono-energetic neutrons; from front to back (a) 0.205 to 5.10 MeV, (b) 5.82 to 20.2 MeV

The distinction between photons and fast neutrons is more readily recognizable by evaluating Figure 70. Between 0.205 MeV and 0.861 MeV, a neutron cloud appears at approximately 3.0 MeV. As this cloud disappears, a second neutron cloud appears at 0.474 MeV that moves to the

right proportionally with the incident neutron energy. This continues to approximately 4.42 MeV. This cloud begins to separate into two components at 3.211 MeV. These two neutron clouds begin to be overtaken and are less recognizable from 4.75 MeV to 8.62 MeV. Beyond 8.62 MeV, a single elongated cloud is observed for neutrons that is distinctly separated from the bottom photon cloud. Although the detected fast neutrons are not readily recognizable (i.e, a peak) in the energy spectra for incident neutrons with a high energy, fast neutrons are readily separated in the PSD plots.

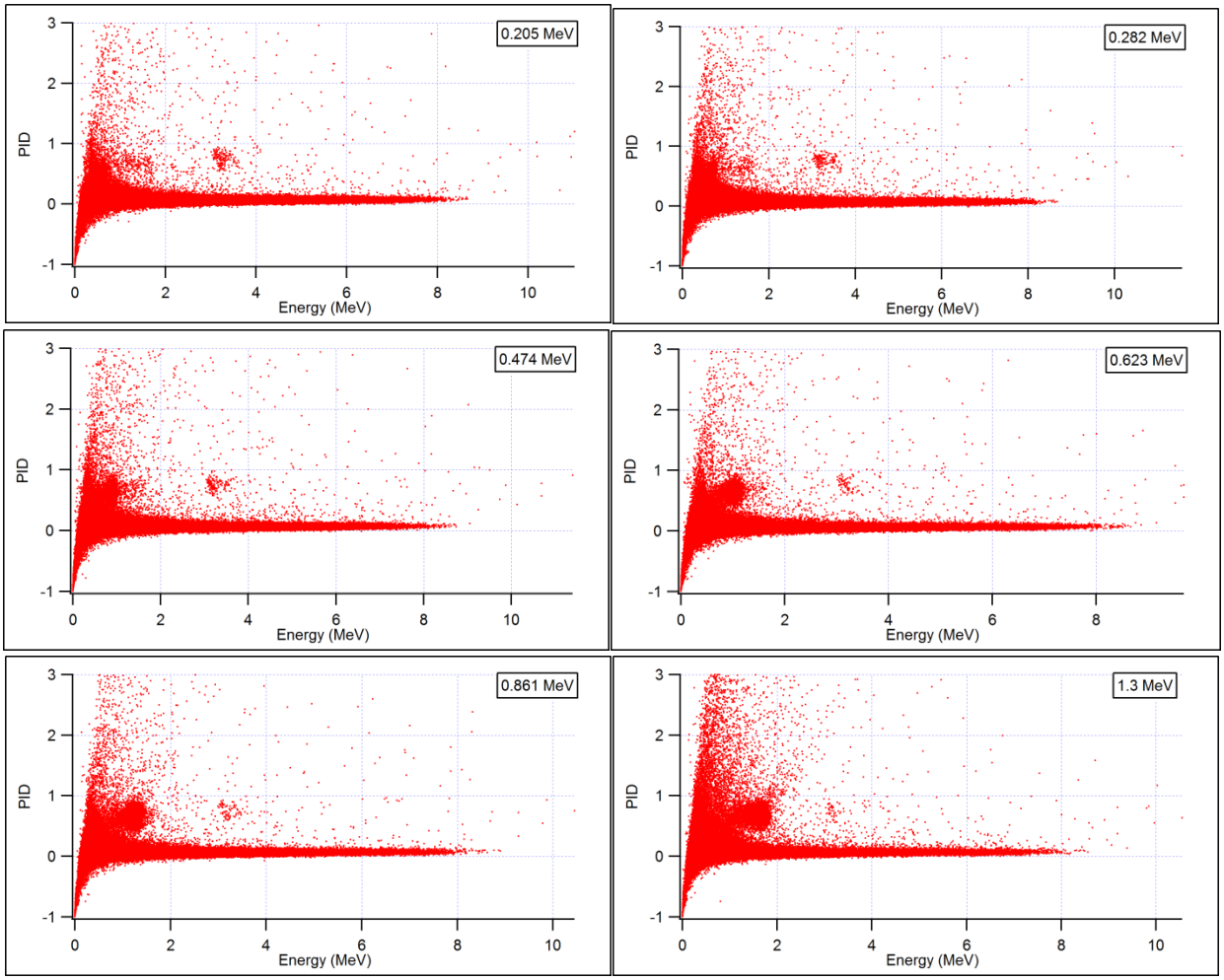

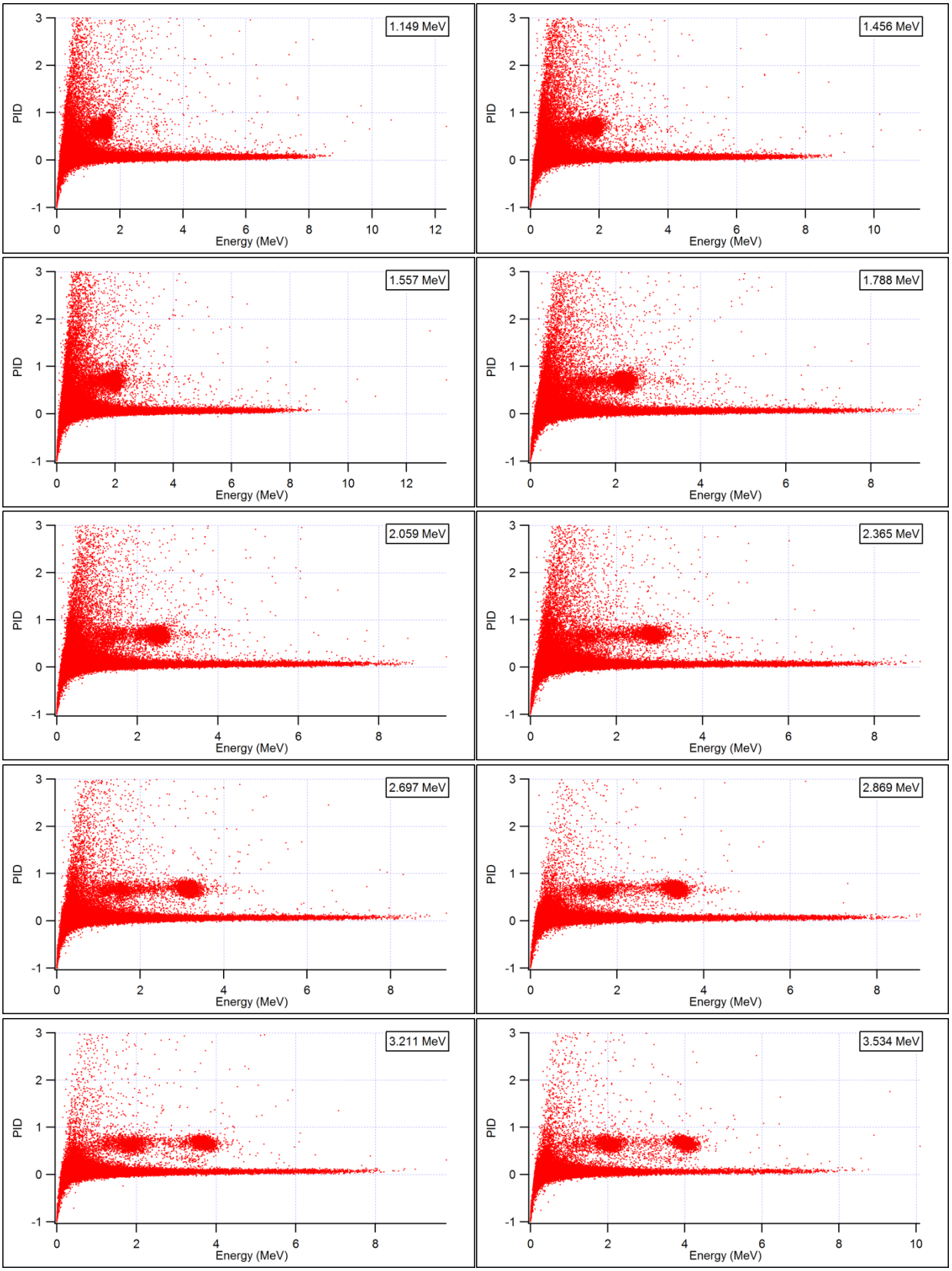
1.149 MeV
1.456 MeV
1.557 MeV
1.788 MeV
2.059 MeV
2.365 MeV
2.697 MeV
2.869 MeV
3.211 MeV
3.534 MeV
PID
Energy (MeV)

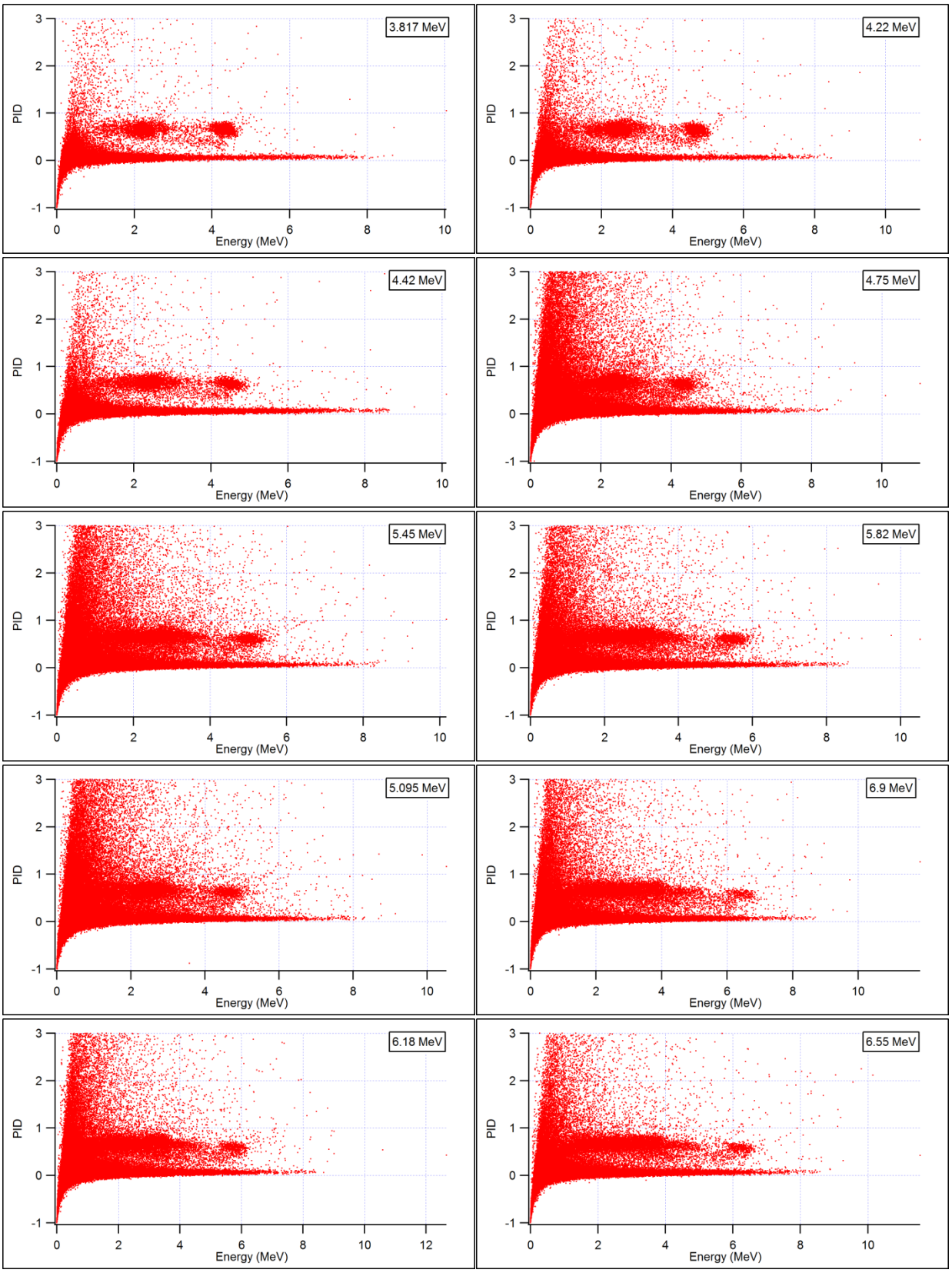
3.817 MeV
4.22 MeV
4.42 MeV
4.75 MeV
5.45 MeV
5.82 MeV
5.095 MeV
6.9 MeV
6.18 MeV
6.55 MeV
PID
Energy (MeV)

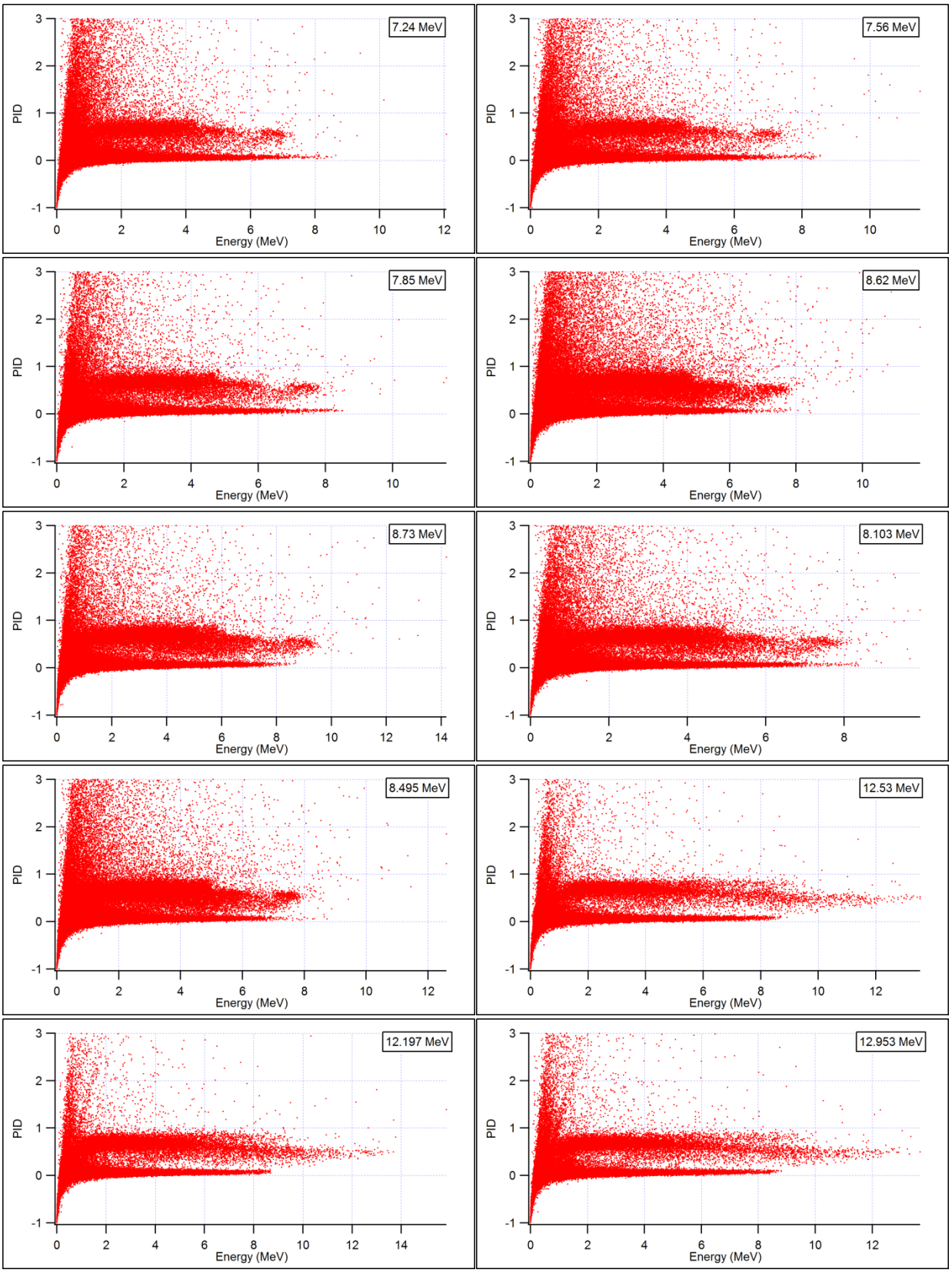
7.24 MeV
7.56 MeV
7.85 MeV
8.62 MeV
8.73 MeV
8.103 MeV
8.495 MeV
12.53 MeV
12.197 MeV
12.953 MeV
PID
Energy (MeV)

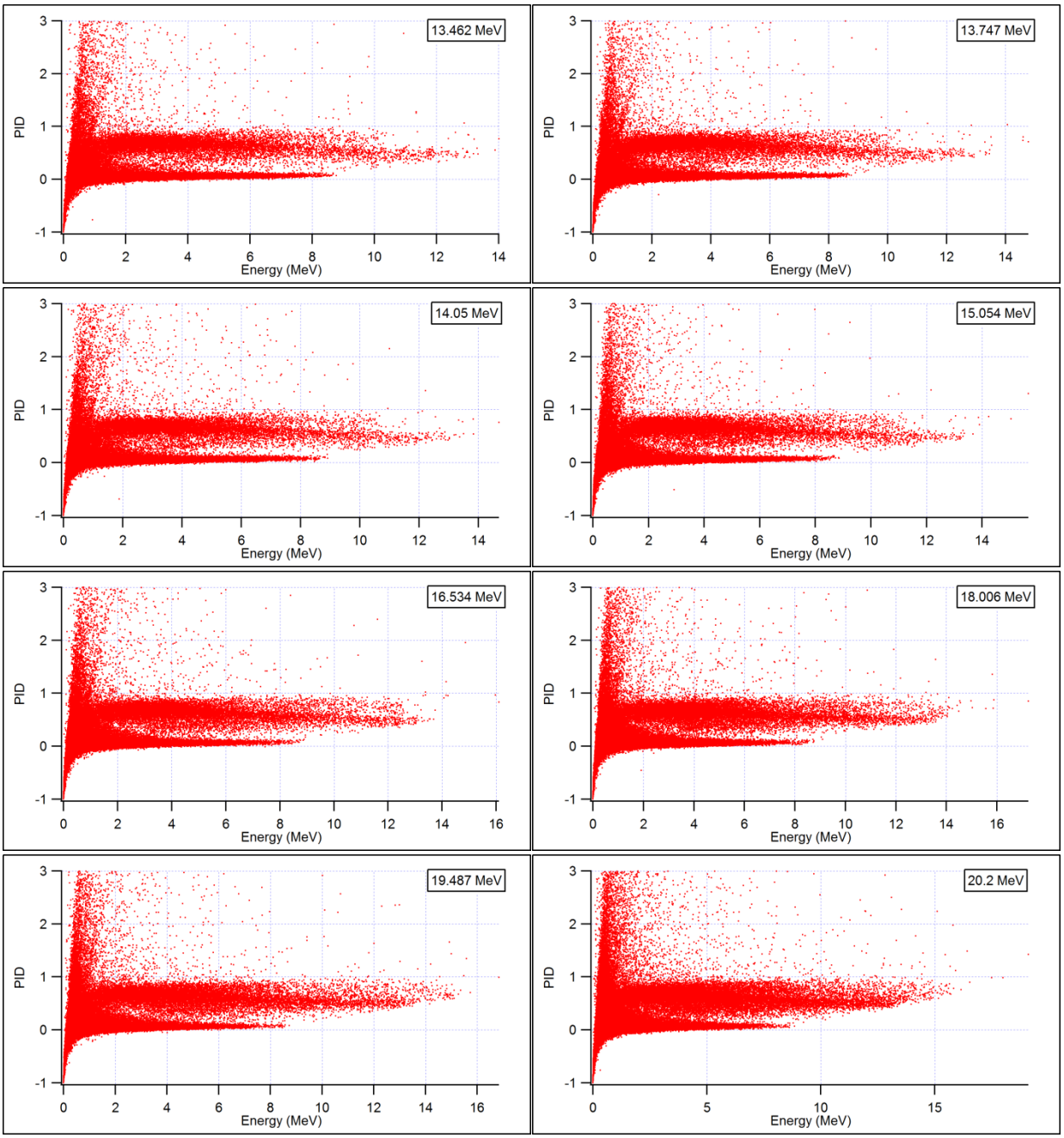

Figure 70. PSD plots of CLYC-7 responses to mono-energetic neutrons from 0.205 MeV to 20.2 MeV

In addition, the responses of CLYC-7 to neutrons from ^{252}Cf and PuBe sources were measured. ^{252}Cf and PuBe are not mono-energetic neutron sources. Thus, the responses appear as continuums. The detector response to neutrons and the PSD plot for the PuBe source is shown in Figure 71. A

small neutron cloud appears to the far left above the photon cloud in each plot. A less-dense, but longer, second neutron cloud appears above the photon cloud of the PuBe PSD plot. This elongated cloud indicates a distribution of neutron energies being measured.

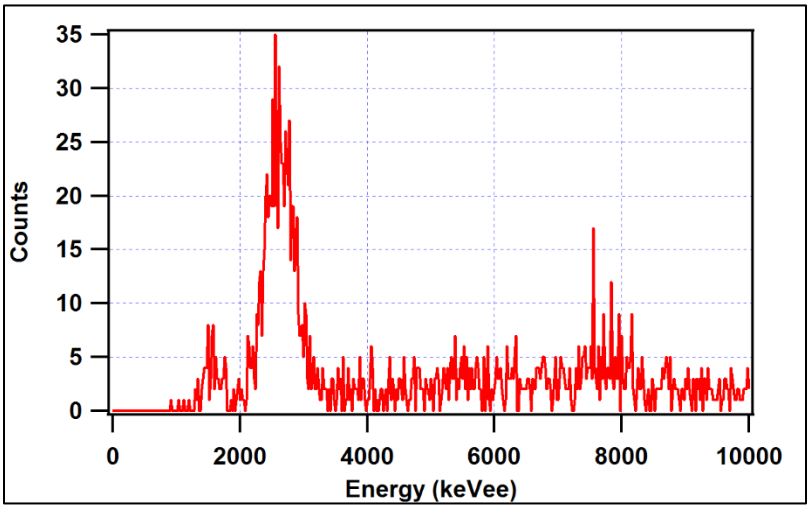

(a)

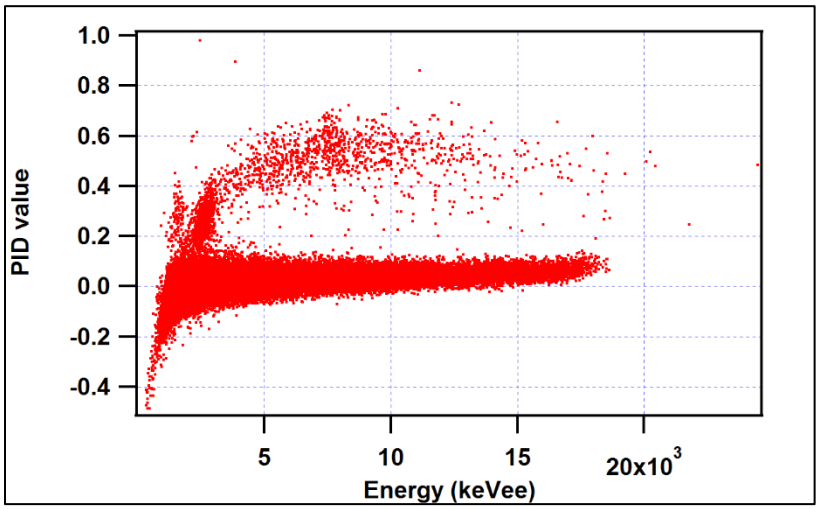

(b)

Figure 71. CLYC-7-measured (a) detector response to neutrons and (b) PSD plot for PuBe

5.3.2 CLYC Handheld Multimode Sensor

5.3.2.1 Laboratory Measurements

The MDS onboard the HMRS provides an easy to use interface to observe count rates, traces, and energy spectra of any measured source. This data was collected with the HMRS for the ^{137}Cs, ^{60}Co, ^{252}Cf, and PuBe sources at the UNLV Nuclear Engineering Laboratory.

Opening the MDS on the HMRS brings the user to the home screen as shown in Figure 72. Here there are four toggle buttons: parameters, count rates, histogram, and traces.

Selecting the "parameters" toggle button takes the user to the parameters screen as shown in Figure 73. The user is able to set the high voltage to the detector, the electronic and digital gain to adjust the compression of the measured spectra, signal threshold, integration time, and hold-off. The parameters shown in Figure 73 were those used for the CLYC-7 scintillator in the HMRS.

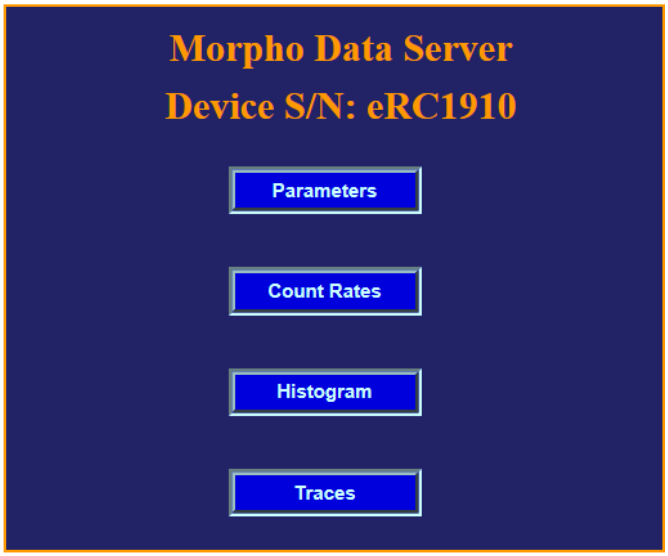

Figure 72. MDS home screen on HMRS

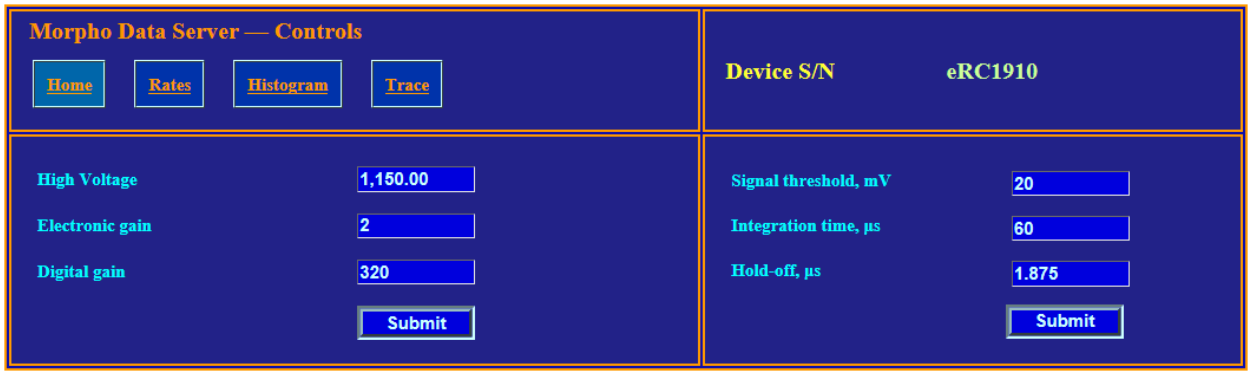

Figure 73. MDS parameter input screen on HMRS

Selecting the "count rates" toggle button allows the user to observe the count rate and various other count rate-related data as shown in Figure 74. This count rate, 996.26 counts per second (cps), was observed from measuring the ^{252}Cf source. Count rates were also collected for the PuBe, ^{137}Cs, and ^{60}Co sources as follows: 3,475.01, 846.79, and 960.56 cps.

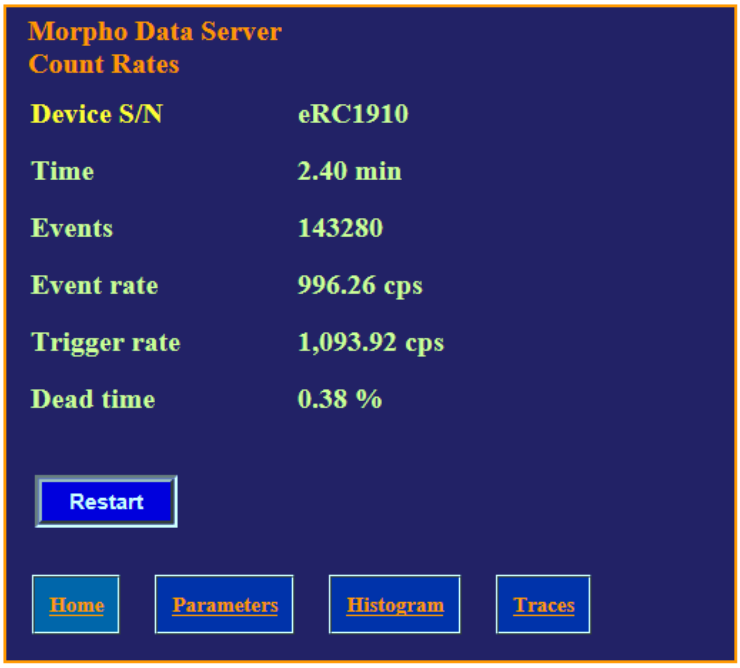

Figure 74. ^{252}Cf count rate collected with HMRS

Selecting the “traces” toggle button enables the user to view the measured traces contributing to the measure spectrum. Both a photon and a neutron traces observed while measuring the ^{252}Cf source are provided in Figure 75. Although not presented by the MDS, the units along the y-axis are arbitrary amplitudes and the units along the x-axis are analog-to-digital (ADC) bins. The photon trace on the left is larger in magnitude and has a faster decay than that of the neutron trace on the right. The ability to view these traces enables the user to confirm that either neutrons or photons, or both, are being detected.

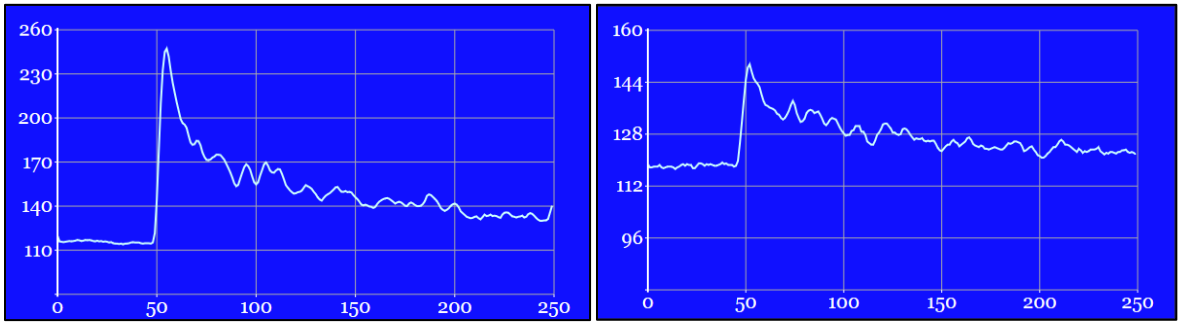

Figure 75. ^{252}Cf photon (left) and neutron (right) traces collected with HMRS

Selecting the “histogram” toggle button enables the user to observe the measured spectrum. Again, units are not provided in the produced plot, but the units along the y-axis are counts and the units along the x-axis are MCA bins. Spectra were collected with the HMRS for ^{252}Cf, PuBe, ^{137}Cs, ^{60}Co, and ^{137}Cs and ^{60}Co together. The detector responses are provided in Figure 76, Figure 77, Figure 78, Figure 79, and Figure 80, respectively.

Both the ^{252}Cf and PuBe detector responses appear as continuum with little or no characteristic peaks. In contrast, both the ^{137}Cs and ^{60}Co spectra yield their respective peaks with 662 keV for ^{137}Cs and 1.17 MeV and 1.33 MeV for ^{60}Co. When the ^{137}Cs and ^{60}Co sources are measured at the same time in the same location, all characteristics peaks from both isotopes are readily observable.

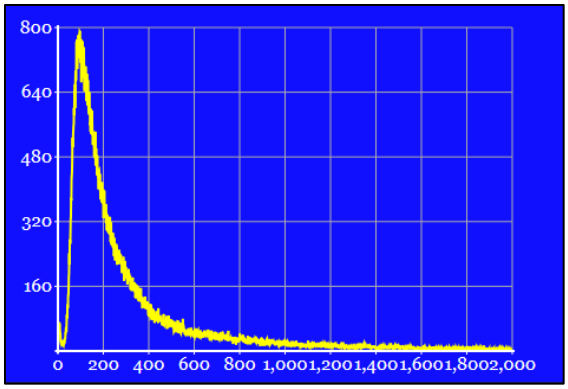

Figure 76. ^{252}Cf detector response collected with HMRS

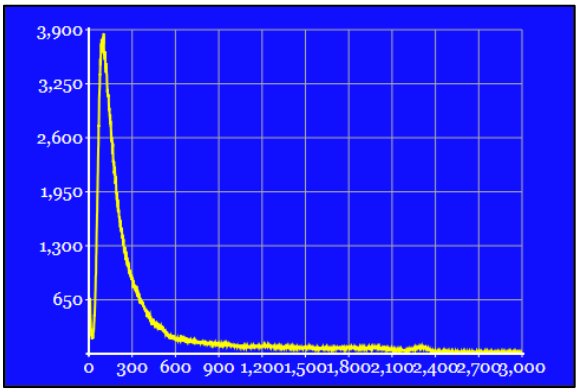

Figure 77. PuBe detector response collected with HMRS

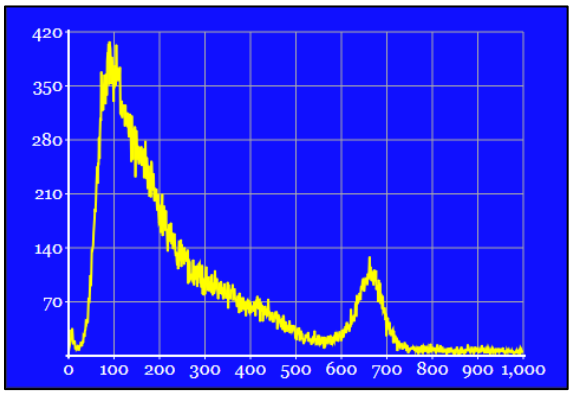

Figure 78. ^{137}Cs energy spectrum collected with HMRS

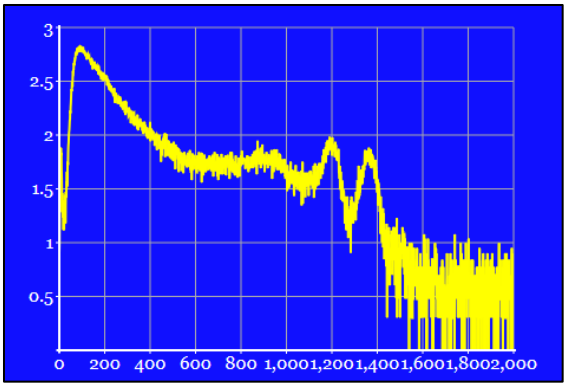

Figure 79. ^{60}Co energy spectrum collected with HMRS

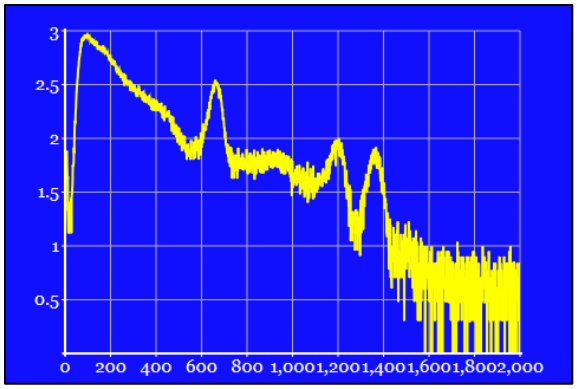

Figure 80. Combined ^{137}Cs and ^{60}Co energy spectrum collected with HMRS

5.3.3 CLYC Collimated Detector

5.3.3.1 Directional Measurements

All measurements of neutron sources collected with the CDRDS were post-processed utilizing the Neutron Separation Tool developed in Igor Pro. PSD list mode data acquired during the measurements was inputted into the Neutron Separation Tool to separate photon and neutron detector responses. Evaluating the integral of the neutron response yielded the neutron counts measured at each time step. Subtracting this value from the integral of the total response yielded the photon counts measured at each time step.

All measurements of photon sources collected with the CDRDS were processed in the eMorpho software in Igor Pro. A Gaussian fit was applied to the characteristic photopeaks that appeared in the measured spectra to determine the total number of photon counts measured at each time step.

The neutron and/or photon counts collected at each time step are stored in a vector for each different configuration and processed with the MLEM algorithm discussed previously and documented in Appendix B. Convergence of the MLEM algorithm yields an estimated image and 2-D location of the measured source. These estimates for Configuration #1 through #5 as described in Section 4.3.2 are described herein.

Measurements of Configuration #1 with the ^{252}Cf source at the 0° mark of the CDRDS were performed to test the functionality of the HDPE collimator on shielding neutrons where designed to. Additionally, the images produced from this neutron source with the HDPE collimator only and with the HDPE plus Pb collimator could be compared to identify any effects that the Pb collimator would have on incident neutrons.

The resulting image is provided in Figure 81. The center of the ^{252}Cf source image appears at (x,y) coordinates of (46, 31). The actual position of the source was at (0, 21). The estimated source position is fairly close to the actual source position with a difference of 12 coordinates in the x-direction and 10 coordinates in the y-direction. It should be noted that low neutrons counts (i.e., 40 to 50 neutrons per time step) were observed for the measurements of Configuration #1. The measured ^{252}Cf source has already decayed several half-lives and thus emits a relatively smaller amount of neutrons than when it was manufactured. These lower neutron counts have an effect on the accuracy of the MLEM-predicted image as can be observed from the significant difference between the estimated source position and the actual source position.

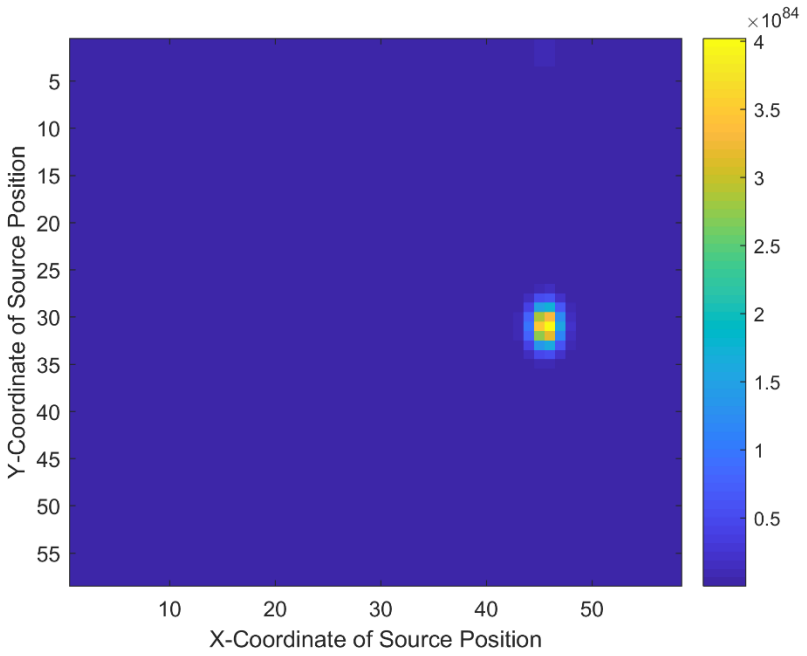

Figure 81. MLEM reconstruction of ^{252}Cf image with HDPE collimator only (200 iterations)

The measurements of Configuration #2 were collected so to determine any effect that the HDPE may have on shielding photons. Although, HDPE is a low-Z (low atomic number), it is capable of scattering photons.

As observed in Figure 82, the HDPE does attenuate photons, but it does not result in the correct imaging of the ^{137}Cs and ^{60}Co sources in the spatial map. There do exist fluctuations in the time-modulated response collected over 360° rotation of the CDRDS, otherwise an image could not be produced. However, these modulations are not different enough to correctly estimate the source positions.

The resultant image does predict that the two sources are in line with one another, but in the incorrect orientation and position. The actual position of the ^{137}Cs and ^{60}Co sources was (28, 10) and (53, 10), respectively. This is a difference of 11 coordinates in the x-direction and 11

coordinates in the y-direction for ^{137}Cs and 17 coordinates in the x-direction and 11 coordinates in the y-direction for ^{60}Co between the estimated source positions and the actual source positions. Based on these results, to successfully image both neutrons and photons, a heterogenous collimator of a low-Z (HDPE) and high-Z (Pb) material is required.

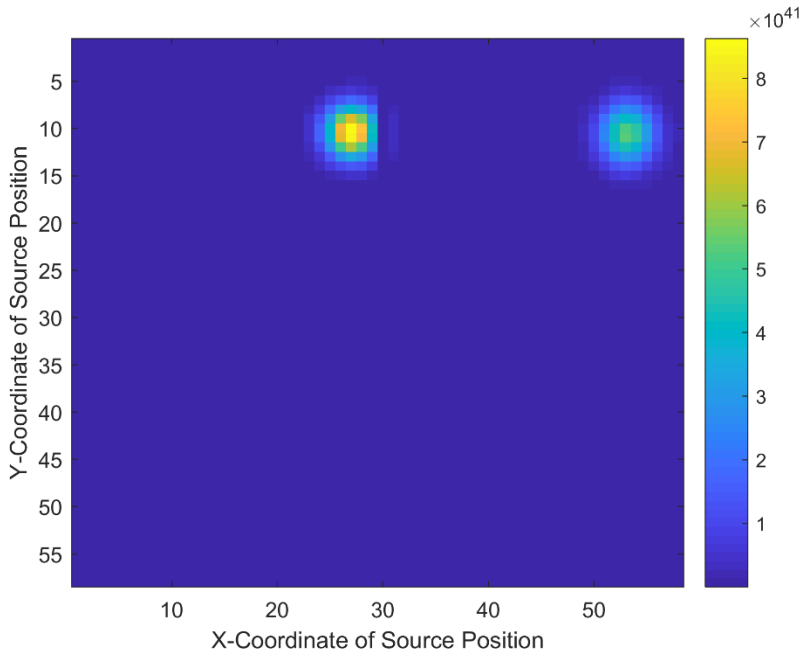

Figure 82. MLEM reconstruction of ^{137}Cs and ^{60}Co image with HDPE collimator only (200 iterations)

For Configuration #3, the Pb collimator was added to the HDPE collimator to enable better imaging of photons. The results were successful for both near field (29 cm) and far field (1 m) measurements. As observed in Figure 83 (a) and (b), both the ^{137}Cs and ^{60}Co sources are imaged in close proximity to their actual positions.

Recall that the ^{137}Cs source was placed at a 30° angle in reference to the 0° mark on the CDRDS at a height of 31 cm above the ground corresponding to an (x, y) coordinate of (5, 36). The ^{60}Co

source was placed at a 60° angle in reference to the 0° mark on the CDRDS at a height of 46 cm above the ground. This corresponds to an (x, y) coordinate of (10, 5). For near field measurements, the estimated source position of the ^{137}Cs and ^{60}Co sources respectively were (5, 37) and (11, 5). This is a difference of 1 bin in the y-direction for ^{137}Cs and 1 bin in the x-direction for ^{60}Co from the actual source positions. For far field measurements, the estimated source position of the ^{137}Cs and ^{60}Co sources respectively were (5, 38) and (10, 5). This is a difference of 1 bin in the y-direction for ^{137}Cs from the actual source position. There was no difference between the estimated and actual source positions for ^{60}Co.

The far field measurements achieve a smaller error in source position estimate. This is largely due to the fact that at larger distances from the CDRDS, the source appears more like a point rather than a distribution. The MURA coded aperture pattern of the CDRDS is better suited for point-like sources [30].

It is evidenced from the images presented in Figure 83 that the addition of the Pb collimator enables successful photon imaging. The standalone success of the HDPE collimator at shielding neutrons and the Pb collimator shielding photons makes possible the simultaneous imaging of both photons and neutrons from measured source.

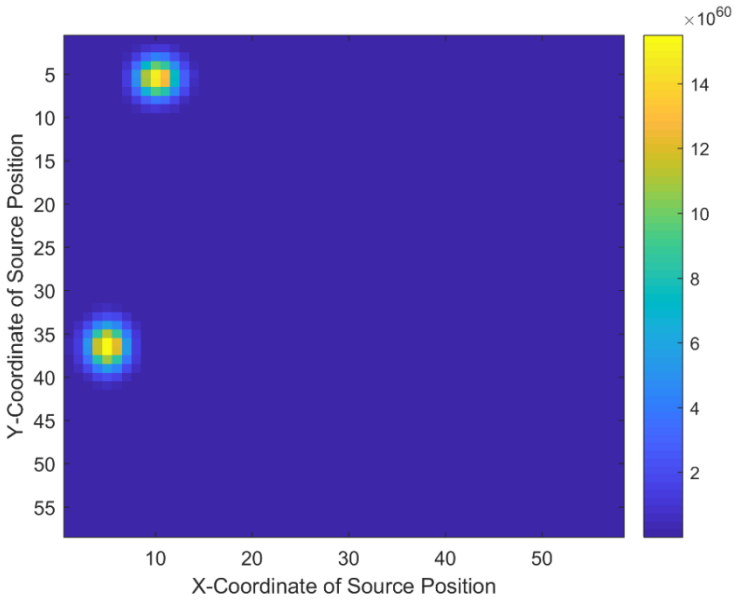

(a)

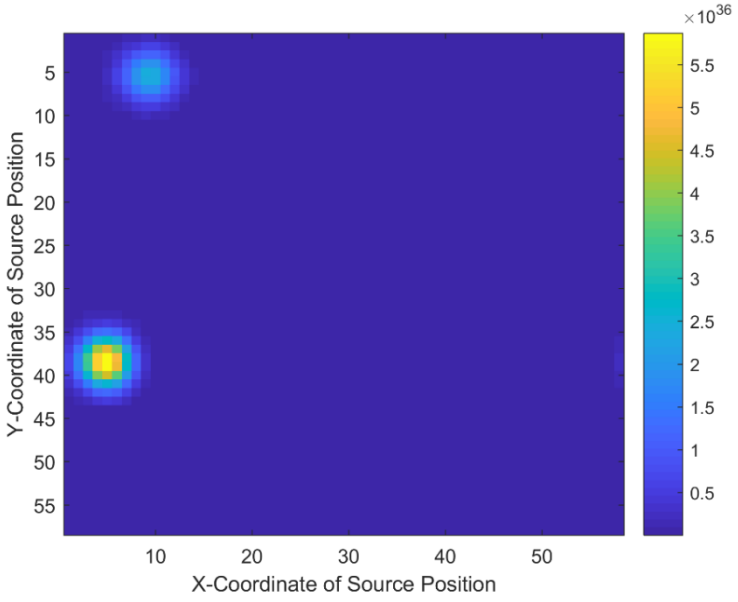

(b)

Figure 83. MLEM reconstruction of ^{137}Cs and ^{60}Co image with HDPE plus Pb collimator (200 iterations)

The measurements of the ^{252}Cf source were repeated with the HDPE plus Pb collimator to determine if any effect would be made on the resultant image by adding Pb to the CDRDS. However, very little effect was observed. As shown in Figure 84, the ^{252}Cf source was imaged to almost the same position as with the measurements with the HDPE collimator only.

The estimated source position of the ^{252}Cf with the HDPE plus Pb collimator measurements was (57, 22). This is in relatively good agreement with the estimated source position with the HDPE collimator only of (6, 28) which demonstrates repeatability. However, this second source position estimate is even closer to the actual source position with only a difference of 2 bins in the x-direction. Although the estimated source position is closer to the actual source position, it can be concluded that the addition of the Pb mask to the collimator has little effect on the shielding of neutrons.

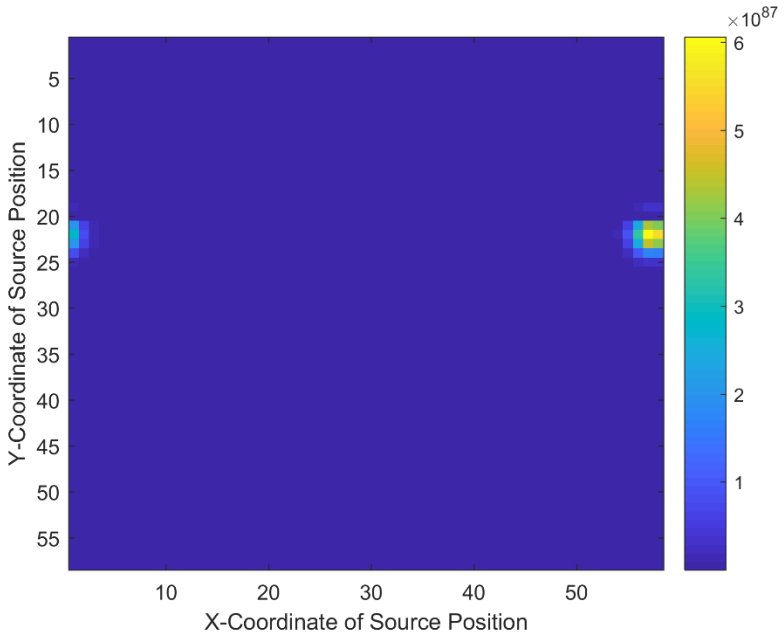

Figure 84. MLEM reconstruction of ^{252}Cf image with HDPE plus Pb collimator (200 iterations)

For Configuration #5, the PuBe source was removed from the 55 gallon drum and thus, its surrounding poly shielding. The CDRDS with both HDPE and Pb masks was used. Recall that the PuBe source was placed at 180° from the 0° marker on the CDRDS. The PuBe source was 40 cm above the ground and 50 cm from the collimator face. This position in spatial coordinates is (30, 17). The estimated source position based on the time-modulation of neutrons was (32, 22) and is shown in Figure 85 (a). This is only a difference of 2 coordinates in the x-direction and 5 coordinates in the y-direction. The estimated source position based on the time-modulation of photons measured from the same PuBe source was (30, 21) and is shown in Figure 85 (b). Not only is the photon-based MLEM estimate very close to the actual source position, it agrees well with the neutron-based MLEM estimate. This is expected since the neutrons and photons are emitted from the same PuBe source at the same location.

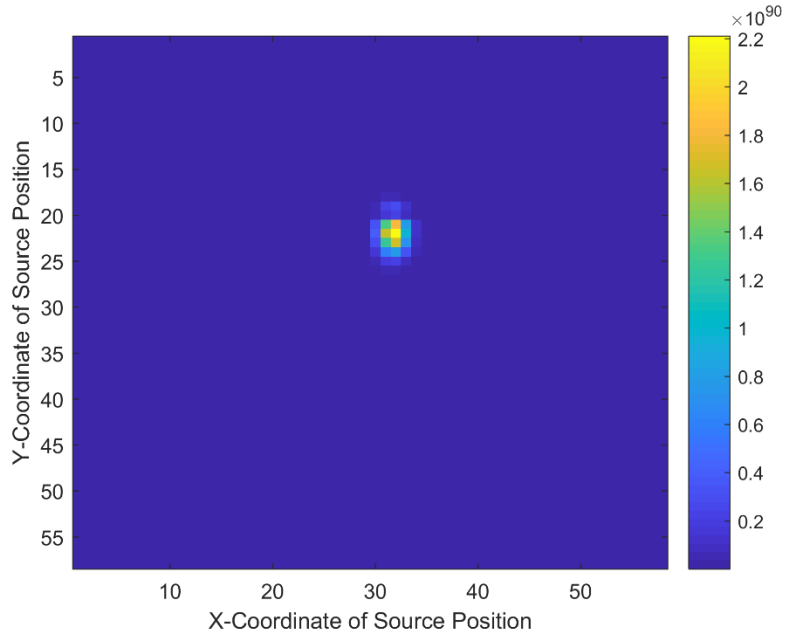

(a)

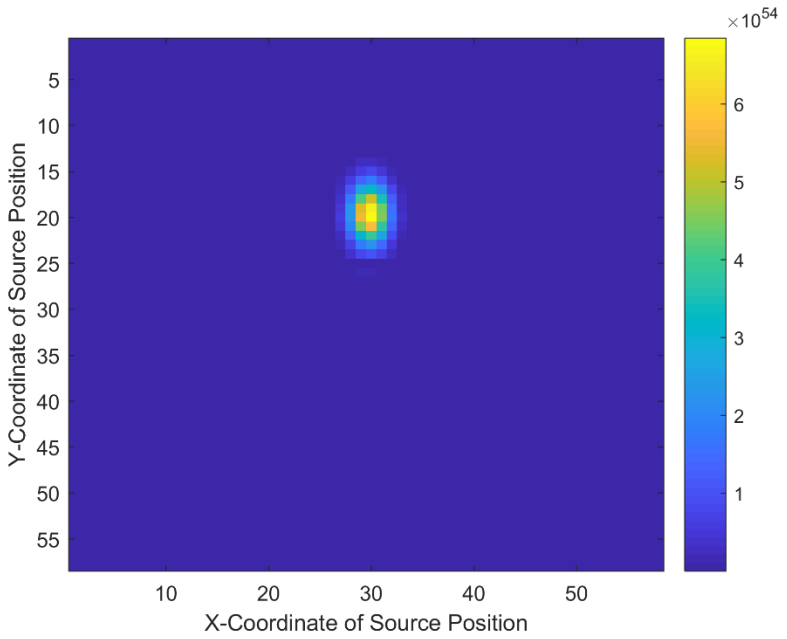

Figure 85. MLEM reconstruction of PuBe at (30,17) based on (a) neutrons and (b) photons (200 iterations)

The PuBe source was then moved down to only 30 cm above the ground and remained 50 cm from the collimator face. This position in spatial coordinates is (30, 38). The estimated source position based on the time-modulation of neutrons was (29, 38) and is shown in Figure 86 (a). This is only a difference of 1 coordinate in the x-direction. The estimated source position based on the time-modulation of photons measured from the same PuBe source was (29, 35) and is shown in Figure 86Figure 85 (b). This is only a difference of 1 coordinate in the x-direction and 3 coordinates in the y-direction. The photon-based MLEM estimates once again agree well with the neutron-based MLEM estimate as expected.

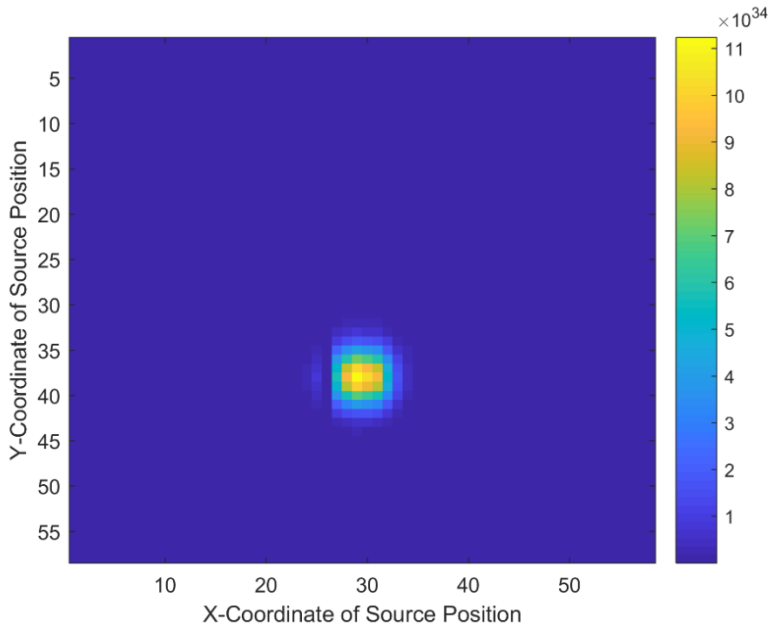

(a)

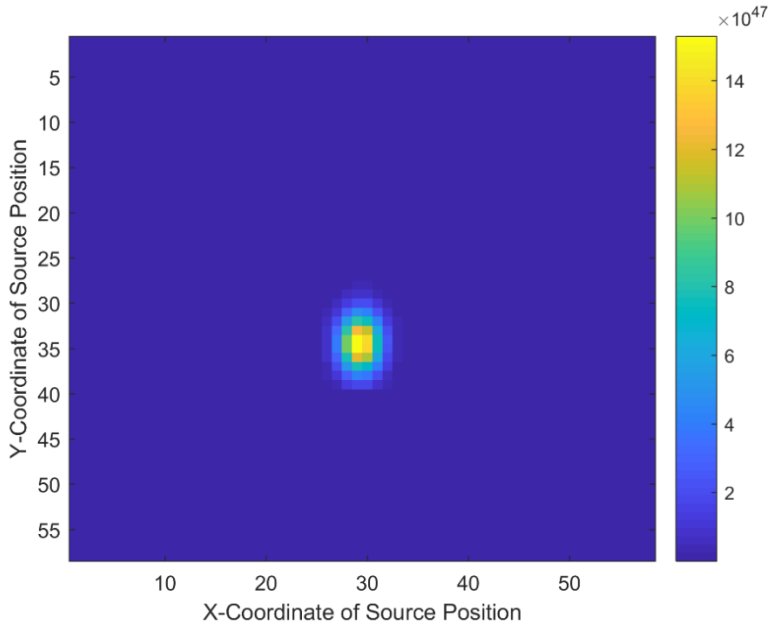

(b)

Figure 86. MLEM reconstruction of PuBe at (30, 38) based on (a) neutrons and (b) photons (200 iterations)

The PuBe source was then moved 1 m away from the face of the CDRDS collimator. It was also moved to 304° from the 0° marker on the CDRDS. It remained at 30 cm above the ground. This position in spatial coordinates is (49, 38). The estimated source position based on the time-modulation of neutrons was (48, 37) and is shown in Figure 87 (a). This is only a difference of 1 coordinate in the x-direction and 2 coordinates in the y-direction. The estimated source position based on the time-modulation of photons measured from the same PuBe source was (51, 42) and is shown in Figure 87 (b). This is only a difference of 2 coordinates in the x-direction and 4 coordinates in the y-direction. The photon-based MLEM estimates again agree well with the neutron-based MLEM estimate as expected.

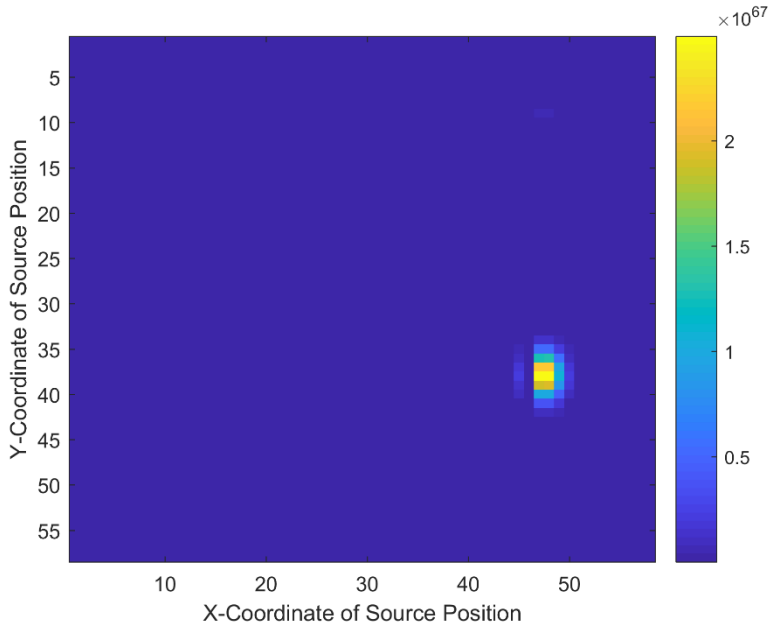

(a)

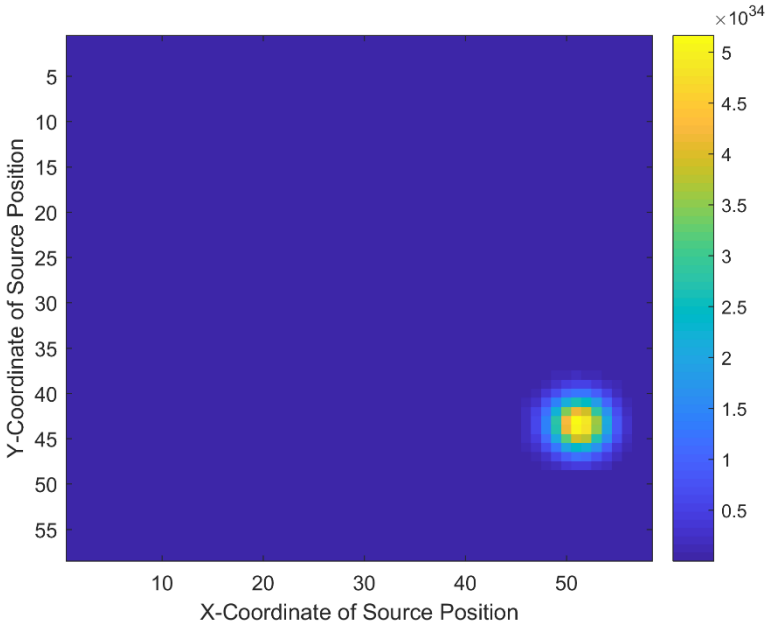

(b)

Figure 87. MLEM reconstruction of PuBe at (30, 38) and 1 m out from the collimator face based on (a) neutrons and (b) photons (200 iterations)

CHAPTER 6

CONCLUSIONS AND FUTURE WORK

The responses to neutrons and photons of the 2 inch-by-2 inch CLYC-7 scintillator used in this study were fully characterized. These responses were evaluated both computationally and experimentally. The computational results provided insight into what to expect during the experimental measurements and a comparison to the experimental results. All computational responses closely reflected the experimentally determined responses to both photons and neutrons. Experimentally, the photon efficiency of the 2 inch-by-2 inch CLYC-7 scintillator was determined over a range of photon energies. Also, the photopeak energy resolution at 662 keV was evaluated to be 6.4%. The response to mono-energetic neutrons produced from the Van de Graaff accelerator was also investigated. Fast neutrons from 0.205 MeV up to 20.2 MeV were measured. It was determined from those measurements that the CLYC-7 scintillator can be applied as a fast neutron spectrometer yielding distinguishable peaks in the neutron spectra from approximately 0.474 MeV to 4.75 MeV. The CLYC-7 scintillator response to mon-energetic neutron sources was also investigated. Signature detector responses for both PuBe and ^{252}Cf were observed.

In future work, the computational and experimental responses of the CLYC-7 scintillator to the various sources investigated in this study can be stored in a library to be used as a part of on-board software to identify measured sources both with the HMRS and the CDRDS. Additional responses to other sources can be simulated or measured to extend this library in the future.

Two applications of the elpasolite scintillator CLYC-7 were designed, developed, and tested. The first, the HMRS, was designed to be end-user friendly and developed using off-the-shelf components. The HMRS is lightweight and easy to hold. The software, MDS, utilized by the HMRS is straight-forward and easy to use. The HMRS was evaluated computationally and tested

experimentally. It proved to be a effecient photon and fast neutron spectrometer and a count rate meter.

Future improvements to the HMRS would include integration of a larger touch screen to allow the end-user to better see and interface with the MDS. Additional access ports on the HMRS housing should be added to allow for easier access to internal components for insertion and removal. Once these modifications have been made to optimize the HMRS, it can be deployed for field testing to ensure that measurements made in the lab are repeatable in the field.

The second application of the CLYC-7 elpasolite was the CDRDS. The CDRDS was designed with the purpose of being autonomous with the intent to monitor and process measurements remotely. The CDRDS was fully functional during tests and measurements were successfully monitored and processed remotely. Coupled with an MLEM algorithm Matlab code, the results from the time-encoded measurements with the CDRDS were post-processed to create an image, or 2-D location, of the measured sources. These measured sources included photon sources and neutron sources at various angles, distances from the CDRDS, and heights. The MLEM-reconstructed images utilizing measurements from the CDRDS (both HDPE and Pb masks) yielded source positions within 5 coordinates in both the x- and y-directions of the actual source position.

It is envisioned that the CDRDS will be revamped in the near future so to enable deployment in the field. It is desired to study the feasibility of the collimator to be made of a single material. Such materials (i.e., a tungsten-plastic filament) can be 3-D printed. The material selection will have to be made based on availability, cost, and ability to successfully modulate incident radiation. Additionally, since MURA coded apertures are best for point-like sources as evaluated in this study, other coded aperture types including a random pattern coded aperture can be investigated

so to be able to optimally image sources that are not point-like in nature. Insulation of the electronics onboard the CDRDS should also be considered to minimize noise in collected signals from incident radiation. In addition to these optimization changes to the CDRDS, it should be packaged so to be able to withstand the outdoors or other harsh environments. The addition of an enclosed housing for all of the electronics and possible protection of the collimator from above should be considered. The current CDRDS weighs approximately 70 lbs. To enable easy movement of it, it is envisioned that the CDRDS be fixed to a remote-controlled drive train with off-road wheels. If the CDRDS will be used for long-term fixed monitoring in a storage or processing facility, this capability may not be needed. Upon completions of these upgrades to the CDRDS, it should be tested in the laboratory to determine its operability and then deployed in the field.

It is ideas and developments such as the HMRS and the CDRDS that keep pushing the envelope of radiation detection technology. These advancements are necessary to prevent and mitigate the radiological and nuclear threats that exist today. For all engineers and scientists who pursue such endeavors, it is their dream and their goal, to make the world a better and safer place through the use of radiation detection technologies.

APPENDIX A: MCNP CODE

HMRS Sample Input

```
C CLYC Scintillator 2x2 in Li-7 Enriched, HEU Source
C ================ CELLS ====================
C Detector cell
   1  1   -3.31  -3        imp:p=1
 C Air in the world
   2  3 -0.001205   -1 2 3  imp:p=1
 C Source cell
   3  2 -19.1   -2      imp:p=1
 C outside world (void)
   4  0         1  imp:p=0

 C ================ SURFACES ==================
 C The world
   1   rpp   -5. 35.  -10. 10.  -10. 10.
C Small sphere to house source
   2   sph     0. 0. 0.   1.0
C Detector
   3   rcc   20. 0. 0   5.0 0. 0.   2.5

C ================ MATERIALS =======================
m1  55133 2.0 3006 0.05 3007 0.95 39089 1.0 17035 4.5456 17037 1.4544 &
   $ CLYC (density = 3.31 g/cc)
m2  92234.    -0.001    92235.   -0.200   92238.   -0.799
m3  6000.     -0.000124 7014.    -0.755268 &
      8016.     -0.231781 18000.   -0.012827 $ Air (density = 0.001205 g/cc)
C ================ SOURCE ========================
mode  n h p a d
sdef  par=n erg=2.53E-8 pos=0 0 0
C ================ TALLIES ========================
f8:p 1
e8   0 2000i 20
ft8 GEB 0.019 0.00065 30.8642
f18:h 1
e18   0 2000i 20
ft18 GEB 0.019 0.00065 30.8642
f28:a 1
e28   0 2000i 20
ft28 GEB 0.019 0.00065 30.8642
f38:d 1
e38   0 2000i 20
ft38 GEB 0.019 0.00065 30.8642
f48:n 1
```

```
e48   0 2000i 20
ft48 cap 3006 3007 17035 GEB 0.019 0.00065 30.8642
fq48 e
C ================ PHYSICS ======================
phys:n j 20 2j    $ physics for neutrons
phys:p  2j 0      $ physics for photons
C ================ CUTOFFS ======================
print
ctme 30
```

CDRDS Sample Input

```
CDRDS Centered Source, HEU
c   CELLS
   1   204 -0.001225 -9 1 7 8 imp:n,p,a,h,d=1
   2   204 -0.001225 -1  fill=1 imp:n,p,a,h,d=1
   3   256    -0.9 -2 3 -4 5  u=1 lat=1 imp:n,p,a,h,d=1 $ROW 1
         fill=-57:58 -28:29 0:0
    1 1 2 2 1 1 1 1 2 1 2 2 2 1 2 2 1 2 2 2 1 2 1 1 1 1 2 2 1 1 1 2 2 $ROW 1
         1 1 1 1 2 1 2 2 2 1 2 2 1 2 2 2 1 2 1 1 1 1 2 2 1 1 1 2 2 1 1 1 1 2
         1 2 2 2 1 2 2 1 2 2 2 1 2 1 1 1 1 2 2 1 1 1 2 2 1 1 1 1 2 1 2 2 2 1
         2 2 1 2 2 2 1 2 1 1 1 1 2 2 1
    1 2 1 1 2 2 2 2 1 2 1 1 1 2 1 1 2 1 1 1 2 1 2 2 2 2 1 1 2 1 2 1 1 $ROW 2
         2 2 2 2 1 2 1 1 1 2 1 1 2 1 1 1 2 1 2 2 2 2 1 1 2 1 2 1 1 2 2 2 2 1
         2 1 1 1 2 1 1 2 1 1 1 2 1 2 2 2 2 1 1 2 1 2 1 1 2 2 2 2 1 2 1 1 1 2
         1 1 2 1 1 1 2 1 2 2 2 2 1 1 2
    1 2 1 1 2 2 2 2 1 2 1 1 1 2 1 1 2 1 1 1 2 1 2 2 2 2 1 1 2 1 2 1 1 $ROW 3
         2 2 2 2 1 2 1 1 1 2 1 1 2 1 1 1 2 1 2 2 2 2 1 1 2 1 2 1 1 2 2 2 2 1
         2 1 1 1 2 1 1 2 1 1 1 2 1 2 2 2 2 1 1 2 1 2 1 1 2 2 2 2 1 2 1 1 1 2
         1 1 2 1 1 1 2 1 2 2 2 2 1 1 2
    1 1 2 2 1 1 1 1 2 1 2 2 2 1 2 2 1 2 2 2 1 2 1 1 1 1 2 2 1 1 1 2 2 $ROW 4
         1 1 1 1 2 1 2 2 2 1 2 2 1 2 2 2 1 2 1 1 1 1 2 2 1 1 1 2 2 1 1 1 1 2
         1 2 2 2 1 2 2 1 2 2 2 1 2 1 1 1 1 2 2 1 1 1 2 2 1 1 1 1 2 1 2 2 2 1
         2 2 1 2 2 2 1 2 1 1 1 1 2 2 1
    1 1 2 2 1 1 1 1 2 1 2 2 2 1 2 2 1 2 2 2 1 2 1 1 1 1 2 2 1 1 1 2 2 $ROW 5
         1 1 1 1 2 1 2 2 2 1 2 2 1 2 2 2 1 2 1 1 1 1 2 2 1 1 1 2 2 1 1 1 1 2
         1 2 2 2 1 2 2 1 2 2 2 1 2 1 1 1 1 2 2 1 1 1 2 2 1 1 1 1 2 1 2 2 2 1
         2 2 1 2 2 2 1 2 1 1 1 1 2 2 1
    1 1 2 2 1 1 1 1 2 1 2 2 2 1 2 2 1 2 2 2 1 2 1 1 1 1 2 2 1 1 1 2 2 $ROW 6
         1 1 1 1 2 1 2 2 2 1 2 2 1 2 2 2 1 2 1 1 1 1 2 2 1 1 1 2 2 1 1 1 1 2
         1 2 2 2 1 2 2 1 2 2 2 1 2 1 1 1 1 2 2 1 1 1 2 2 1 1 1 1 2 1 2 2 2 1
         2 2 1 2 2 2 1 2 1 1 1 1 2 2 1
    1 1 2 2 1 1 1 1 2 1 2 2 2 1 2 2 1 2 2 2 1 2 1 1 1 1 2 2 1 1 1 2 2 $ROW 7
         1 1 1 1 2 1 2 2 2 1 2 2 1 2 2 2 1 2 1 1 1 1 2 2 1 1 1 2 2 1 1 1 1 2
         1 2 2 2 1 2 2 1 2 2 2 1 2 1 1 1 1 2 2 1 1 1 2 2 1 1 1 1 2 1 2 2 2 1
         2 2 1 2 2 2 1 2 1 1 1 1 2 2 1
```

1 2 1 1 2 2 2 2 1 2 1 1 1 2 1 1 2 1 1 1 2 1 2 2 2 2 1 1 2 1 2 1 1 $ROW 8
2 2 2 2 1 2 1 1 1 2 1 1 2 1 1 1 2 1 2 2 2 2 1 1 2 1 2 1 1 2 2 2 2 1
2 1 1 1 2 1 1 2 1 1 1 2 1 2 2 2 2 1 1 2 1 2 1 1 2 2 2 2 1 2 1 1 1 2
1 1 2 1 1 1 2 1 2 2 2 2 1 1 2
1 1 2 2 1 1 1 1 2 1 2 2 2 1 2 2 1 2 2 2 1 2 1 1 1 1 2 2 1 1 1 2 2 $ROW 9
1 1 1 1 2 1 2 2 2 1 2 2 1 2 2 2 1 2 1 1 1 1 2 2 1 1 1 2 2 1 1 1 1 2
1 2 2 2 1 2 2 1 2 2 2 1 2 1 1 1 1 2 2 1 1 1 2 2 1 1 1 1 2 1 2 2 2 1
2 2 1 2 2 2 1 2 1 1 1 1 2 2 1
1 2 1 1 2 2 2 2 1 2 1 1 1 2 1 1 2 1 1 1 2 1 2 2 2 2 1 1 2 1 2 1 1 $ROW 10
1 2 2 2 2 1 2 1 1 1 2 1 1 2 1 1 1 2 1 2 2 2 2 1 1 2 1 2 1 1 2 2 2 2
1 2 1 1 1 2 1 1 2 1 1 1 2 1 2 2 2 2 1 1 2 1 2 1 1 2 2 2 2 1 2 1 1 1
2 1 1 2 1 1 1 2 1 2 2 2 2 1 1 2
1 2 1 1 2 2 2 2 1 2 1 1 1 2 1 1 2 1 1 1 2 1 2 2 2 2 1 1 2 1 2 1 1 $ROW 11
1 2 2 2 2 1 2 1 1 1 2 1 1 2 1 1 1 2 1 2 2 2 2 1 1 2 1 2 1 1 2 2 2 2
1 2 1 1 1 2 1 1 2 1 1 1 2 1 2 2 2 2 1 1 2 1 2 1 1 2 2 2 2 1 2 1 1 1
2 1 1 2 1 1 1 2 1 2 2 2 2 1 1 2
1 2 1 1 2 2 2 2 1 2 1 1 1 2 1 1 2 1 1 1 2 1 2 2 2 2 1 1 2 1 2 1 1 $ROW 12
1 2 2 2 2 1 2 1 1 1 2 1 1 2 1 1 1 2 1 2 2 2 2 1 1 2 1 2 1 1 2 2 2 2
1 2 1 1 1 2 1 1 2 1 1 1 2 1 2 2 2 2 1 1 2 1 2 1 1 2 2 2 2 1 2 1 1 1
2 1 1 2 1 1 1 2 1 2 2 2 2 1 1 2
1 1 2 2 1 1 1 1 2 1 2 2 2 1 2 2 1 2 2 2 1 2 1 1 1 1 2 2 1 1 1 2 $ROW 13
2 1 1 1 1 2 1 2 2 2 1 2 2 1 2 2 2 1 2 1 1 1 1 2 2 1 1 1 2 2 1 1 1 1
2 1 2 2 2 1 2 2 1 2 2 2 1 2 1 1 1 1 2 2 1 1 1 2 2 1 1 1 1 2 1 2 2 2
1 2 2 1 2 2 2 1 2 1 1 1 1 2 2 1
1 2 1 1 2 2 2 2 1 2 1 1 1 2 1 1 2 1 1 1 2 1 2 2 2 2 1 1 2 1 2 1 1 $ROW 14
1 2 2 2 2 1 2 1 1 1 2 1 1 2 1 1 1 2 1 2 2 2 2 1 1 2 1 2 1 1 2 2 2 2
1 2 1 1 1 2 1 1 2 1 1 1 2 1 2 2 2 2 1 1 2 1 2 1 1 2 2 2 2 1 2 1 1 1
2 1 1 2 1 1 1 2 1 2 2 2 2 1 1 2
1 2 1 1 2 2 2 2 1 2 1 1 1 2 1 1 2 1 1 1 2 1 2 2 2 2 1 1 2 1 2 1 1 $ROW 15
1 2 2 2 2 1 2 1 1 1 2 1 1 2 1 1 1 2 1 2 2 2 2 1 1 2 1 2 1 1 2 2 2 2
1 2 1 1 1 2 1 1 2 1 1 1 2 1 2 2 2 2 1 1 2 1 2 1 1 2 2 2 2 1 2 1 1 1
2 1 1 2 1 1 1 2 1 2 2 2 2 1 1 2
1 1 2 2 1 1 1 1 2 1 2 2 2 1 2 2 1 2 2 2 1 2 1 1 1 1 2 2 1 1 1 2 $ROW 16
2 1 1 1 1 2 1 2 2 2 1 2 2 1 2 2 2 1 2 1 1 1 1 2 2 1 1 1 2 2 1 1 1 1
2 1 2 2 2 1 2 2 1 2 2 2 1 2 1 1 1 1 2 2 1 1 1 2 2 1 1 1 1 2 1 2 2 2
1 2 2 1 2 2 2 1 2 1 1 1 1 2 2 1
1 2 1 1 2 2 2 2 1 2 1 1 1 2 1 1 2 1 1 1 2 1 2 2 2 2 1 1 2 1 2 1 1 $ROW 17
1 2 2 2 2 1 2 1 1 1 2 1 1 2 1 1 1 2 1 2 2 2 2 1 1 2 1 2 1 1 2 2 2 2
1 2 1 1 1 2 1 1 2 1 1 1 2 1 2 2 2 2 1 1 2 1 2 1 1 2 2 2 2 1 2 1 1 1
2 1 1 2 1 1 1 2 1 2 2 2 2 1 1 2
1 2 1 1 2 2 2 2 1 2 1 1 1 2 1 1 2 1 1 1 2 1 2 2 2 2 1 1 2 1 2 1 1 $ROW 18
1 2 2 2 2 1 2 1 1 1 2 1 1 2 1 1 1 2 1 2 2 2 2 1 1 2 1 2 1 1 2 2 2 2
1 2 1 1 1 2 1 1 2 1 1 1 2 1 2 2 2 2 1 1 2 1 2 1 1 2 2 2 2 1 2 1 1 1
2 1 1 2 1 1 1 2 1 2 2 2 2 1 1 2
1 2 1 1 2 2 2 2 1 2 1 1 1 2 1 1 2 1 1 1 2 1 2 2 2 2 1 1 2 1 2 1 1 $ROW 19
1 2 2 2 2 1 2 1 1 1 2 1 1 2 1 1 1 2 1 2 2 2 2 1 1 2 1 2 1 1 2 2 2 2

1 2 1 1 1 2 1 1 2 1 1 1 2 1 2 2 2 2 1 1 2 1 2 1 1 2 2 2 2 1 2 1 1 1
2 1 1 2 1 1 1 2 1 2 2 2 2 1 1 2
1 1 2 2 1 1 1 1 2 1 2 2 2 1 2 2 1 2 2 2 1 2 1 1 1 1 2 2 1 1 1 2 $ROW 20
2 1 1 1 1 2 1 2 2 2 1 2 2 1 2 2 2 1 2 1 1 1 1 2 2 1 1 1 2 2 1 1 1 1
2 1 2 2 2 1 2 2 1 2 2 2 1 2 1 1 1 1 2 2 1 1 1 2 2 1 1 1 1 2 1 2 2 2
1 2 2 1 2 2 2 1 2 1 1 1 1 2 2 1
1 2 1 1 2 2 2 2 1 2 1 1 1 2 1 1 2 1 1 1 2 1 2 2 2 2 1 1 2 1 2 1 $ROW 21
1 2 2 2 2 1 2 1 1 1 2 1 1 2 1 1 1 2 1 2 2 2 2 1 1 2 1 2 1 1 2 2 2 2
1 2 1 1 1 2 1 1 2 1 1 1 2 1 2 2 2 2 1 1 2 1 2 1 1 2 2 2 2 1 2 1 1 1
2 1 1 2 1 1 1 2 1 2 2 2 2 1 1 2
1 1 2 2 1 1 1 1 2 1 2 2 2 1 2 2 1 2 2 2 1 2 1 1 1 1 2 2 1 1 1 2 $ROW 22
2 1 1 1 1 2 1 2 2 2 1 2 2 1 2 2 2 1 2 1 1 1 1 2 2 1 1 1 2 2 1 1 1 1
2 1 2 2 2 1 2 2 1 2 2 2 1 2 1 1 1 1 2 2 1 1 1 2 2 1 1 1 1 2 1 2 2 2
1 2 2 1 2 2 2 1 2 1 1 1 1 2 2 1
1 1 2 2 1 1 1 1 2 1 2 2 2 1 2 2 1 2 2 2 1 2 1 1 1 1 2 2 1 1 1 2 $ROW 23
2 1 1 1 1 2 1 2 2 2 1 2 2 1 2 2 2 1 2 1 1 1 1 2 2 1 1 1 2 2 1 1 1 1
2 1 2 2 2 1 2 2 1 2 2 2 1 2 1 1 1 1 2 2 1 1 1 2 2 1 1 1 1 2 1 2 2 2
1 2 2 1 2 2 2 1 2 1 1 1 1 2 2 1
1 1 2 2 1 1 1 1 2 1 2 2 2 1 2 2 1 2 2 2 1 2 1 1 1 1 2 2 1 1 1 2 $ROW 24
2 1 1 1 1 2 1 2 2 2 1 2 2 1 2 2 2 1 2 1 1 1 1 2 2 1 1 1 2 2 1 1 1 1
2 1 2 2 2 1 2 2 1 2 2 2 1 2 1 1 1 1 2 2 1 1 1 2 2 1 1 1 1 2 1 2 2 2
1 2 2 1 2 2 2 1 2 1 1 1 1 2 2 1
1 1 2 2 1 1 1 1 2 1 2 2 2 1 2 2 1 2 2 2 1 2 1 1 1 1 2 2 1 1 1 2 $ROW 25
2 1 1 1 1 2 1 2 2 2 1 2 2 1 2 2 2 1 2 1 1 1 1 2 2 1 1 1 2 2 1 1 1 1
2 1 2 2 2 1 2 2 1 2 2 2 1 2 1 1 1 1 2 2 1 1 1 2 2 1 1 1 1 2 1 2 2 2
1 2 2 1 2 2 2 1 2 1 1 1 1 2 2 1
1 2 1 1 2 2 2 2 1 2 1 1 1 2 1 1 2 1 1 1 2 1 2 2 2 2 1 1 2 1 2 1 $ROW 26
1 2 2 2 2 1 2 1 1 1 2 1 1 2 1 1 1 2 1 2 2 2 2 1 1 2 1 2 1 1 2 2 2 2
1 2 1 1 1 2 1 1 2 1 1 1 2 1 2 2 2 2 1 1 2 1 2 1 1 2 2 2 2 1 2 1 1 1
2 1 1 2 1 1 1 2 1 2 2 2 2 1 1 2
1 2 1 1 2 2 2 2 1 2 1 1 1 2 1 1 2 1 1 1 2 1 2 2 2 2 1 1 2 1 2 1 $ROW 27
1 2 2 2 2 1 2 1 1 1 2 1 1 2 1 1 1 2 1 2 2 2 2 1 1 2 1 2 1 1 2 2 2 2
1 2 1 1 1 2 1 1 2 1 1 1 2 1 2 2 2 2 1 1 2 1 2 1 1 2 2 2 2 1 2 1 1 1
2 1 1 2 1 1 1 2 1 2 2 2 2 1 1 2
1 1 2 2 1 1 1 1 2 1 2 2 2 1 2 2 1 2 2 2 1 2 1 1 1 1 2 2 1 1 1 2 $ROW 28
2 1 1 1 1 2 1 2 2 2 1 2 2 1 2 2 2 1 2 1 1 1 1 2 2 1 1 1 2 2 1 1 1 1
2 1 2 2 2 1 2 2 1 2 2 2 1 2 1 1 1 1 2 2 1 1 1 2 2 1 1 1 1 2 1 2 2 2
1 2 2 1 2 2 2 1 2 1 1 1 1 2 2 1
2 2 2 2 2 2 2 2 2 2 2 2 2 2 2 2 2 2 2 2 2 2 2 2 2 2 2 2 2 2 2 2 $ROW 29
2 2 2 2 2 2 2 2 2 2 2 2 2 2 2 2 2 2 2 2 2 2 2 2 2 2 2 2 2 2 2 2 2 2
2 2 2 2 2 2 2 2 2 2 2 2 2 2 2 2 2 2 2 2 2 2 2 2 2 2 2 2 2 2 2 2 2 2
2 2 2 2 2 2 2 2 2 2 2 2 2 2 2 2
1 1 2 2 1 1 1 1 2 1 2 2 2 1 2 2 1 2 2 2 1 2 1 1 1 1 2 2 1 1 1 2 $ROW 30
2 1 1 1 1 2 1 2 2 2 1 2 2 1 2 2 2 1 2 1 1 1 1 2 2 1 1 1 2 2 1 1 1 1
2 1 2 2 2 1 2 2 1 2 2 2 1 2 1 1 1 1 2 2 1 1 1 2 2 1 1 1 1 2 1 2 2 2
1 2 2 1 2 2 2 1 2 1 1 1 1 2 2 1

1 2 1 1 2 2 2 2 1 2 1 1 1 2 1 1 2 1 1 1 2 1 2 2 2 2 1 1 2 1 2 1 $ROW 31
1 2 2 2 2 1 2 1 1 1 2 1 1 2 1 1 1 2 1 2 2 2 2 1 1 2 1 2 1 1 2 2 2 2
1 2 1 1 1 2 1 1 2 1 1 1 2 1 2 2 2 2 1 1 2 1 2 1 1 2 2 2 2 1 2 1 1 1
2 1 1 2 1 1 1 2 1 2 2 2 2 1 1 2
1 2 1 1 2 2 2 2 1 2 1 1 1 2 1 1 2 1 1 1 2 1 2 2 2 2 1 1 2 1 2 1 $ROW 32
1 2 2 2 2 1 2 1 1 1 2 1 1 2 1 1 1 2 1 2 2 2 2 1 1 2 1 2 1 1 2 2 2 2
1 2 1 1 1 2 1 1 2 1 1 1 2 1 2 2 2 2 1 1 2 1 2 1 1 2 2 2 2 1 2 1 1 1
2 1 1 2 1 1 1 2 1 2 2 2 2 1 1 2
1 1 2 2 1 1 1 1 2 1 2 2 2 1 2 2 1 2 2 2 1 2 1 1 1 1 2 2 1 1 1 2 $ROW 33
2 1 1 1 1 2 1 2 2 2 1 2 2 1 2 2 2 1 2 1 1 1 1 2 2 1 1 1 2 2 1 1 1 1
2 1 2 2 2 1 2 2 1 2 2 2 1 2 1 1 1 1 2 2 1 1 1 2 2 1 1 1 1 2 1 2 2 2
1 2 2 1 2 2 2 1 2 1 1 1 1 2 2 1
1 1 2 2 1 1 1 1 2 1 2 2 2 1 2 2 1 2 2 2 1 2 1 1 1 1 2 2 1 1 1 2 $ROW 34
2 1 1 1 1 2 1 2 2 2 1 2 2 1 2 2 2 1 2 1 1 1 1 2 2 1 1 1 2 2 1 1 1 1
2 1 2 2 2 1 2 2 1 2 2 2 1 2 1 1 1 1 2 2 1 1 1 2 2 1 1 1 1 2 1 2 2 2
1 2 2 1 2 2 2 1 2 1 1 1 1 2 2 1
1 1 2 2 1 1 1 1 2 1 2 2 2 1 2 2 1 2 2 2 1 2 1 1 1 1 2 2 1 1 1 2 $ROW 35
2 1 1 1 1 2 1 2 2 2 1 2 2 1 2 2 2 1 2 1 1 1 1 2 2 1 1 1 2 2 1 1 1 1
2 1 2 2 2 1 2 2 1 2 2 2 1 2 1 1 1 1 2 2 1 1 1 2 2 1 1 1 1 2 1 2 2 2
1 2 2 1 2 2 2 1 2 1 1 1 1 2 2 1
1 1 2 2 1 1 1 1 2 1 2 2 2 1 2 2 1 2 2 2 1 2 1 1 1 1 2 2 1 1 1 2 $ROW 36
2 1 1 1 1 2 1 2 2 2 1 2 2 1 2 2 2 1 2 1 1 1 1 2 2 1 1 1 2 2 1 1 1 1
2 1 2 2 2 1 2 2 1 2 2 2 1 2 1 1 1 1 2 2 1 1 1 2 2 1 1 1 1 2 1 2 2 2
1 2 2 1 2 2 2 1 2 1 1 1 1 2 2 1
1 2 1 1 2 2 2 2 1 2 1 1 1 2 1 1 2 1 1 1 2 1 2 2 2 2 1 1 2 1 2 1 $ROW 37
1 2 2 2 2 1 2 1 1 1 2 1 1 2 1 1 1 2 1 2 2 2 2 1 1 2 1 2 1 1 2 2 2 2
1 2 1 1 1 2 1 1 2 1 1 1 2 1 2 2 2 2 1 1 2 1 2 1 1 2 2 2 2 1 2 1 1 1
2 1 1 2 1 1 1 2 1 2 2 2 2 1 1 2
1 1 2 2 1 1 1 1 2 1 2 2 2 1 2 2 1 2 2 2 1 2 1 1 1 1 2 2 1 1 1 2 $ROW 38
2 1 1 1 1 2 1 2 2 2 1 2 2 1 2 2 2 1 2 1 1 1 1 2 2 1 1 1 2 2 1 1 1 1
2 1 2 2 2 1 2 2 1 2 2 2 1 2 1 1 1 1 2 2 1 1 1 2 2 1 1 1 1 2 1 2 2 2
1 2 2 1 2 2 2 1 2 1 1 1 1 2 2 1
1 2 1 1 2 2 2 2 1 2 1 1 1 2 1 1 2 1 1 1 2 1 2 2 2 2 1 1 2 1 2 1 $ROW 39
1 2 2 2 2 1 2 1 1 1 2 1 1 2 1 1 1 2 1 2 2 2 2 1 1 2 1 2 1 1 2 2 2 2
1 2 1 1 1 2 1 1 2 1 1 1 2 1 2 2 2 2 1 1 2 1 2 1 1 2 2 2 2 1 2 1 1 1
2 1 1 2 1 1 1 2 1 2 2 2 2 1 1 2
1 2 1 1 2 2 2 2 1 2 1 1 1 2 1 1 2 1 1 1 2 1 2 2 2 2 1 1 2 1 2 1 $ROW 40
1 2 2 2 2 1 2 1 1 1 2 1 1 2 1 1 1 2 1 2 2 2 2 1 1 2 1 2 1 1 2 2 2 2
1 2 1 1 1 2 1 1 2 1 1 1 2 1 2 2 2 2 1 1 2 1 2 1 1 2 2 2 2 1 2 1 1 1
2 1 1 2 1 1 1 2 1 2 2 2 2 1 1 2
1 2 1 1 2 2 2 2 1 2 1 1 1 2 1 1 2 1 1 1 2 1 2 2 2 2 1 1 2 1 2 1 $ROW 41
1 2 2 2 2 1 2 1 1 1 2 1 1 2 1 1 1 2 1 2 2 2 2 1 1 2 1 2 1 1 2 2 2 2
1 2 1 1 1 2 1 1 2 1 1 1 2 1 2 2 2 2 1 1 2 1 2 1 1 2 2 2 2 1 2 1 1 1
2 1 1 2 1 1 1 2 1 2 2 2 2 1 1 2
1 1 2 2 1 1 1 1 2 1 2 2 2 1 2 2 1 2 2 2 1 2 1 1 1 1 2 2 1 1 1 2 $ROW 42
2 1 1 1 1 2 1 2 2 2 1 2 2 1 2 2 2 1 2 1 1 1 1 2 2 1 1 1 2 2 1 1 1 1

2 1 2 2 2 1 2 2 1 2 2 2 1 2 1 1 1 1 2 2 1 1 1 2 2 1 1 1 1 2 1 2 2 2
1 2 2 1 2 2 2 1 2 1 1 1 1 2 2 1
1 2 1 1 2 2 2 2 1 2 1 1 1 2 1 1 2 1 1 1 2 1 2 2 2 2 1 1 2 1 2 1 $ROW 43
1 2 2 2 2 1 2 1 1 1 2 1 1 2 1 1 1 2 1 2 2 2 2 1 1 2 1 2 1 1 2 2 2 2
1 2 1 1 1 2 1 1 2 1 1 1 2 1 2 2 2 2 1 1 2 1 2 1 1 2 2 2 2 1 2 1 1 1
2 1 1 2 1 1 1 2 1 2 2 2 2 1 1 2
1 2 1 1 2 2 2 2 1 2 1 1 1 2 1 1 2 1 1 1 2 1 2 2 2 2 1 1 2 1 2 1 $ROW 44
1 2 2 2 2 1 2 1 1 1 2 1 1 2 1 1 1 2 1 2 2 2 2 1 1 2 1 2 1 1 2 2 2 2
1 2 1 1 1 2 1 1 2 1 1 1 2 1 2 2 2 2 1 1 2 1 2 1 1 2 2 2 2 1 2 1 1 1
2 1 1 2 1 1 1 2 1 2 2 2 2 1 1 2
1 1 2 2 1 1 1 1 2 1 2 2 2 1 2 2 1 2 2 2 1 2 1 1 1 1 2 2 1 1 1 2 $ROW 45
2 1 1 1 1 2 1 2 2 2 1 2 2 1 2 2 2 1 2 1 1 1 1 2 2 1 1 1 2 2 1 1 1 1
2 1 2 2 2 1 2 2 1 2 2 2 1 2 1 1 1 1 2 2 1 1 1 2 2 1 1 1 1 2 1 2 2 2
1 2 2 1 2 2 2 1 2 1 1 1 1 2 2 1
1 2 1 1 2 2 2 2 1 2 1 1 1 2 1 1 2 1 1 1 2 1 2 2 2 2 1 1 2 1 2 1 $ROW 46
1 2 2 2 2 1 2 1 1 1 2 1 1 2 1 1 1 2 1 2 2 2 2 1 1 2 1 2 1 1 2 2 2 2
1 2 1 1 1 2 1 1 2 1 1 1 2 1 2 2 2 2 1 1 2 1 2 1 1 2 2 2 2 1 2 1 1 1
2 1 1 2 1 1 1 2 1 2 2 2 2 1 1 2
1 2 1 1 2 2 2 2 1 2 1 1 1 2 1 1 2 1 1 1 2 1 2 2 2 2 1 1 2 1 2 1 $ROW 47
1 2 2 2 2 1 2 1 1 1 2 1 1 2 1 1 1 2 1 2 2 2 2 1 1 2 1 2 1 1 2 2 2 2
1 2 1 1 1 2 1 1 2 1 1 1 2 1 2 2 2 2 1 1 2 1 2 1 1 2 2 2 2 1 2 1 1 1
2 1 1 2 1 1 1 2 1 2 2 2 2 1 1 2
1 2 1 1 2 2 2 2 1 2 1 1 1 2 1 1 2 1 1 1 2 1 2 2 2 2 1 1 2 1 2 1 $ROW 48
1 2 2 2 2 1 2 1 1 1 2 1 1 2 1 1 1 2 1 2 2 2 2 1 1 2 1 2 1 1 2 2 2 2
1 2 1 1 1 2 1 1 2 1 1 1 2 1 2 2 2 2 1 1 2 1 2 1 1 2 2 2 2 1 2 1 1 1
2 1 1 2 1 1 1 2 1 2 2 2 2 1 1 2
1 1 2 2 1 1 1 1 2 1 2 2 2 1 2 2 1 2 2 2 1 2 1 1 1 1 2 2 1 1 1 2 $ROW 49
2 1 1 1 1 2 1 2 2 2 1 2 2 1 2 2 2 1 2 1 1 1 1 2 2 1 1 1 2 2 1 1 1 1
2 1 2 2 2 1 2 2 1 2 2 2 1 2 1 1 1 1 2 2 1 1 1 2 2 1 1 1 1 2 1 2 2 2
1 2 2 1 2 2 2 1 2 1 1 1 1 2 2 1
1 2 1 1 2 2 2 2 1 2 1 1 1 2 1 1 2 1 1 1 2 1 2 2 2 2 1 1 2 1 2 1 $ROW 50
1 2 2 2 2 1 2 1 1 1 2 1 1 2 1 1 1 2 1 2 2 2 2 1 1 2 1 2 1 1 2 2 2 2
1 2 1 1 1 2 1 1 2 1 1 1 2 1 2 2 2 2 1 1 2 1 2 1 1 2 2 2 2 1 2 1 1 1
2 1 1 2 1 1 1 2 1 2 2 2 2 1 1 2
1 1 2 2 1 1 1 1 2 1 2 2 2 1 2 2 1 2 2 2 1 2 1 1 1 1 2 2 1 1 1 2 $ROW 51
2 1 1 1 1 2 1 2 2 2 1 2 2 1 2 2 2 1 2 1 1 1 1 2 2 1 1 1 2 2 1 1 1 1
2 1 2 2 2 1 2 2 1 2 2 2 1 2 1 1 1 1 2 2 1 1 1 2 2 1 1 1 1 2 1 2 2 2
1 2 2 1 2 2 2 1 2 1 1 1 1 2 2 1
1 1 2 2 1 1 1 1 2 1 2 2 2 1 2 2 1 2 2 2 1 2 1 1 1 1 2 2 1 1 1 2 $ROW 52
2 1 1 1 1 2 1 2 2 2 1 2 2 1 2 2 2 1 2 1 1 1 1 2 2 1 1 1 2 2 1 1 1 1
2 1 2 2 2 1 2 2 1 2 2 2 1 2 1 1 1 1 2 2 1 1 1 2 2 1 1 1 1 2 1 2 2 2
1 2 2 1 2 2 2 1 2 1 1 1 1 2 2 1
1 1 2 2 1 1 1 1 2 1 2 2 2 1 2 2 1 2 2 2 1 2 1 1 1 1 2 2 1 1 1 2 $ROW 53
2 1 1 1 1 2 1 2 2 2 1 2 2 1 2 2 2 1 2 1 1 1 1 2 2 1 1 1 2 2 1 1 1 1
2 1 2 2 2 1 2 2 1 2 2 2 1 2 1 1 1 1 2 2 1 1 1 2 2 1 1 1 1 2 1 2 2 2
1 2 2 1 2 2 2 1 2 1 1 1 1 2 2 1

```
     1 1 2 2 1 1 1 1 2 1 2 2 2 1 2 2 1 2 2 2 1 2 1 1 1 1 2 2 1 1 1 2 $ROW 54
          2 1 1 1 1 2 1 2 2 2 1 2 2 1 2 2 2 1 2 1 1 1 1 2 2 1 1 1 2 2 1 1 1 1
          2 1 2 2 2 1 2 2 1 2 2 2 1 2 1 1 1 1 2 2 1 1 1 2 2 1 1 1 1 2 1 2 2 2
          1 2 2 1 2 2 2 1 2 1 1 1 1 2 2 1
     1 2 1 1 2 2 2 2 1 2 1 1 1 2 1 1 2 1 1 1 2 1 2 2 2 2 1 1 2 1 2 1 $ROW 55
          1 2 2 2 2 1 2 1 1 1 2 1 1 2 1 1 1 2 1 2 2 2 2 1 1 2 1 2 1 1 2 2 2 2
          1 2 1 1 1 2 1 1 2 1 1 1 2 1 2 2 2 2 1 1 2 1 2 1 1 2 2 2 2 1 2 1 1 1
          2 1 1 2 1 1 1 2 1 2 2 2 2 1 1 2
     1 2 1 1 2 2 2 2 1 2 1 1 1 2 1 1 2 1 1 1 2 1 2 2 2 2 1 1 2 1 2 1 $ROW 56
          1 2 2 2 2 1 2 1 1 1 2 1 1 2 1 1 1 2 1 2 2 2 2 1 1 2 1 2 1 1 2 2 2 2
          1 2 1 1 1 2 1 1 2 1 1 1 2 1 2 2 2 2 1 1 2 1 2 1 1 2 2 2 2 1 2 1 1 1
          2 1 1 2 1 1 1 2 1 2 2 2 2 1 1 2
     1 1 2 2 1 1 1 1 2 1 2 2 2 1 2 2 1 2 2 2 1 2 1 1 1 1 2 2 1 1 1 2 $ROW 57
          2 1 1 1 1 2 1 2 2 2 1 2 2 1 2 2 2 1 2 1 1 1 1 2 2 1 1 1 2 2 1 1 1 1
          2 1 2 2 2 1 2 2 1 2 2 2 1 2 1 1 1 1 2 2 1 1 1 2 2 1 1 1 1 2 1 2 2 2
          1 2 2 1 2 2 2 1 2 1 1 1 1 2 2 1
     2 2 2 2 2 2 2 2 2 2 2 2 2 2 2 2 2 2 2 2 2 2 2 2 2 2 2 2 2 2 2 2 $ROW 58
          2 2 2 2 2 2 2 2 2 2 2 2 2 2 2 2 2 2 2 2 2 2 2 2 2 2 2 2 2 2 2 2 2 2
          2 2 2 2 2 2 2 2 2 2 2 2 2 2 2 2 2 2 2 2 2 2 2 2 2 2 2 2 2 2 2 2 2 2
          2 2 2 2 2 2 2 2 2 2 2 2 2 2 2 2
   4   252  -11.35 -6  u=2 imp:n,p,a,h,d=1
   5   204 -0.001225 6  u=2 imp:n,p,a,h,d=1
   6   101   -3.31 -7 imp:n,p,a,h,d=1
   7   502  -18.95 -8 imp:n,p,a,h,d=1
   8     0   9 imp:n,p,a,h,d=0

   1       rpp -142.3 144.8 -12.4 12.92 -3.81 3.81
   2        px 1.238
   3        px -1.238
   4        py 0.219
   5        py -0.219
   6       rpp -1.238 1.238 -0.219 0.219 -3.81 3.81
   7       rcc 70.5748 -2.54 19.05 0 5.08 0 2.54
   8       sph 70.5748 -2.54 -203.81 5
   9       rpp -400 400 -400 400 -400 400

mode  n p h a d
sdef par=n pos=70.5748 -2.54 -203.81 erg=2.53E-8
m101  55133.70c            2  $ CLYC (density = 3.31 g/cc)
     3006.70c          0.05 3007.70c          0.95 39089.70c             1
     17035.70c        4.5456 17037.70c        1.4544
m204  7014.70c      -0.755636  $air (US S. Atm at sea level)
     8016.70c      -0.231475 18036.70c     -3.9e-005 18038.70c       -8e-006
     18040.70c     -0.012842
m252  82206.70c     -0.242902  $lead
     82207.70c     -0.223827 82208.70c      -0.53327
```

```
m256  1001.70c      -0.143711  $polyethylene
     6000.70c      -0.856289
m502  92234.70c       -0.0098  $HEU, US Average,
     92235.70c      -0.93155 92236.70c       -0.0045 92238.70c      -0.05415
   f8:p 6
   ft8 GEB 0.019 0.00065 30.8642
   f18:h 6
   ft18 GEB 0.019 0.00065 30.8642
   f28:a 6
   ft28 GEB 0.019 0.00065 30.8642
   f38:d 6
   ft38 GEB 0.019 0.00065 30.8642
   f48:n 6
   ft48 GEB 0.019 0.00065 30.8642
phys:n j 20 2j    $ physics for neutrons
phys:p  2j 0      $ physics for photons
nps 1000000
```

APPENDIX B: MATLAB CODE EXAMPLE

Neutron-based MLEM Estimate

```
clc,clear,close all;
lambda = ones(58,58);
a = [1.18E+02 1.12E+02 1.19E+02 1.23E+02 1.25E+02 1.28E+02
        1.19E+02 1.23E+02 1.25E+02 1.27E+02 1.39E+02 1.20E+02
        1.17E+02 1.39E+02 1.10E+02 1.20E+02 1.34E+02 1.25E+02
        1.28E+02 1.13E+02 1.29E+02 1.31E+02 1.17E+02 1.27E+02
        1.31E+02 1.36E+02 1.39E+02 1.26E+02 1.36E+02 1.26E+02
        1.25E+02 1.30E+02 1.23E+02 1.41E+02 1.39E+02 1.26E+02
        1.33E+02 1.25E+02 1.41E+02 1.43E+02 1.24E+02 1.34E+02
        1.47E+02 1.20E+02 1.33E+02 1.45E+02 1.24E+02 1.25E+02
        1.24E+02 1.37E+02 1.33E+02 1.31E+02 1.41E+02 1.25E+02
        1.40E+02 1.41E+02 1.42E+02 1.36E+02
];
angle = [0 6.2069 12.4138 18.6207 24.8276 31.0345 37.2414
        43.4483 49.6552 55.8621 62.069 68.2759 74.4828
        80.6897 86.8966 93.1035 99.3104 105.5173 111.7242
        117.9311 124.138 130.3449 136.5518 142.7587 148.9656
        155.1725 161.3794 167.5863 173.7932 180.0001 186.207
        192.4139 198.6208 204.8277 211.0346 217.2415 223.4484
        229.6553 235.8622 242.0691 248.276 254.4829 260.6898
        266.8967 273.1036 279.3105 285.5174 291.7243 297.9312
        304.1381 310.345 316.5519 322.7588 328.9657 335.1726
        341.3795 347.5864 353.7933
6.2069 12.4138 18.6207 24.8276 31.0345 37.2414 43.4483
        49.6552 55.8621 62.069 68.2759 74.4828 80.6897
        86.8966 93.1035 99.3104 105.5173 111.7242 117.9311
        124.138 130.3449 136.5518 142.7587 148.9656 155.1725
        161.3794 167.5863 173.7932 180.0001 186.207 192.4139
        198.6208 204.8277 211.0346 217.2415 223.4484 229.6553
        235.8622 242.0691 248.276 254.4829 260.6898 266.8967
        273.1036 279.3105 285.5174 291.7243 297.9312 304.1381
        310.345 316.5519 322.7588 328.9657 335.1726 341.3795
        347.5864 353.7933 360.0002
12.4138 18.6207 24.8276 31.0345 37.2414 43.4483
        49.6552 55.8621 62.069 68.2759 74.4828 80.6897
        86.8966 93.1035 99.3104 105.5173 111.7242 117.9311
        124.138 130.3449 136.5518 142.7587 148.9656 155.1725
        161.3794 167.5863 173.7932 180.0001 186.207 192.4139
        198.6208 204.8277 211.0346 217.2415 223.4484 229.6553
        235.8622 242.0691 248.276 254.4829 260.6898 266.8967
        273.1036 279.3105 285.5174 291.7243 297.9312 304.1381
        310.345 316.5519 322.7588 328.9657 335.1726 341.3795
        347.5864 353.7933 360.0002 366.2071
```

18.6207 24.8276 31.0345 37.2414 43.4483 49.6552
55.8621 62.069 68.2759 74.4828 80.6897 86.8966
93.1035 99.3104 105.5173 111.7242 117.9311 124.138
130.3449 136.5518 142.7587 148.9656 155.1725 161.3794
167.5863 173.7932 180.0001 186.207 192.4139 198.6208
204.8277 211.0346 217.2415 223.4484 229.6553 235.8622
242.0691 248.276 254.4829 260.6898 266.8967 273.1036
279.3105 285.5174 291.7243 297.9312 304.1381 310.345
316.5519 322.7588 328.9657 335.1726 341.3795 347.5864
353.7933 360.0002 366.2071 372.414
24.8276 31.0345 37.2414 43.4483 49.6552 55.8621 62.069
68.2759 74.4828 80.6897 86.8966 93.1035 99.3104
105.5173 111.7242 117.9311 124.138 130.3449 136.5518
142.7587 148.9656 155.1725 161.3794 167.5863 173.7932
180.0001 186.207 192.4139 198.6208 204.8277 211.0346
217.2415 223.4484 229.6553 235.8622 242.0691 248.276
254.4829 260.6898 266.8967 273.1036 279.3105 285.5174
291.7243 297.9312 304.1381 310.345 316.5519 322.7588
328.9657 335.1726 341.3795 347.5864 353.7933 360.0002
366.2071 372.414 378.6209
31.0345 37.2414 43.4483 49.6552 55.8621 62.069 68.2759
74.4828 80.6897 86.8966 93.1035 99.3104 105.5173
111.7242 117.9311 124.138 130.3449 136.5518 142.7587
148.9656 155.1725 161.3794 167.5863 173.7932 180.0001
186.207 192.4139 198.6208 204.8277 211.0346 217.2415
223.4484 229.6553 235.8622 242.0691 248.276 254.4829
260.6898 266.8967 273.1036 279.3105 285.5174 291.7243
297.9312 304.1381 310.345 316.5519 322.7588 328.9657
335.1726 341.3795 347.5864 353.7933 360.0002 366.2071
372.414 378.6209 384.8278
37.2414 43.4483 49.6552 55.8621 62.069 68.2759 74.4828
80.6897 86.8966 93.1035 99.3104 105.5173 111.7242
117.9311 124.138 130.3449 136.5518 142.7587 148.9656
155.1725 161.3794 167.5863 173.7932 180.0001 186.207
192.4139 198.6208 204.8277 211.0346 217.2415 223.4484
229.6553 235.8622 242.0691 248.276 254.4829 260.6898
266.8967 273.1036 279.3105 285.5174 291.7243 297.9312
304.1381 310.345 316.5519 322.7588 328.9657 335.1726
341.3795 347.5864 353.7933 360.0002 366.2071 372.414
378.6209 384.8278 391.0347
43.4483 49.6552 55.8621 62.069 68.2759 74.4828 80.6897
86.8966 93.1035 99.3104 105.5173 111.7242 117.9311
124.138 130.3449 136.5518 142.7587 148.9656 155.1725
161.3794 167.5863 173.7932 180.0001 186.207 192.4139
198.6208 204.8277 211.0346 217.2415 223.4484 229.6553
235.8622 242.0691 248.276 254.4829 260.6898 266.8967

273.1036 279.3105 285.5174 291.7243 297.9312 304.1381
310.345 316.5519 322.7588 328.9657 335.1726 341.3795
347.5864 353.7933 360.0002 366.2071 372.414 378.6209
384.8278 391.0347 397.2416
49.6552 55.8621 62.069 68.2759 74.4828 80.6897 86.8966
93.1035 99.3104 105.5173 111.7242 117.9311 124.138
130.3449 136.5518 142.7587 148.9656 155.1725 161.3794
167.5863 173.7932 180.0001 186.207 192.4139 198.6208
204.8277 211.0346 217.2415 223.4484 229.6553 235.8622
242.0691 248.276 254.4829 260.6898 266.8967 273.1036
279.3105 285.5174 291.7243 297.9312 304.1381 310.345
316.5519 322.7588 328.9657 335.1726 341.3795 347.5864
353.7933 360.0002 366.2071 372.414 378.6209 384.8278
391.0347 397.2416 403.4485
55.8621 62.069 68.2759 74.4828 80.6897 86.8966 93.1035
99.3104 105.5173 111.7242 117.9311 124.138 130.3449
136.5518 142.7587 148.9656 155.1725 161.3794 167.5863
173.7932 180.0001 186.207 192.4139 198.6208 204.8277
211.0346 217.2415 223.4484 229.6553 235.8622 242.0691
248.276 254.4829 260.6898 266.8967 273.1036 279.3105
285.5174 291.7243 297.9312 304.1381 310.345 316.5519
322.7588 328.9657 335.1726 341.3795 347.5864 353.7933
360.0002 366.2071 372.414 378.6209 384.8278 391.0347
397.2416 403.4485 409.6554
62.069 68.2759 74.4828 80.6897 86.8966 93.1035 99.3104
105.5173 111.7242 117.9311 124.138 130.3449 136.5518
142.7587 148.9656 155.1725 161.3794 167.5863 173.7932
180.0001 186.207 192.4139 198.6208 204.8277 211.0346
217.2415 223.4484 229.6553 235.8622 242.0691 248.276
254.4829 260.6898 266.8967 273.1036 279.3105 285.5174
291.7243 297.9312 304.1381 310.345 316.5519 322.7588
328.9657 335.1726 341.3795 347.5864 353.7933 360.0002
366.2071 372.414 378.6209 384.8278 391.0347 397.2416
403.4485 409.6554 415.8623
68.2759 74.4828 80.6897 86.8966 93.1035 99.3104
105.5173 111.7242 117.9311 124.138 130.3449 136.5518
142.7587 148.9656 155.1725 161.3794 167.5863 173.7932
180.0001 186.207 192.4139 198.6208 204.8277 211.0346
217.2415 223.4484 229.6553 235.8622 242.0691 248.276
254.4829 260.6898 266.8967 273.1036 279.3105 285.5174
291.7243 297.9312 304.1381 310.345 316.5519 322.7588
328.9657 335.1726 341.3795 347.5864 353.7933 360.0002
366.2071 372.414 378.6209 384.8278 391.0347 397.2416
403.4485 409.6554 415.8623 422.0692
74.4828 80.6897 86.8966 93.1035 99.3104 105.5173
111.7242 117.9311 124.138 130.3449 136.5518 142.7587

148.9656 155.1725 161.3794 167.5863 173.7932 180.0001
186.207 192.4139 198.6208 204.8277 211.0346 217.2415
223.4484 229.6553 235.8622 242.0691 248.276 254.4829
260.6898 266.8967 273.1036 279.3105 285.5174 291.7243
297.9312 304.1381 310.345 316.5519 322.7588 328.9657
335.1726 341.3795 347.5864 353.7933 360.0002 366.2071
372.414 378.6209 384.8278 391.0347 397.2416 403.4485
409.6554 415.8623 422.0692 428.2761

80.6897 86.8966 93.1035 99.3104 105.5173 111.7242
117.9311 124.138 130.3449 136.5518 142.7587 148.9656
155.1725 161.3794 167.5863 173.7932 180.0001 186.207
192.4139 198.6208 204.8277 211.0346 217.2415 223.4484
229.6553 235.8622 242.0691 248.276 254.4829 260.6898
266.8967 273.1036 279.3105 285.5174 291.7243 297.9312
304.1381 310.345 316.5519 322.7588 328.9657 335.1726
341.3795 347.5864 353.7933 360.0002 366.2071 372.414
378.6209 384.8278 391.0347 397.2416 403.4485 409.6554
415.8623 422.0692 428.2761 434.483

86.8966 93.1035 99.3104 105.5173 111.7242 117.9311
124.138 130.3449 136.5518 142.7587 148.9656 155.1725
161.3794 167.5863 173.7932 180.0001 186.207 192.4139
198.6208 204.8277 211.0346 217.2415 223.4484 229.6553
235.8622 242.0691 248.276 254.4829 260.6898 266.8967
273.1036 279.3105 285.5174 291.7243 297.9312 304.1381
310.345 316.5519 322.7588 328.9657 335.1726 341.3795
347.5864 353.7933 360.0002 366.2071 372.414 378.6209
384.8278 391.0347 397.2416 403.4485 409.6554 415.8623
422.0692 428.2761 434.483 440.6899

93.1035 99.3104 105.5173 111.7242 117.9311 124.138
130.3449 136.5518 142.7587 148.9656 155.1725 161.3794
167.5863 173.7932 180.0001 186.207 192.4139 198.6208
204.8277 211.0346 217.2415 223.4484 229.6553 235.8622
242.0691 248.276 254.4829 260.6898 266.8967 273.1036
279.3105 285.5174 291.7243 297.9312 304.1381 310.345
316.5519 322.7588 328.9657 335.1726 341.3795 347.5864
353.7933 360.0002 366.2071 372.414 378.6209 384.8278
391.0347 397.2416 403.4485 409.6554 415.8623 422.0692
428.2761 434.483 440.6899 446.8968

99.3104 105.5173 111.7242 117.9311 124.138 130.3449
136.5518 142.7587 148.9656 155.1725 161.3794 167.5863
173.7932 180.0001 186.207 192.4139 198.6208 204.8277
211.0346 217.2415 223.4484 229.6553 235.8622 242.0691
248.276 254.4829 260.6898 266.8967 273.1036 279.3105
285.5174 291.7243 297.9312 304.1381 310.345 316.5519
322.7588 328.9657 335.1726 341.3795 347.5864 353.7933
360.0002 366.2071 372.414 378.6209 384.8278 391.0347

397.2416 403.4485 409.6554 415.8623 422.0692 428.2761
434.483 440.6899 446.8968 453.1037
105.5173 111.7242 117.9311 124.138 130.3449 136.5518
142.7587 148.9656 155.1725 161.3794 167.5863 173.7932
180.0001 186.207 192.4139 198.6208 204.8277 211.0346
217.2415 223.4484 229.6553 235.8622 242.0691 248.276
254.4829 260.6898 266.8967 273.1036 279.3105 285.5174
291.7243 297.9312 304.1381 310.345 316.5519 322.7588
328.9657 335.1726 341.3795 347.5864 353.7933 360.0002
366.2071 372.414 378.6209 384.8278 391.0347 397.2416
403.4485 409.6554 415.8623 422.0692 428.2761 434.483
440.6899 446.8968 453.1037 459.3106
111.7242 117.9311 124.138 130.3449 136.5518 142.7587
148.9656 155.1725 161.3794 167.5863 173.7932 180.0001
186.207 192.4139 198.6208 204.8277 211.0346 217.2415
223.4484 229.6553 235.8622 242.0691 248.276 254.4829
260.6898 266.8967 273.1036 279.3105 285.5174 291.7243
297.9312 304.1381 310.345 316.5519 322.7588 328.9657
335.1726 341.3795 347.5864 353.7933 360.0002 366.2071
372.414 378.6209 384.8278 391.0347 397.2416 403.4485
409.6554 415.8623 422.0692 428.2761 434.483 440.6899
446.8968 453.1037 459.3106 465.5175
117.9311 124.138 130.3449 136.5518 142.7587 148.9656
155.1725 161.3794 167.5863 173.7932 180.0001 186.207
192.4139 198.6208 204.8277 211.0346 217.2415 223.4484
229.6553 235.8622 242.0691 248.276 254.4829 260.6898
266.8967 273.1036 279.3105 285.5174 291.7243 297.9312
304.1381 310.345 316.5519 322.7588 328.9657 335.1726
341.3795 347.5864 353.7933 360.0002 366.2071 372.414
378.6209 384.8278 391.0347 397.2416 403.4485 409.6554
415.8623 422.0692 428.2761 434.483 440.6899 446.8968
453.1037 459.3106 465.5175 471.7244
124.138 130.3449 136.5518 142.7587 148.9656 155.1725
161.3794 167.5863 173.7932 180.0001 186.207 192.4139
198.6208 204.8277 211.0346 217.2415 223.4484 229.6553
235.8622 242.0691 248.276 254.4829 260.6898 266.8967
273.1036 279.3105 285.5174 291.7243 297.9312 304.1381
310.345 316.5519 322.7588 328.9657 335.1726 341.3795
347.5864 353.7933 360.0002 366.2071 372.414 378.6209
384.8278 391.0347 397.2416 403.4485 409.6554 415.8623
422.0692 428.2761 434.483 440.6899 446.8968 453.1037
459.3106 465.5175 471.7244 477.9313
130.3449 136.5518 142.7587 148.9656 155.1725 161.3794
167.5863 173.7932 180.0001 186.207 192.4139 198.6208
204.8277 211.0346 217.2415 223.4484 229.6553 235.8622
242.0691 248.276 254.4829 260.6898 266.8967 273.1036

279.3105 285.5174 291.7243 297.9312 304.1381 310.345
316.5519 322.7588 328.9657 335.1726 341.3795 347.5864
353.7933 360.0002 366.2071 372.414 378.6209 384.8278
391.0347 397.2416 403.4485 409.6554 415.8623 422.0692
428.2761 434.483 440.6899 446.8968 453.1037 459.3106
465.5175 471.7244 477.9313 484.1382
136.5518 142.7587 148.9656 155.1725 161.3794 167.5863
173.7932 180.0001 186.207 192.4139 198.6208 204.8277
211.0346 217.2415 223.4484 229.6553 235.8622 242.0691
248.276 254.4829 260.6898 266.8967 273.1036 279.3105
285.5174 291.7243 297.9312 304.1381 310.345 316.5519
322.7588 328.9657 335.1726 341.3795 347.5864 353.7933
360.0002 366.2071 372.414 378.6209 384.8278 391.0347
397.2416 403.4485 409.6554 415.8623 422.0692 428.2761
434.483 440.6899 446.8968 453.1037 459.3106 465.5175
471.7244 477.9313 484.1382 490.3451
142.7587 148.9656 155.1725 161.3794 167.5863 173.7932
180.0001 186.207 192.4139 198.6208 204.8277 211.0346
217.2415 223.4484 229.6553 235.8622 242.0691 248.276
254.4829 260.6898 266.8967 273.1036 279.3105 285.5174
291.7243 297.9312 304.1381 310.345 316.5519 322.7588
328.9657 335.1726 341.3795 347.5864 353.7933 360.0002
366.2071 372.414 378.6209 384.8278 391.0347 397.2416
403.4485 409.6554 415.8623 422.0692 428.2761 434.483
440.6899 446.8968 453.1037 459.3106 465.5175 471.7244
477.9313 484.1382 490.3451 496.552
148.9656 155.1725 161.3794 167.5863 173.7932 180.0001
186.207 192.4139 198.6208 204.8277 211.0346 217.2415
223.4484 229.6553 235.8622 242.0691 248.276 254.4829
260.6898 266.8967 273.1036 279.3105 285.5174 291.7243
297.9312 304.1381 310.345 316.5519 322.7588 328.9657
335.1726 341.3795 347.5864 353.7933 360.0002 366.2071
372.414 378.6209 384.8278 391.0347 397.2416 403.4485
409.6554 415.8623 422.0692 428.2761 434.483 440.6899
446.8968 453.1037 459.3106 465.5175 471.7244 477.9313
484.1382 490.3451 496.552 502.7589
155.1725 161.3794 167.5863 173.7932 180.0001 186.207
192.4139 198.6208 204.8277 211.0346 217.2415 223.4484
229.6553 235.8622 242.0691 248.276 254.4829 260.6898
266.8967 273.1036 279.3105 285.5174 291.7243 297.9312
304.1381 310.345 316.5519 322.7588 328.9657 335.1726
341.3795 347.5864 353.7933 360.0002 366.2071 372.414
378.6209 384.8278 391.0347 397.2416 403.4485 409.6554
415.8623 422.0692 428.2761 434.483 440.6899 446.8968
453.1037 459.3106 465.5175 471.7244 477.9313 484.1382
490.3451 496.552 502.7589 508.9658

161.3794 167.5863 173.7932 180.0001 186.207 192.4139
198.6208 204.8277 211.0346 217.2415 223.4484 229.6553
235.8622 242.0691 248.276 254.4829 260.6898 266.8967
273.1036 279.3105 285.5174 291.7243 297.9312 304.1381
310.345 316.5519 322.7588 328.9657 335.1726 341.3795
347.5864 353.7933 360.0002 366.2071 372.414 378.6209
384.8278 391.0347 397.2416 403.4485 409.6554 415.8623
422.0692 428.2761 434.483 440.6899 446.8968 453.1037
459.3106 465.5175 471.7244 477.9313 484.1382 490.3451
496.552 502.7589 508.9658 515.1727
167.5863 173.7932 180.0001 186.207 192.4139 198.6208
204.8277 211.0346 217.2415 223.4484 229.6553 235.8622
242.0691 248.276 254.4829 260.6898 266.8967 273.1036
279.3105 285.5174 291.7243 297.9312 304.1381 310.345
316.5519 322.7588 328.9657 335.1726 341.3795 347.5864
353.7933 360.0002 366.2071 372.414 378.6209 384.8278
391.0347 397.2416 403.4485 409.6554 415.8623 422.0692
428.2761 434.483 440.6899 446.8968 453.1037 459.3106
465.5175 471.7244 477.9313 484.1382 490.3451 496.552
502.7589 508.9658 515.1727 521.3796
173.7932 180.0001 186.207 192.4139 198.6208 204.8277
211.0346 217.2415 223.4484 229.6553 235.8622 242.0691
248.276 254.4829 260.6898 266.8967 273.1036 279.3105
285.5174 291.7243 297.9312 304.1381 310.345 316.5519
322.7588 328.9657 335.1726 341.3795 347.5864 353.7933
360.0002 366.2071 372.414 378.6209 384.8278 391.0347
397.2416 403.4485 409.6554 415.8623 422.0692 428.2761
434.483 440.6899 446.8968 453.1037 459.3106 465.5175
471.7244 477.9313 484.1382 490.3451 496.552 502.7589
508.9658 515.1727 521.3796 527.5865
180.0001 186.207 192.4139 198.6208 204.8277 211.0346
217.2415 223.4484 229.6553 235.8622 242.0691 248.276
254.4829 260.6898 266.8967 273.1036 279.3105 285.5174
291.7243 297.9312 304.1381 310.345 316.5519 322.7588
328.9657 335.1726 341.3795 347.5864 353.7933 360.0002
366.2071 372.414 378.6209 384.8278 391.0347 397.2416
403.4485 409.6554 415.8623 422.0692 428.2761 434.483
440.6899 446.8968 453.1037 459.3106 465.5175 471.7244
477.9313 484.1382 490.3451 496.552 502.7589 508.9658
515.1727 521.3796 527.5865 533.7934
186.207 192.4139 198.6208 204.8277 211.0346 217.2415
223.4484 229.6553 235.8622 242.0691 248.276 254.4829
260.6898 266.8967 273.1036 279.3105 285.5174 291.7243
297.9312 304.1381 310.345 316.5519 322.7588 328.9657
335.1726 341.3795 347.5864 353.7933 360.0002 366.2071
372.414 378.6209 384.8278 391.0347 397.2416 403.4485

409.6554 415.8623 422.0692 428.2761 434.483 440.6899
446.8968 453.1037 459.3106 465.5175 471.7244 477.9313
484.1382 490.3451 496.552 502.7589 508.9658 515.1727
521.3796 527.5865 533.7934 540.0003
192.4139 198.6208 204.8277 211.0346 217.2415 223.4484
229.6553 235.8622 242.0691 248.276 254.4829 260.6898
266.8967 273.1036 279.3105 285.5174 291.7243 297.9312
304.1381 310.345 316.5519 322.7588 328.9657 335.1726
341.3795 347.5864 353.7933 360.0002 366.2071 372.414
378.6209 384.8278 391.0347 397.2416 403.4485 409.6554
415.8623 422.0692 428.2761 434.483 440.6899 446.8968
453.1037 459.3106 465.5175 471.7244 477.9313 484.1382
490.3451 496.552 502.7589 508.9658 515.1727 521.3796
527.5865 533.7934 540.0003 546.2072
198.6208 204.8277 211.0346 217.2415 223.4484 229.6553
235.8622 242.0691 248.276 254.4829 260.6898 266.8967
273.1036 279.3105 285.5174 291.7243 297.9312 304.1381
310.345 316.5519 322.7588 328.9657 335.1726 341.3795
347.5864 353.7933 360.0002 366.2071 372.414 378.6209
384.8278 391.0347 397.2416 403.4485 409.6554 415.8623
422.0692 428.2761 434.483 440.6899 446.8968 453.1037
459.3106 465.5175 471.7244 477.9313 484.1382 490.3451
496.552 502.7589 508.9658 515.1727 521.3796 527.5865
533.7934 540.0003 546.2072 552.4141
204.8277 211.0346 217.2415 223.4484 229.6553 235.8622
242.0691 248.276 254.4829 260.6898 266.8967 273.1036
279.3105 285.5174 291.7243 297.9312 304.1381 310.345
316.5519 322.7588 328.9657 335.1726 341.3795 347.5864
353.7933 360.0002 366.2071 372.414 378.6209 384.8278
391.0347 397.2416 403.4485 409.6554 415.8623 422.0692
428.2761 434.483 440.6899 446.8968 453.1037 459.3106
465.5175 471.7244 477.9313 484.1382 490.3451 496.552
502.7589 508.9658 515.1727 521.3796 527.5865 533.7934
540.0003 546.2072 552.4141 558.621
211.0346 217.2415 223.4484 229.6553 235.8622 242.0691
248.276 254.4829 260.6898 266.8967 273.1036 279.3105
285.5174 291.7243 297.9312 304.1381 310.345 316.5519
322.7588 328.9657 335.1726 341.3795 347.5864 353.7933
360.0002 366.2071 372.414 378.6209 384.8278 391.0347
397.2416 403.4485 409.6554 415.8623 422.0692 428.2761
434.483 440.6899 446.8968 453.1037 459.3106 465.5175
471.7244 477.9313 484.1382 490.3451 496.552 502.7589
508.9658 515.1727 521.3796 527.5865 533.7934 540.0003
546.2072 552.4141 558.621 564.8279
217.2415 223.4484 229.6553 235.8622 242.0691 248.276
254.4829 260.6898 266.8967 273.1036 279.3105 285.5174

291.7243 297.9312 304.1381 310.345 316.5519 322.7588
328.9657 335.1726 341.3795 347.5864 353.7933 360.0002
366.2071 372.414 378.6209 384.8278 391.0347 397.2416
403.4485 409.6554 415.8623 422.0692 428.2761 434.483
440.6899 446.8968 453.1037 459.3106 465.5175 471.7244
477.9313 484.1382 490.3451 496.552 502.7589 508.9658
515.1727 521.3796 527.5865 533.7934 540.0003 546.2072
552.4141 558.621 564.8279 571.0348
223.4484 229.6553 235.8622 242.0691 248.276 254.4829
260.6898 266.8967 273.1036 279.3105 285.5174 291.7243
297.9312 304.1381 310.345 316.5519 322.7588 328.9657
335.1726 341.3795 347.5864 353.7933 360.0002 366.2071
372.414 378.6209 384.8278 391.0347 397.2416 403.4485
409.6554 415.8623 422.0692 428.2761 434.483 440.6899
446.8968 453.1037 459.3106 465.5175 471.7244 477.9313
484.1382 490.3451 496.552 502.7589 508.9658 515.1727
521.3796 527.5865 533.7934 540.0003 546.2072 552.4141
558.621 564.8279 571.0348 577.2417
229.6553 235.8622 242.0691 248.276 254.4829 260.6898
266.8967 273.1036 279.3105 285.5174 291.7243 297.9312
304.1381 310.345 316.5519 322.7588 328.9657 335.1726
341.3795 347.5864 353.7933 360.0002 366.2071 372.414
378.6209 384.8278 391.0347 397.2416 403.4485 409.6554
415.8623 422.0692 428.2761 434.483 440.6899 446.8968
453.1037 459.3106 465.5175 471.7244 477.9313 484.1382
490.3451 496.552 502.7589 508.9658 515.1727 521.3796
527.5865 533.7934 540.0003 546.2072 552.4141 558.621
564.8279 571.0348 577.2417 583.4486
235.8622 242.0691 248.276 254.4829 260.6898 266.8967
273.1036 279.3105 285.5174 291.7243 297.9312 304.1381
310.345 316.5519 322.7588 328.9657 335.1726 341.3795
347.5864 353.7933 360.0002 366.2071 372.414 378.6209
384.8278 391.0347 397.2416 403.4485 409.6554 415.8623
422.0692 428.2761 434.483 440.6899 446.8968 453.1037
459.3106 465.5175 471.7244 477.9313 484.1382 490.3451
496.552 502.7589 508.9658 515.1727 521.3796 527.5865
533.7934 540.0003 546.2072 552.4141 558.621 564.8279
571.0348 577.2417 583.4486 589.6555
242.0691 248.276 254.4829 260.6898 266.8967 273.1036
279.3105 285.5174 291.7243 297.9312 304.1381 310.345
316.5519 322.7588 328.9657 335.1726 341.3795 347.5864
353.7933 360.0002 366.2071 372.414 378.6209 384.8278
391.0347 397.2416 403.4485 409.6554 415.8623 422.0692
428.2761 434.483 440.6899 446.8968 453.1037 459.3106
465.5175 471.7244 477.9313 484.1382 490.3451 496.552
502.7589 508.9658 515.1727 521.3796 527.5865 533.7934

540.0003 546.2072 552.4141 558.621 564.8279 571.0348
577.2417 583.4486 589.6555 595.8624
248.276 254.4829 260.6898 266.8967 273.1036 279.3105
285.5174 291.7243 297.9312 304.1381 310.345 316.5519
322.7588 328.9657 335.1726 341.3795 347.5864 353.7933
360.0002 366.2071 372.414 378.6209 384.8278 391.0347
397.2416 403.4485 409.6554 415.8623 422.0692 428.2761
434.483 440.6899 446.8968 453.1037 459.3106 465.5175
471.7244 477.9313 484.1382 490.3451 496.552 502.7589
508.9658 515.1727 521.3796 527.5865 533.7934 540.0003
546.2072 552.4141 558.621 564.8279 571.0348 577.2417
583.4486 589.6555 595.8624 602.0693
254.4829 260.6898 266.8967 273.1036 279.3105 285.5174
291.7243 297.9312 304.1381 310.345 316.5519 322.7588
328.9657 335.1726 341.3795 347.5864 353.7933 360.0002
366.2071 372.414 378.6209 384.8278 391.0347 397.2416
403.4485 409.6554 415.8623 422.0692 428.2761 434.483
440.6899 446.8968 453.1037 459.3106 465.5175 471.7244
477.9313 484.1382 490.3451 496.552 502.7589 508.9658
515.1727 521.3796 527.5865 533.7934 540.0003 546.2072
552.4141 558.621 564.8279 571.0348 577.2417 583.4486
589.6555 595.8624 602.0693 608.2762
260.6898 266.8967 273.1036 279.3105 285.5174 291.7243
297.9312 304.1381 310.345 316.5519 322.7588 328.9657
335.1726 341.3795 347.5864 353.7933 360.0002 366.2071
372.414 378.6209 384.8278 391.0347 397.2416 403.4485
409.6554 415.8623 422.0692 428.2761 434.483 440.6899
446.8968 453.1037 459.3106 465.5175 471.7244 477.9313
484.1382 490.3451 496.552 502.7589 508.9658 515.1727
521.3796 527.5865 533.7934 540.0003 546.2072 552.4141
558.621 564.8279 571.0348 577.2417 583.4486 589.6555
595.8624 602.0693 608.2762 614.4831
266.8967 273.1036 279.3105 285.5174 291.7243 297.9312
304.1381 310.345 316.5519 322.7588 328.9657 335.1726
341.3795 347.5864 353.7933 360.0002 366.2071 372.414
378.6209 384.8278 391.0347 397.2416 403.4485 409.6554
415.8623 422.0692 428.2761 434.483 440.6899 446.8968
453.1037 459.3106 465.5175 471.7244 477.9313 484.1382
490.3451 496.552 502.7589 508.9658 515.1727 521.3796
527.5865 533.7934 540.0003 546.2072 552.4141 558.621
564.8279 571.0348 577.2417 583.4486 589.6555 595.8624
602.0693 608.2762 614.4831 620.69
273.1036 279.3105 285.5174 291.7243 297.9312 304.1381
310.345 316.5519 322.7588 328.9657 335.1726 341.3795
347.5864 353.7933 360.0002 366.2071 372.414 378.6209
384.8278 391.0347 397.2416 403.4485 409.6554 415.8623

422.0692 428.2761 434.483 440.6899 446.8968 453.1037
459.3106 465.5175 471.7244 477.9313 484.1382 490.3451
496.552 502.7589 508.9658 515.1727 521.3796 527.5865
533.7934 540.0003 546.2072 552.4141 558.621 564.8279
571.0348 577.2417 583.4486 589.6555 595.8624 602.0693
608.2762 614.4831 620.69 626.8969
279.3105 285.5174 291.7243 297.9312 304.1381 310.345
316.5519 322.7588 328.9657 335.1726 341.3795 347.5864
353.7933 360.0002 366.2071 372.414 378.6209 384.8278
391.0347 397.2416 403.4485 409.6554 415.8623 422.0692
428.2761 434.483 440.6899 446.8968 453.1037 459.3106
465.5175 471.7244 477.9313 484.1382 490.3451 496.552
502.7589 508.9658 515.1727 521.3796 527.5865 533.7934
540.0003 546.2072 552.4141 558.621 564.8279 571.0348
577.2417 583.4486 589.6555 595.8624 602.0693 608.2762
614.4831 620.69 626.8969 633.1038
285.5174 291.7243 297.9312 304.1381 310.345 316.5519
322.7588 328.9657 335.1726 341.3795 347.5864 353.7933
360.0002 366.2071 372.414 378.6209 384.8278 391.0347
397.2416 403.4485 409.6554 415.8623 422.0692 428.2761
434.483 440.6899 446.8968 453.1037 459.3106 465.5175
471.7244 477.9313 484.1382 490.3451 496.552 502.7589
508.9658 515.1727 521.3796 527.5865 533.7934 540.0003
546.2072 552.4141 558.621 564.8279 571.0348 577.2417
583.4486 589.6555 595.8624 602.0693 608.2762 614.4831
620.69 626.8969 633.1038 639.3107
291.7243 297.9312 304.1381 310.345 316.5519 322.7588
328.9657 335.1726 341.3795 347.5864 353.7933 360.0002
366.2071 372.414 378.6209 384.8278 391.0347 397.2416
403.4485 409.6554 415.8623 422.0692 428.2761 434.483
440.6899 446.8968 453.1037 459.3106 465.5175 471.7244
477.9313 484.1382 490.3451 496.552 502.7589 508.9658
515.1727 521.3796 527.5865 533.7934 540.0003 546.2072
552.4141 558.621 564.8279 571.0348 577.2417 583.4486
589.6555 595.8624 602.0693 608.2762 614.4831 620.69
626.8969 633.1038 639.3107 645.5176
297.9312 304.1381 310.345 316.5519 322.7588 328.9657
335.1726 341.3795 347.5864 353.7933 360.0002 366.2071
372.414 378.6209 384.8278 391.0347 397.2416 403.4485
409.6554 415.8623 422.0692 428.2761 434.483 440.6899
446.8968 453.1037 459.3106 465.5175 471.7244 477.9313
484.1382 490.3451 496.552 502.7589 508.9658 515.1727
521.3796 527.5865 533.7934 540.0003 546.2072 552.4141
558.621 564.8279 571.0348 577.2417 583.4486 589.6555
595.8624 602.0693 608.2762 614.4831 620.69 626.8969
633.1038 639.3107 645.5176 651.7245

304.1381 310.345 316.5519 322.7588 328.9657 335.1726
341.3795 347.5864 353.7933 360.0002 366.2071 372.414
378.6209 384.8278 391.0347 397.2416 403.4485 409.6554
415.8623 422.0692 428.2761 434.483 440.6899 446.8968
453.1037 459.3106 465.5175 471.7244 477.9313 484.1382
490.3451 496.552 502.7589 508.9658 515.1727 521.3796
527.5865 533.7934 540.0003 546.2072 552.4141 558.621
564.8279 571.0348 577.2417 583.4486 589.6555 595.8624
602.0693 608.2762 614.4831 620.69 626.8969 633.1038
639.3107 645.5176 651.7245 657.9314
310.345 316.5519 322.7588 328.9657 335.1726 341.3795
347.5864 353.7933 360.0002 366.2071 372.414 378.6209
384.8278 391.0347 397.2416 403.4485 409.6554 415.8623
422.0692 428.2761 434.483 440.6899 446.8968 453.1037
459.3106 465.5175 471.7244 477.9313 484.1382 490.3451
496.552 502.7589 508.9658 515.1727 521.3796 527.5865
533.7934 540.0003 546.2072 552.4141 558.621 564.8279
571.0348 577.2417 583.4486 589.6555 595.8624 602.0693
608.2762 614.4831 620.69 626.8969 633.1038 639.3107
645.5176 651.7245 657.9314 664.1383
316.5519 322.7588 328.9657 335.1726 341.3795 347.5864
353.7933 360.0002 366.2071 372.414 378.6209 384.8278
391.0347 397.2416 403.4485 409.6554 415.8623 422.0692
428.2761 434.483 440.6899 446.8968 453.1037 459.3106
465.5175 471.7244 477.9313 484.1382 490.3451 496.552
502.7589 508.9658 515.1727 521.3796 527.5865 533.7934
540.0003 546.2072 552.4141 558.621 564.8279 571.0348
577.2417 583.4486 589.6555 595.8624 602.0693 608.2762
614.4831 620.69 626.8969 633.1038 639.3107 645.5176
651.7245 657.9314 664.1383 670.3452
322.7588 328.9657 335.1726 341.3795 347.5864 353.7933
360.0002 366.2071 372.414 378.6209 384.8278 391.0347
397.2416 403.4485 409.6554 415.8623 422.0692 428.2761
434.483 440.6899 446.8968 453.1037 459.3106 465.5175
471.7244 477.9313 484.1382 490.3451 496.552 502.7589
508.9658 515.1727 521.3796 527.5865 533.7934 540.0003
546.2072 552.4141 558.621 564.8279 571.0348 577.2417
583.4486 589.6555 595.8624 602.0693 608.2762 614.4831
620.69 626.8969 633.1038 639.3107 645.5176 651.7245
657.9314 664.1383 670.3452 676.5521
328.9657 335.1726 341.3795 347.5864 353.7933 360.0002
366.2071 372.414 378.6209 384.8278 391.0347 397.2416
403.4485 409.6554 415.8623 422.0692 428.2761 434.483
440.6899 446.8968 453.1037 459.3106 465.5175 471.7244
477.9313 484.1382 490.3451 496.552 502.7589 508.9658
515.1727 521.3796 527.5865 533.7934 540.0003 546.2072

552.4141 558.621 564.8279 571.0348 577.2417 583.4486
589.6555 595.8624 602.0693 608.2762 614.4831 620.69
626.8969 633.1038 639.3107 645.5176 651.7245 657.9314
664.1383 670.3452 676.5521 682.759
335.1726 341.3795 347.5864 353.7933 360.0002 366.2071
372.414 378.6209 384.8278 391.0347 397.2416 403.4485
409.6554 415.8623 422.0692 428.2761 434.483 440.6899
446.8968 453.1037 459.3106 465.5175 471.7244 477.9313
484.1382 490.3451 496.552 502.7589 508.9658 515.1727
521.3796 527.5865 533.7934 540.0003 546.2072 552.4141
558.621 564.8279 571.0348 577.2417 583.4486 589.6555
595.8624 602.0693 608.2762 614.4831 620.69 626.8969
633.1038 639.3107 645.5176 651.7245 657.9314 664.1383
670.3452 676.5521 682.759 688.9659
341.3795 347.5864 353.7933 360.0002 366.2071 372.414
378.6209 384.8278 391.0347 397.2416 403.4485 409.6554
415.8623 422.0692 428.2761 434.483 440.6899 446.8968
453.1037 459.3106 465.5175 471.7244 477.9313 484.1382
490.3451 496.552 502.7589 508.9658 515.1727 521.3796
527.5865 533.7934 540.0003 546.2072 552.4141 558.621
564.8279 571.0348 577.2417 583.4486 589.6555 595.8624
602.0693 608.2762 614.4831 620.69 626.8969 633.1038
639.3107 645.5176 651.7245 657.9314 664.1383 670.3452
676.5521 682.759 688.9659 695.1728
347.5864 353.7933 360.0002 366.2071 372.414 378.6209
384.8278 391.0347 397.2416 403.4485 409.6554 415.8623
422.0692 428.2761 434.483 440.6899 446.8968 453.1037
459.3106 465.5175 471.7244 477.9313 484.1382 490.3451
496.552 502.7589 508.9658 515.1727 521.3796 527.5865
533.7934 540.0003 546.2072 552.4141 558.621 564.8279
571.0348 577.2417 583.4486 589.6555 595.8624 602.0693
608.2762 614.4831 620.69 626.8969 633.1038 639.3107
645.5176 651.7245 657.9314 664.1383 670.3452 676.5521
682.759 688.9659 695.1728 701.3797
353.7933 360.0002 366.2071 372.414 378.6209 384.8278
391.0347 397.2416 403.4485 409.6554 415.8623 422.0692
428.2761 434.483 440.6899 446.8968 453.1037 459.3106
465.5175 471.7244 477.9313 484.1382 490.3451 496.552
502.7589 508.9658 515.1727 521.3796 527.5865 533.7934
540.0003 546.2072 552.4141 558.621 564.8279 571.0348
577.2417 583.4486 589.6555 595.8624 602.0693 608.2762
614.4831 620.69 626.8969 633.1038 639.3107 645.5176
651.7245 657.9314 664.1383 670.3452 676.5521 682.759
688.9659 695.1728 701.3797 707.5866
];

m = [0.530332229 0.530332229 0.530332229 0.530332229 0.530332229 0.530332229
0.530332229 0.530332229 0.530332229 0.530332229 0.530332229 0.530332229
0.530332229 0.530332229 0.530332229 0.530332229 0.530332229 0.530332229
0.530332229 0.530332229 0.530332229 0.530332229 0.530332229 0.530332229
0.530332229 0.530332229 0.530332229 0.530332229 0.530332229 0.530332229
0.530332229 0.530332229 0.530332229 0.530332229 0.530332229 0.530332229
0.530332229 0.530332229 0.530332229 0.530332229 0.530332229 0.530332229
0.530332229 0.530332229 0.530332229 0.530332229
0.530332229 0.530332229 0.952382455 0.952382455 0.530332229 0.530332229
0.530332229 0.530332229 0.952382455 0.530332229 0.952382455 0.952382455
0.952382455 0.530332229 0.952382455 0.952382455 0.530332229 0.952382455
0.952382455 0.952382455 0.530332229 0.952382455 0.530332229 0.530332229
0.530332229 0.530332229 0.952382455 0.952382455 0.530332229 0.530332229
0.530332229 0.952382455 0.952382455 0.530332229 0.530332229 0.530332229
0.530332229 0.952382455 0.530332229 0.952382455 0.952382455 0.952382455
0.530332229 0.952382455 0.952382455 0.530332229 0.952382455 0.952382455
0.952382455 0.530332229 0.952382455 0.530332229 0.530332229 0.530332229
0.530332229 0.952382455 0.952382455 0.530332229
0.530332229 0.952382455 0.530332229 0.530332229 0.952382455 0.952382455
0.952382455 0.952382455 0.530332229 0.952382455 0.530332229 0.530332229
0.530332229 0.952382455 0.530332229 0.530332229 0.952382455 0.530332229
0.530332229 0.530332229 0.952382455 0.530332229 0.952382455 0.952382455
0.952382455 0.952382455 0.530332229 0.530332229 0.952382455 0.530332229
0.952382455 0.530332229 0.530332229 0.952382455 0.952382455 0.952382455
0.952382455 0.530332229 0.952382455 0.530332229 0.530332229 0.530332229
0.952382455 0.530332229 0.530332229 0.952382455 0.530332229 0.530332229
0.530332229 0.952382455 0.530332229 0.952382455 0.952382455 0.952382455
0.952382455 0.530332229 0.530332229 0.952382455
0.530332229 0.952382455 0.530332229 0.530332229 0.952382455 0.952382455
0.952382455 0.952382455 0.530332229 0.952382455 0.530332229 0.530332229
0.530332229 0.952382455 0.530332229 0.530332229 0.952382455 0.530332229
0.530332229 0.530332229 0.952382455 0.530332229 0.952382455 0.952382455
0.952382455 0.952382455 0.530332229 0.530332229 0.952382455 0.530332229
0.952382455 0.530332229 0.530332229 0.952382455 0.952382455 0.952382455
0.952382455 0.530332229 0.952382455 0.530332229 0.530332229 0.530332229
0.952382455 0.530332229 0.530332229 0.952382455 0.530332229 0.530332229
0.530332229 0.952382455 0.530332229 0.952382455 0.952382455 0.952382455
0.952382455 0.530332229 0.530332229 0.952382455
0.530332229 0.530332229 0.952382455 0.952382455 0.530332229 0.530332229
0.530332229 0.530332229 0.952382455 0.530332229 0.952382455 0.952382455
0.952382455 0.530332229 0.952382455 0.952382455 0.530332229 0.952382455
0.952382455 0.952382455 0.530332229 0.952382455 0.530332229 0.530332229
0.530332229 0.530332229 0.952382455 0.952382455 0.530332229 0.530332229
0.530332229 0.952382455 0.952382455 0.530332229 0.530332229 0.530332229

```
        0.530332229  0.952382455  0.530332229  0.952382455  0.952382455  0.952382455
        0.530332229  0.952382455  0.952382455  0.530332229  0.952382455  0.952382455
        0.952382455  0.530332229  0.952382455  0.530332229  0.530332229  0.530332229
        0.530332229  0.952382455  0.952382455  0.530332229
0.530332229  0.530332229  0.952382455  0.952382455  0.530332229  0.530332229
        0.530332229  0.530332229  0.952382455  0.530332229  0.952382455  0.952382455
        0.952382455  0.530332229  0.952382455  0.952382455  0.530332229  0.952382455
        0.952382455  0.952382455  0.530332229  0.952382455  0.530332229  0.530332229
        0.530332229  0.530332229  0.952382455  0.952382455  0.530332229  0.530332229
        0.530332229  0.952382455  0.952382455  0.530332229  0.530332229  0.530332229
        0.530332229  0.952382455  0.530332229  0.952382455  0.952382455  0.952382455
        0.530332229  0.952382455  0.952382455  0.530332229  0.952382455  0.952382455
        0.952382455  0.530332229  0.952382455  0.530332229  0.530332229  0.530332229
        0.530332229  0.952382455  0.952382455  0.530332229
0.530332229  0.530332229  0.952382455  0.952382455  0.530332229  0.530332229
        0.530332229  0.530332229  0.952382455  0.530332229  0.952382455  0.952382455
        0.952382455  0.530332229  0.952382455  0.952382455  0.530332229  0.952382455
        0.952382455  0.952382455  0.530332229  0.952382455  0.530332229  0.530332229
        0.530332229  0.530332229  0.952382455  0.952382455  0.530332229  0.530332229
        0.530332229  0.952382455  0.952382455  0.530332229  0.530332229  0.530332229
        0.530332229  0.952382455  0.530332229  0.952382455  0.952382455  0.952382455
        0.530332229  0.952382455  0.952382455  0.530332229  0.952382455  0.952382455
        0.952382455  0.530332229  0.952382455  0.530332229  0.530332229  0.530332229
        0.530332229  0.952382455  0.952382455  0.530332229
0.530332229  0.530332229  0.952382455  0.952382455  0.530332229  0.530332229
        0.530332229  0.530332229  0.952382455  0.530332229  0.952382455  0.952382455
        0.952382455  0.530332229  0.952382455  0.952382455  0.530332229  0.952382455
        0.952382455  0.952382455  0.530332229  0.952382455  0.530332229  0.530332229
        0.530332229  0.530332229  0.952382455  0.952382455  0.530332229  0.530332229
        0.530332229  0.952382455  0.952382455  0.530332229  0.530332229  0.530332229
        0.530332229  0.952382455  0.530332229  0.952382455  0.952382455  0.952382455
        0.530332229  0.952382455  0.952382455  0.530332229  0.952382455  0.952382455
        0.952382455  0.530332229  0.952382455  0.530332229  0.530332229  0.530332229
        0.530332229  0.952382455  0.952382455  0.530332229
0.530332229  0.952382455  0.530332229  0.530332229  0.952382455  0.952382455
        0.952382455  0.952382455  0.530332229  0.952382455  0.530332229  0.530332229
        0.530332229  0.952382455  0.530332229  0.530332229  0.952382455  0.530332229
        0.530332229  0.530332229  0.952382455  0.530332229  0.952382455  0.952382455
        0.952382455  0.952382455  0.530332229  0.530332229  0.952382455  0.530332229
        0.952382455  0.530332229  0.530332229  0.952382455  0.952382455  0.952382455
        0.952382455  0.530332229  0.952382455  0.530332229  0.530332229  0.530332229
        0.952382455  0.530332229  0.530332229  0.952382455  0.530332229  0.530332229
        0.530332229  0.952382455  0.530332229  0.952382455  0.952382455  0.952382455
        0.952382455  0.530332229  0.530332229  0.952382455
0.530332229  0.530332229  0.952382455  0.952382455  0.530332229  0.530332229
        0.530332229  0.530332229  0.952382455  0.530332229  0.952382455  0.952382455
```

```
    0.952382455  0.530332229  0.952382455  0.952382455  0.530332229  0.952382455
    0.952382455  0.952382455  0.530332229  0.952382455  0.530332229  0.530332229
    0.530332229  0.530332229  0.952382455  0.952382455  0.530332229  0.530332229
    0.530332229  0.952382455  0.952382455  0.530332229  0.530332229  0.530332229
    0.530332229  0.952382455  0.530332229  0.952382455  0.952382455  0.952382455
    0.530332229  0.952382455  0.952382455  0.530332229  0.952382455  0.952382455
    0.952382455  0.530332229  0.952382455  0.530332229  0.530332229  0.530332229
    0.530332229  0.952382455  0.952382455  0.530332229
0.530332229  0.952382455  0.530332229  0.530332229  0.952382455  0.952382455
    0.952382455  0.952382455  0.530332229  0.952382455  0.530332229  0.530332229
    0.530332229  0.952382455  0.530332229  0.530332229  0.952382455  0.530332229
    0.530332229  0.530332229  0.952382455  0.530332229  0.952382455  0.952382455
    0.952382455  0.952382455  0.530332229  0.530332229  0.952382455  0.530332229
    0.952382455  0.530332229  0.530332229  0.952382455  0.952382455  0.952382455
    0.952382455  0.530332229  0.952382455  0.530332229  0.530332229  0.530332229
    0.952382455  0.530332229  0.530332229  0.952382455  0.530332229  0.530332229
    0.530332229  0.952382455  0.530332229  0.952382455  0.952382455  0.952382455
    0.952382455  0.530332229  0.530332229  0.952382455
0.530332229  0.952382455  0.530332229  0.530332229  0.952382455  0.952382455
    0.952382455  0.952382455  0.530332229  0.952382455  0.530332229  0.530332229
    0.530332229  0.952382455  0.530332229  0.530332229  0.952382455  0.530332229
    0.530332229  0.530332229  0.952382455  0.530332229  0.952382455  0.952382455
    0.952382455  0.952382455  0.530332229  0.530332229  0.952382455  0.530332229
    0.952382455  0.530332229  0.530332229  0.952382455  0.952382455  0.952382455
    0.952382455  0.530332229  0.952382455  0.530332229  0.530332229  0.530332229
    0.952382455  0.530332229  0.530332229  0.952382455  0.530332229  0.530332229
    0.530332229  0.952382455  0.530332229  0.952382455  0.952382455  0.952382455
    0.952382455  0.530332229  0.530332229  0.952382455
0.530332229  0.952382455  0.530332229  0.530332229  0.952382455  0.952382455
    0.952382455  0.952382455  0.530332229  0.952382455  0.530332229  0.530332229
    0.530332229  0.952382455  0.530332229  0.530332229  0.952382455  0.530332229
    0.530332229  0.530332229  0.952382455  0.530332229  0.952382455  0.952382455
    0.952382455  0.952382455  0.530332229  0.530332229  0.952382455  0.530332229
    0.952382455  0.530332229  0.530332229  0.952382455  0.952382455  0.952382455
    0.952382455  0.530332229  0.952382455  0.530332229  0.530332229  0.530332229
    0.952382455  0.530332229  0.530332229  0.952382455  0.530332229  0.530332229
    0.530332229  0.952382455  0.530332229  0.952382455  0.952382455  0.952382455
    0.952382455  0.530332229  0.530332229  0.952382455
0.530332229  0.530332229  0.952382455  0.952382455  0.530332229  0.530332229
    0.530332229  0.530332229  0.952382455  0.530332229  0.952382455  0.952382455
    0.952382455  0.530332229  0.952382455  0.952382455  0.530332229  0.952382455
    0.952382455  0.952382455  0.530332229  0.952382455  0.530332229  0.530332229
    0.530332229  0.530332229  0.952382455  0.952382455  0.530332229  0.530332229
    0.530332229  0.952382455  0.952382455  0.530332229  0.530332229  0.530332229
    0.530332229  0.952382455  0.530332229  0.952382455  0.952382455  0.952382455
    0.530332229  0.952382455  0.952382455  0.530332229  0.952382455  0.952382455
```

0.952382455 0.530332229 0.952382455 0.530332229 0.530332229 0.530332229
0.530332229 0.952382455 0.952382455 0.530332229
0.530332229 0.952382455 0.530332229 0.530332229 0.952382455 0.952382455
0.952382455 0.952382455 0.530332229 0.952382455 0.530332229 0.530332229
0.530332229 0.952382455 0.530332229 0.530332229 0.952382455 0.530332229
0.530332229 0.530332229 0.952382455 0.530332229 0.952382455 0.952382455
0.952382455 0.952382455 0.530332229 0.530332229 0.952382455 0.530332229
0.952382455 0.530332229 0.530332229 0.952382455 0.952382455 0.952382455
0.952382455 0.530332229 0.952382455 0.530332229 0.530332229 0.530332229
0.952382455 0.530332229 0.530332229 0.952382455 0.530332229 0.530332229
0.530332229 0.952382455 0.530332229 0.952382455 0.952382455 0.952382455
0.952382455 0.530332229 0.530332229 0.952382455
0.530332229 0.952382455 0.530332229 0.530332229 0.952382455 0.952382455
0.952382455 0.952382455 0.530332229 0.952382455 0.530332229 0.530332229
0.530332229 0.952382455 0.530332229 0.530332229 0.952382455 0.530332229
0.530332229 0.530332229 0.952382455 0.530332229 0.952382455 0.952382455
0.952382455 0.952382455 0.530332229 0.530332229 0.952382455 0.530332229
0.952382455 0.530332229 0.530332229 0.952382455 0.952382455 0.952382455
0.952382455 0.530332229 0.952382455 0.530332229 0.530332229 0.530332229
0.952382455 0.530332229 0.530332229 0.952382455 0.530332229 0.530332229
0.530332229 0.952382455 0.530332229 0.952382455 0.952382455 0.952382455
0.952382455 0.530332229 0.530332229 0.952382455
0.530332229 0.530332229 0.952382455 0.952382455 0.530332229 0.530332229
0.530332229 0.530332229 0.952382455 0.530332229 0.952382455 0.952382455
0.952382455 0.530332229 0.952382455 0.952382455 0.530332229 0.952382455
0.952382455 0.952382455 0.530332229 0.952382455 0.530332229 0.530332229
0.530332229 0.530332229 0.952382455 0.952382455 0.530332229 0.530332229
0.530332229 0.952382455 0.952382455 0.530332229 0.530332229 0.530332229
0.530332229 0.952382455 0.530332229 0.952382455 0.952382455 0.952382455
0.530332229 0.952382455 0.952382455 0.530332229 0.952382455 0.952382455
0.952382455 0.530332229 0.952382455 0.530332229 0.530332229 0.530332229
0.530332229 0.952382455 0.952382455 0.530332229
0.530332229 0.952382455 0.530332229 0.530332229 0.952382455 0.952382455
0.952382455 0.952382455 0.530332229 0.952382455 0.530332229 0.530332229
0.530332229 0.952382455 0.530332229 0.530332229 0.952382455 0.530332229
0.530332229 0.530332229 0.952382455 0.530332229 0.952382455 0.952382455
0.952382455 0.952382455 0.530332229 0.530332229 0.952382455 0.530332229
0.952382455 0.530332229 0.530332229 0.952382455 0.952382455 0.952382455
0.952382455 0.530332229 0.530332229 0.952382455
0.530332229 0.952382455 0.530332229 0.530332229 0.952382455 0.952382455
0.952382455 0.952382455 0.530332229 0.952382455 0.530332229 0.530332229
0.530332229 0.952382455 0.530332229 0.530332229 0.952382455 0.530332229
0.530332229 0.530332229 0.952382455 0.530332229 0.952382455 0.952382455

0.952382455 0.952382455 0.530332229 0.530332229 0.952382455 0.530332229
0.952382455 0.530332229 0.530332229 0.952382455 0.952382455 0.952382455
0.952382455 0.530332229 0.952382455 0.530332229 0.530332229 0.530332229
0.952382455 0.530332229 0.530332229 0.952382455 0.530332229 0.530332229
0.530332229 0.952382455 0.530332229 0.952382455 0.952382455 0.952382455
0.952382455 0.530332229 0.530332229 0.952382455
0.530332229 0.952382455 0.530332229 0.530332229 0.952382455 0.952382455
0.952382455 0.952382455 0.530332229 0.952382455 0.530332229 0.530332229
0.530332229 0.952382455 0.530332229 0.530332229 0.952382455 0.530332229
0.530332229 0.530332229 0.952382455 0.530332229 0.952382455 0.952382455
0.952382455 0.952382455 0.530332229 0.530332229 0.952382455 0.530332229
0.952382455 0.530332229 0.530332229 0.952382455 0.952382455 0.952382455
0.952382455 0.530332229 0.952382455 0.530332229 0.530332229 0.530332229
0.952382455 0.530332229 0.530332229 0.952382455 0.530332229 0.530332229
0.530332229 0.952382455 0.530332229 0.952382455 0.952382455 0.952382455
0.952382455 0.530332229 0.530332229 0.952382455
0.530332229 0.530332229 0.952382455 0.952382455 0.530332229 0.530332229
0.530332229 0.530332229 0.952382455 0.530332229 0.952382455 0.952382455
0.952382455 0.530332229 0.952382455 0.952382455 0.530332229 0.952382455
0.952382455 0.952382455 0.530332229 0.952382455 0.530332229 0.530332229
0.530332229 0.530332229 0.952382455 0.952382455 0.530332229 0.530332229
0.530332229 0.952382455 0.952382455 0.530332229 0.530332229 0.530332229
0.530332229 0.952382455 0.530332229 0.952382455 0.952382455 0.952382455
0.530332229 0.952382455 0.952382455 0.530332229 0.952382455 0.952382455
0.952382455 0.530332229 0.952382455 0.530332229 0.530332229 0.530332229
0.530332229 0.952382455 0.952382455 0.530332229
0.530332229 0.952382455 0.530332229 0.530332229 0.952382455 0.952382455
0.952382455 0.952382455 0.530332229 0.952382455 0.530332229 0.530332229
0.530332229 0.952382455 0.530332229 0.530332229 0.952382455 0.530332229
0.530332229 0.530332229 0.952382455 0.530332229 0.952382455 0.952382455
0.952382455 0.952382455 0.530332229 0.530332229 0.952382455 0.530332229
0.952382455 0.530332229 0.530332229 0.952382455 0.952382455 0.952382455
0.952382455 0.530332229 0.530332229 0.952382455 0.530332229 0.530332229
0.530332229 0.952382455 0.530332229 0.952382455 0.952382455 0.952382455
0.952382455 0.530332229 0.530332229 0.952382455
0.530332229 0.530332229 0.952382455 0.952382455 0.530332229 0.530332229
0.530332229 0.530332229 0.952382455 0.530332229 0.952382455 0.952382455
0.952382455 0.530332229 0.952382455 0.952382455 0.530332229 0.952382455
0.952382455 0.952382455 0.530332229 0.952382455 0.530332229 0.530332229
0.530332229 0.530332229 0.952382455 0.952382455 0.530332229 0.530332229
0.530332229 0.952382455 0.952382455 0.530332229 0.530332229 0.530332229
0.530332229 0.952382455 0.530332229 0.952382455 0.952382455 0.952382455
0.530332229 0.952382455 0.952382455 0.530332229 0.952382455 0.952382455
0.952382455 0.530332229 0.952382455 0.530332229 0.530332229 0.530332229
0.530332229 0.952382455 0.952382455 0.530332229

```
0.530332229  0.530332229  0.952382455  0.952382455  0.530332229  0.530332229
    0.530332229  0.530332229  0.952382455  0.530332229  0.952382455  0.952382455
    0.952382455  0.530332229  0.952382455  0.952382455  0.530332229  0.952382455
    0.952382455  0.952382455  0.530332229  0.952382455  0.530332229  0.530332229
    0.530332229  0.530332229  0.952382455  0.952382455  0.530332229  0.530332229
    0.530332229  0.952382455  0.952382455  0.530332229  0.530332229  0.530332229
    0.530332229  0.952382455  0.530332229  0.952382455  0.952382455  0.952382455
    0.530332229  0.952382455  0.952382455  0.530332229  0.952382455  0.952382455
    0.952382455  0.530332229  0.952382455  0.530332229  0.530332229  0.530332229
    0.530332229  0.952382455  0.952382455  0.530332229
0.530332229  0.530332229  0.952382455  0.952382455  0.530332229  0.530332229
    0.530332229  0.530332229  0.952382455  0.530332229  0.952382455  0.952382455
    0.952382455  0.530332229  0.952382455  0.952382455  0.530332229  0.952382455
    0.952382455  0.952382455  0.530332229  0.952382455  0.530332229  0.530332229
    0.530332229  0.530332229  0.952382455  0.952382455  0.530332229  0.530332229
    0.530332229  0.952382455  0.952382455  0.530332229  0.530332229  0.530332229
    0.530332229  0.952382455  0.530332229  0.952382455  0.952382455  0.952382455
    0.530332229  0.952382455  0.952382455  0.530332229  0.952382455  0.952382455
    0.952382455  0.530332229  0.952382455  0.530332229  0.530332229  0.530332229
    0.530332229  0.952382455  0.952382455  0.530332229
0.530332229  0.530332229  0.952382455  0.952382455  0.530332229  0.530332229
    0.530332229  0.530332229  0.952382455  0.530332229  0.952382455  0.952382455
    0.952382455  0.530332229  0.952382455  0.952382455  0.530332229  0.952382455
    0.952382455  0.952382455  0.530332229  0.952382455  0.530332229  0.530332229
    0.530332229  0.530332229  0.952382455  0.952382455  0.530332229  0.530332229
    0.530332229  0.952382455  0.952382455  0.530332229  0.530332229  0.530332229
    0.530332229  0.952382455  0.530332229  0.952382455  0.952382455  0.952382455
    0.530332229  0.952382455  0.952382455  0.530332229  0.952382455  0.952382455
    0.952382455  0.530332229  0.952382455  0.530332229  0.530332229  0.530332229
    0.530332229  0.952382455  0.952382455  0.530332229
0.530332229  0.952382455  0.530332229  0.530332229  0.952382455  0.952382455
    0.952382455  0.952382455  0.530332229  0.952382455  0.530332229  0.530332229
    0.530332229  0.952382455  0.530332229  0.530332229  0.952382455  0.530332229
    0.530332229  0.530332229  0.952382455  0.530332229  0.952382455  0.952382455
    0.952382455  0.952382455  0.530332229  0.530332229  0.952382455  0.530332229
    0.952382455  0.530332229  0.530332229  0.952382455  0.952382455  0.952382455
    0.952382455  0.530332229  0.952382455  0.530332229  0.530332229  0.530332229
    0.952382455  0.530332229  0.530332229  0.952382455  0.530332229  0.530332229
    0.530332229  0.952382455  0.530332229  0.952382455  0.952382455  0.952382455
    0.952382455  0.530332229  0.530332229  0.952382455
0.530332229  0.952382455  0.530332229  0.530332229  0.952382455  0.952382455
    0.952382455  0.952382455  0.530332229  0.952382455  0.530332229  0.530332229
    0.530332229  0.952382455  0.530332229  0.530332229  0.952382455  0.530332229
    0.530332229  0.530332229  0.952382455  0.530332229  0.952382455  0.952382455
    0.952382455  0.952382455  0.530332229  0.530332229  0.952382455  0.530332229
    0.952382455  0.530332229  0.530332229  0.952382455  0.952382455  0.952382455
```

0.952382455 0.530332229 0.952382455 0.530332229 0.530332229 0.530332229
0.952382455 0.530332229 0.530332229 0.952382455 0.530332229 0.530332229
0.530332229 0.952382455 0.530332229 0.952382455 0.952382455 0.952382455
0.952382455 0.530332229 0.530332229 0.952382455
0.530332229 0.530332229 0.952382455 0.952382455 0.530332229 0.530332229
0.530332229 0.530332229 0.952382455 0.530332229 0.952382455 0.952382455
0.952382455 0.530332229 0.952382455 0.952382455 0.530332229 0.952382455
0.952382455 0.952382455 0.530332229 0.952382455 0.530332229 0.530332229
0.530332229 0.530332229 0.952382455 0.952382455 0.530332229 0.530332229
0.530332229 0.952382455 0.952382455 0.530332229 0.530332229 0.530332229
0.530332229 0.952382455 0.530332229 0.952382455 0.952382455 0.952382455
0.530332229 0.952382455 0.952382455 0.530332229 0.952382455 0.952382455
0.952382455 0.530332229 0.952382455 0.530332229 0.530332229 0.530332229
0.530332229 0.952382455 0.952382455 0.530332229
0.530332229 0.530332229 0.530332229 0.530332229 0.530332229 0.530332229
0.530332229 0.530332229 0.530332229 0.530332229 0.530332229 0.530332229
0.530332229 0.530332229 0.530332229 0.530332229 0.530332229 0.530332229
0.530332229 0.530332229 0.530332229 0.530332229 0.530332229 0.530332229
0.530332229 0.530332229 0.530332229 0.530332229 0.530332229 0.530332229
0.530332229 0.530332229 0.530332229 0.530332229 0.530332229 0.530332229
0.530332229 0.530332229 0.530332229 0.530332229 0.530332229 0.530332229
0.530332229 0.530332229 0.530332229 0.530332229 0.530332229 0.530332229
0.530332229 0.530332229 0.530332229 0.530332229
0.530332229 0.530332229 0.952382455 0.952382455 0.530332229 0.530332229
0.530332229 0.530332229 0.952382455 0.530332229 0.952382455 0.952382455
0.952382455 0.530332229 0.952382455 0.952382455 0.530332229 0.952382455
0.952382455 0.952382455 0.530332229 0.952382455 0.530332229 0.530332229
0.530332229 0.530332229 0.952382455 0.952382455 0.530332229 0.530332229
0.530332229 0.952382455 0.952382455 0.530332229 0.530332229 0.530332229
0.530332229 0.952382455 0.530332229 0.952382455 0.952382455 0.952382455
0.530332229 0.952382455 0.952382455 0.530332229 0.952382455 0.952382455
0.952382455 0.530332229 0.952382455 0.530332229 0.530332229 0.530332229
0.530332229 0.952382455 0.952382455 0.530332229
0.530332229 0.952382455 0.530332229 0.530332229 0.952382455 0.952382455
0.952382455 0.952382455 0.530332229 0.952382455 0.530332229 0.530332229
0.530332229 0.952382455 0.530332229 0.530332229 0.952382455 0.530332229
0.530332229 0.530332229 0.952382455 0.530332229 0.952382455 0.952382455
0.952382455 0.952382455 0.530332229 0.530332229 0.952382455 0.530332229
0.952382455 0.530332229 0.530332229 0.952382455 0.952382455 0.952382455
0.952382455 0.530332229 0.952382455 0.530332229 0.530332229 0.530332229
0.530332229 0.952382455 0.530332229 0.952382455 0.952382455 0.952382455
0.952382455 0.530332229 0.530332229 0.952382455
0.530332229 0.952382455 0.530332229 0.530332229 0.952382455 0.952382455
0.952382455 0.952382455 0.530332229 0.952382455 0.530332229 0.530332229

```
    0.530332229  0.952382455  0.530332229  0.530332229  0.952382455  0.530332229
    0.530332229  0.530332229  0.952382455  0.530332229  0.952382455  0.952382455
    0.952382455  0.952382455  0.530332229  0.530332229  0.952382455  0.530332229
    0.952382455  0.530332229  0.530332229  0.952382455  0.952382455  0.952382455
    0.952382455  0.530332229  0.952382455  0.530332229  0.530332229  0.530332229
    0.952382455  0.530332229  0.530332229  0.952382455  0.530332229  0.530332229
    0.530332229  0.952382455  0.530332229  0.952382455  0.952382455  0.952382455
    0.952382455  0.530332229  0.530332229  0.952382455
0.530332229  0.530332229  0.952382455  0.952382455  0.530332229  0.530332229
    0.530332229  0.530332229  0.952382455  0.530332229  0.952382455  0.952382455
    0.952382455  0.530332229  0.952382455  0.952382455  0.530332229  0.952382455
    0.952382455  0.952382455  0.530332229  0.952382455  0.530332229  0.530332229
    0.530332229  0.530332229  0.952382455  0.952382455  0.530332229  0.530332229
    0.530332229  0.952382455  0.952382455  0.530332229  0.530332229  0.530332229
    0.530332229  0.952382455  0.530332229  0.952382455  0.952382455  0.952382455
    0.530332229  0.952382455  0.952382455  0.530332229  0.952382455  0.952382455
    0.952382455  0.530332229  0.952382455  0.530332229  0.530332229  0.530332229
    0.530332229  0.952382455  0.952382455  0.530332229
0.530332229  0.530332229  0.952382455  0.952382455  0.530332229  0.530332229
    0.530332229  0.530332229  0.952382455  0.530332229  0.952382455  0.952382455
    0.952382455  0.530332229  0.952382455  0.952382455  0.530332229  0.952382455
    0.952382455  0.952382455  0.530332229  0.952382455  0.530332229  0.530332229
    0.530332229  0.530332229  0.952382455  0.952382455  0.530332229  0.530332229
    0.530332229  0.952382455  0.952382455  0.530332229  0.530332229  0.530332229
    0.530332229  0.952382455  0.530332229  0.952382455  0.952382455  0.952382455
    0.530332229  0.952382455  0.952382455  0.530332229  0.952382455  0.952382455
    0.952382455  0.530332229  0.952382455  0.530332229  0.530332229  0.530332229
    0.530332229  0.952382455  0.952382455  0.530332229
0.530332229  0.530332229  0.952382455  0.952382455  0.530332229  0.530332229
    0.530332229  0.530332229  0.952382455  0.530332229  0.952382455  0.952382455
    0.952382455  0.530332229  0.952382455  0.952382455  0.530332229  0.952382455
    0.952382455  0.952382455  0.530332229  0.952382455  0.530332229  0.530332229
    0.530332229  0.530332229  0.952382455  0.952382455  0.530332229  0.530332229
    0.530332229  0.952382455  0.952382455  0.530332229  0.530332229  0.530332229
    0.530332229  0.952382455  0.530332229  0.952382455  0.952382455  0.952382455
    0.530332229  0.952382455  0.952382455  0.530332229  0.952382455  0.952382455
    0.952382455  0.530332229  0.952382455  0.530332229  0.530332229  0.530332229
    0.530332229  0.952382455  0.952382455  0.530332229
0.530332229  0.530332229  0.952382455  0.952382455  0.530332229  0.530332229
    0.530332229  0.530332229  0.952382455  0.530332229  0.952382455  0.952382455
    0.952382455  0.530332229  0.952382455  0.952382455  0.530332229  0.952382455
    0.952382455  0.952382455  0.530332229  0.952382455  0.530332229  0.530332229
    0.530332229  0.530332229  0.952382455  0.952382455  0.530332229  0.530332229
    0.530332229  0.952382455  0.952382455  0.530332229  0.530332229  0.530332229
    0.530332229  0.952382455  0.530332229  0.952382455  0.952382455  0.952382455
    0.530332229  0.952382455  0.952382455  0.530332229  0.952382455  0.952382455
```

0.952382455 0.530332229 0.952382455 0.530332229 0.530332229 0.530332229
0.530332229 0.952382455 0.952382455 0.530332229
0.530332229 0.952382455 0.530332229 0.530332229 0.952382455 0.952382455
0.952382455 0.952382455 0.530332229 0.952382455 0.530332229 0.530332229
0.530332229 0.952382455 0.530332229 0.530332229 0.952382455 0.530332229
0.530332229 0.530332229 0.952382455 0.530332229 0.952382455 0.952382455
0.952382455 0.952382455 0.530332229 0.530332229 0.952382455 0.530332229
0.952382455 0.530332229 0.530332229 0.952382455 0.952382455 0.952382455
0.952382455 0.530332229 0.952382455 0.530332229 0.530332229 0.530332229
0.952382455 0.530332229 0.530332229 0.952382455 0.530332229 0.530332229
0.530332229 0.952382455 0.530332229 0.952382455 0.952382455 0.952382455
0.952382455 0.530332229 0.530332229 0.952382455
0.530332229 0.530332229 0.952382455 0.952382455 0.530332229 0.530332229
0.530332229 0.530332229 0.952382455 0.530332229 0.952382455 0.952382455
0.952382455 0.530332229 0.952382455 0.952382455 0.530332229 0.952382455
0.952382455 0.952382455 0.530332229 0.952382455 0.530332229 0.530332229
0.530332229 0.530332229 0.952382455 0.952382455 0.530332229 0.530332229
0.530332229 0.952382455 0.952382455 0.530332229 0.530332229 0.530332229
0.530332229 0.952382455 0.530332229 0.952382455 0.952382455 0.952382455
0.530332229 0.952382455 0.952382455 0.530332229 0.952382455 0.952382455
0.952382455 0.530332229 0.952382455 0.530332229 0.530332229 0.530332229
0.530332229 0.952382455 0.952382455 0.530332229
0.530332229 0.952382455 0.530332229 0.530332229 0.952382455 0.952382455
0.952382455 0.952382455 0.530332229 0.952382455 0.530332229 0.530332229
0.530332229 0.952382455 0.530332229 0.530332229 0.952382455 0.530332229
0.530332229 0.530332229 0.952382455 0.530332229 0.952382455 0.952382455
0.952382455 0.952382455 0.530332229 0.530332229 0.952382455 0.530332229
0.952382455 0.530332229 0.530332229 0.952382455 0.952382455 0.952382455
0.952382455 0.530332229 0.952382455 0.530332229 0.530332229 0.530332229
0.952382455 0.530332229 0.530332229 0.952382455 0.530332229 0.530332229
0.530332229 0.952382455 0.530332229 0.952382455 0.952382455 0.952382455
0.952382455 0.530332229 0.530332229 0.952382455
0.530332229 0.952382455 0.530332229 0.530332229 0.952382455 0.952382455
0.952382455 0.952382455 0.530332229 0.952382455 0.530332229 0.530332229
0.530332229 0.952382455 0.530332229 0.530332229 0.952382455 0.530332229
0.530332229 0.530332229 0.952382455 0.530332229 0.952382455 0.952382455
0.952382455 0.952382455 0.530332229 0.530332229 0.952382455 0.530332229
0.952382455 0.530332229 0.530332229 0.952382455 0.952382455 0.952382455
0.952382455 0.530332229 0.952382455 0.530332229 0.530332229 0.530332229
0.952382455 0.530332229 0.530332229 0.952382455 0.530332229 0.530332229
0.530332229 0.952382455 0.530332229 0.952382455 0.952382455 0.952382455
0.952382455 0.530332229 0.530332229 0.952382455
0.530332229 0.952382455 0.530332229 0.530332229 0.952382455 0.952382455
0.952382455 0.952382455 0.530332229 0.952382455 0.530332229 0.530332229
0.530332229 0.952382455 0.530332229 0.530332229 0.952382455 0.530332229
0.530332229 0.530332229 0.952382455 0.530332229 0.952382455 0.952382455

0.952382455 0.952382455 0.530332229 0.530332229 0.952382455 0.530332229
0.952382455 0.530332229 0.530332229 0.952382455 0.952382455 0.952382455
0.952382455 0.530332229 0.952382455 0.530332229 0.530332229 0.530332229
0.952382455 0.530332229 0.530332229 0.952382455 0.530332229 0.530332229
0.530332229 0.952382455 0.530332229 0.952382455 0.952382455 0.952382455
0.952382455 0.530332229 0.530332229 0.952382455
0.530332229 0.530332229 0.952382455 0.952382455 0.530332229 0.530332229
0.530332229 0.530332229 0.952382455 0.530332229 0.952382455 0.952382455
0.952382455 0.530332229 0.952382455 0.952382455 0.530332229 0.952382455
0.952382455 0.952382455 0.530332229 0.952382455 0.530332229 0.530332229
0.530332229 0.530332229 0.952382455 0.952382455 0.530332229 0.530332229
0.530332229 0.952382455 0.952382455 0.530332229 0.530332229 0.530332229
0.530332229 0.952382455 0.530332229 0.952382455 0.952382455 0.952382455
0.530332229 0.952382455 0.952382455 0.530332229 0.952382455 0.952382455
0.952382455 0.530332229 0.952382455 0.530332229 0.530332229 0.530332229
0.530332229 0.952382455 0.952382455 0.530332229
0.530332229 0.952382455 0.530332229 0.530332229 0.952382455 0.952382455
0.952382455 0.952382455 0.530332229 0.952382455 0.530332229 0.530332229
0.530332229 0.952382455 0.530332229 0.530332229 0.952382455 0.530332229
0.530332229 0.530332229 0.952382455 0.530332229 0.952382455 0.952382455
0.952382455 0.952382455 0.530332229 0.530332229 0.952382455 0.530332229
0.952382455 0.530332229 0.530332229 0.952382455 0.952382455 0.952382455
0.952382455 0.530332229 0.952382455 0.530332229 0.530332229 0.530332229
0.952382455 0.530332229 0.530332229 0.952382455 0.530332229 0.530332229
0.530332229 0.952382455 0.530332229 0.952382455 0.952382455 0.952382455
0.952382455 0.530332229 0.530332229 0.952382455
0.530332229 0.952382455 0.530332229 0.530332229 0.952382455 0.952382455
0.952382455 0.952382455 0.530332229 0.952382455 0.530332229 0.530332229
0.530332229 0.952382455 0.530332229 0.530332229 0.952382455 0.530332229
0.530332229 0.530332229 0.952382455 0.530332229 0.952382455 0.952382455
0.952382455 0.952382455 0.530332229 0.530332229 0.952382455 0.530332229
0.952382455 0.530332229 0.530332229 0.952382455 0.952382455 0.952382455
0.952382455 0.530332229 0.952382455 0.530332229 0.530332229 0.530332229
0.952382455 0.530332229 0.530332229 0.952382455 0.530332229 0.530332229
0.530332229 0.952382455 0.530332229 0.952382455 0.952382455 0.952382455
0.952382455 0.530332229 0.530332229 0.952382455
0.530332229 0.530332229 0.952382455 0.952382455 0.530332229 0.530332229
0.530332229 0.530332229 0.952382455 0.530332229 0.952382455 0.952382455
0.952382455 0.530332229 0.952382455 0.952382455 0.530332229 0.952382455
0.952382455 0.952382455 0.530332229 0.952382455 0.530332229 0.530332229
0.530332229 0.530332229 0.952382455 0.952382455 0.530332229 0.530332229
0.530332229 0.952382455 0.952382455 0.530332229 0.530332229 0.530332229
0.530332229 0.952382455 0.530332229 0.952382455 0.952382455 0.952382455
0.530332229 0.952382455 0.952382455 0.530332229 0.952382455 0.952382455
0.952382455 0.530332229 0.952382455 0.530332229 0.530332229 0.530332229
0.530332229 0.952382455 0.952382455 0.530332229

```
0.530332229   0.952382455   0.530332229   0.530332229   0.952382455   0.952382455
          0.952382455   0.952382455   0.530332229   0.952382455   0.530332229   0.530332229
          0.530332229   0.952382455   0.530332229   0.530332229   0.952382455   0.530332229
          0.530332229   0.530332229   0.952382455   0.530332229   0.952382455   0.952382455
          0.952382455   0.952382455   0.530332229   0.530332229   0.952382455   0.530332229
          0.952382455   0.530332229   0.530332229   0.952382455   0.952382455   0.952382455
          0.952382455   0.530332229   0.952382455   0.530332229   0.530332229   0.530332229
          0.952382455   0.530332229   0.530332229   0.952382455   0.530332229   0.530332229
          0.530332229   0.952382455   0.530332229   0.952382455   0.952382455   0.952382455
          0.952382455   0.530332229   0.530332229   0.952382455
0.530332229   0.952382455   0.530332229   0.530332229   0.952382455   0.952382455
          0.952382455   0.952382455   0.530332229   0.952382455   0.530332229   0.530332229
          0.530332229   0.952382455   0.530332229   0.530332229   0.952382455   0.530332229
          0.530332229   0.530332229   0.952382455   0.530332229   0.952382455   0.952382455
          0.952382455   0.952382455   0.530332229   0.530332229   0.952382455   0.530332229
          0.952382455   0.530332229   0.530332229   0.952382455   0.952382455   0.952382455
          0.952382455   0.530332229   0.952382455   0.530332229   0.530332229   0.530332229
          0.952382455   0.530332229   0.530332229   0.952382455   0.530332229   0.530332229
          0.530332229   0.952382455   0.530332229   0.952382455   0.952382455   0.952382455
          0.952382455   0.530332229   0.530332229   0.952382455
0.530332229   0.952382455   0.530332229   0.530332229   0.952382455   0.952382455
          0.952382455   0.952382455   0.530332229   0.952382455   0.530332229   0.530332229
          0.530332229   0.952382455   0.530332229   0.530332229   0.952382455   0.530332229
          0.530332229   0.530332229   0.952382455   0.530332229   0.952382455   0.952382455
          0.952382455   0.952382455   0.530332229   0.530332229   0.952382455   0.530332229
          0.952382455   0.530332229   0.530332229   0.952382455   0.952382455   0.952382455
          0.952382455   0.530332229   0.952382455   0.530332229   0.530332229   0.530332229
          0.952382455   0.530332229   0.530332229   0.952382455   0.530332229   0.530332229
          0.530332229   0.952382455   0.530332229   0.952382455   0.952382455   0.952382455
          0.952382455   0.530332229   0.530332229   0.952382455
0.530332229   0.530332229   0.952382455   0.952382455   0.530332229   0.530332229
          0.530332229   0.530332229   0.952382455   0.530332229   0.952382455   0.952382455
          0.952382455   0.530332229   0.952382455   0.952382455   0.530332229   0.952382455
          0.952382455   0.952382455   0.530332229   0.952382455   0.530332229   0.530332229
          0.530332229   0.530332229   0.952382455   0.952382455   0.530332229   0.530332229
          0.530332229   0.952382455   0.952382455   0.530332229   0.530332229   0.530332229
          0.530332229   0.952382455   0.530332229   0.952382455   0.952382455   0.952382455
          0.530332229   0.952382455   0.952382455   0.530332229   0.952382455   0.952382455
          0.952382455   0.530332229   0.952382455   0.530332229   0.530332229   0.530332229
          0.530332229   0.952382455   0.952382455   0.530332229
0.530332229   0.952382455   0.530332229   0.530332229   0.952382455   0.952382455
          0.952382455   0.952382455   0.530332229   0.952382455   0.530332229   0.530332229
          0.530332229   0.952382455   0.530332229   0.530332229   0.952382455   0.530332229
          0.530332229   0.530332229   0.952382455   0.530332229   0.952382455   0.952382455
          0.952382455   0.952382455   0.530332229   0.530332229   0.952382455   0.530332229
          0.952382455   0.530332229   0.530332229   0.952382455   0.952382455   0.952382455
```

```
    0.952382455   0.530332229   0.952382455   0.530332229   0.530332229   0.530332229
    0.952382455   0.530332229   0.530332229   0.952382455   0.530332229   0.530332229
    0.530332229   0.952382455   0.530332229   0.952382455   0.952382455   0.952382455
    0.952382455   0.530332229   0.530332229   0.952382455
0.530332229   0.530332229   0.952382455   0.952382455   0.530332229   0.530332229
    0.530332229   0.530332229   0.952382455   0.530332229   0.952382455   0.952382455
    0.952382455   0.530332229   0.952382455   0.952382455   0.530332229   0.952382455
    0.952382455   0.952382455   0.530332229   0.952382455   0.530332229   0.530332229
    0.530332229   0.530332229   0.952382455   0.952382455   0.530332229   0.530332229
    0.530332229   0.952382455   0.952382455   0.530332229   0.530332229   0.530332229
    0.530332229   0.952382455   0.530332229   0.952382455   0.952382455   0.952382455
    0.530332229   0.952382455   0.952382455   0.530332229   0.952382455   0.952382455
    0.952382455   0.530332229   0.952382455   0.530332229   0.530332229   0.530332229
    0.530332229   0.952382455   0.952382455   0.530332229
0.530332229   0.530332229   0.952382455   0.952382455   0.530332229   0.530332229
    0.530332229   0.530332229   0.952382455   0.530332229   0.952382455   0.952382455
    0.952382455   0.530332229   0.952382455   0.952382455   0.530332229   0.952382455
    0.952382455   0.952382455   0.530332229   0.952382455   0.530332229   0.530332229
    0.530332229   0.530332229   0.952382455   0.952382455   0.530332229   0.530332229
    0.530332229   0.952382455   0.952382455   0.530332229   0.530332229   0.530332229
    0.530332229   0.952382455   0.530332229   0.952382455   0.952382455   0.952382455
    0.530332229   0.952382455   0.952382455   0.530332229   0.952382455   0.952382455
    0.952382455   0.530332229   0.952382455   0.530332229   0.530332229   0.530332229
    0.530332229   0.952382455   0.952382455   0.530332229
0.530332229   0.530332229   0.952382455   0.952382455   0.530332229   0.530332229
    0.530332229   0.530332229   0.952382455   0.530332229   0.952382455   0.952382455
    0.952382455   0.530332229   0.952382455   0.952382455   0.530332229   0.952382455
    0.952382455   0.952382455   0.530332229   0.952382455   0.530332229   0.530332229
    0.530332229   0.530332229   0.952382455   0.952382455   0.530332229   0.530332229
    0.530332229   0.952382455   0.952382455   0.530332229   0.530332229   0.530332229
    0.530332229   0.952382455   0.530332229   0.952382455   0.952382455   0.952382455
    0.530332229   0.952382455   0.952382455   0.530332229   0.952382455   0.952382455
    0.952382455   0.530332229   0.952382455   0.530332229   0.530332229   0.530332229
    0.530332229   0.952382455   0.952382455   0.530332229
0.530332229   0.530332229   0.952382455   0.952382455   0.530332229   0.530332229
    0.530332229   0.530332229   0.952382455   0.530332229   0.952382455   0.952382455
    0.952382455   0.530332229   0.952382455   0.952382455   0.530332229   0.952382455
    0.952382455   0.952382455   0.530332229   0.952382455   0.530332229   0.530332229
    0.530332229   0.530332229   0.952382455   0.952382455   0.530332229   0.530332229
    0.530332229   0.952382455   0.952382455   0.530332229   0.530332229   0.530332229
    0.530332229   0.952382455   0.530332229   0.952382455   0.952382455   0.952382455
    0.530332229   0.952382455   0.952382455   0.530332229   0.952382455   0.952382455
    0.952382455   0.530332229   0.952382455   0.530332229   0.530332229   0.530332229
    0.530332229   0.952382455   0.952382455   0.530332229
0.530332229   0.952382455   0.530332229   0.530332229   0.952382455   0.952382455
    0.952382455   0.952382455   0.530332229   0.952382455   0.530332229   0.530332229
```

```
        0.530332229   0.952382455   0.530332229   0.530332229   0.952382455   0.530332229
        0.530332229   0.530332229   0.952382455   0.530332229   0.952382455   0.952382455
        0.952382455   0.952382455   0.530332229   0.530332229   0.952382455   0.530332229
        0.952382455   0.530332229   0.530332229   0.952382455   0.952382455   0.952382455
        0.952382455   0.530332229   0.952382455   0.530332229   0.530332229   0.530332229
        0.952382455   0.530332229   0.530332229   0.952382455   0.530332229   0.530332229
        0.530332229   0.952382455   0.530332229   0.952382455   0.952382455   0.952382455
        0.952382455   0.530332229   0.530332229   0.952382455
0.530332229   0.952382455   0.530332229   0.530332229   0.952382455   0.952382455
        0.952382455   0.952382455   0.530332229   0.952382455   0.530332229   0.530332229
        0.530332229   0.952382455   0.530332229   0.530332229   0.952382455   0.530332229
        0.530332229   0.530332229   0.952382455   0.530332229   0.952382455   0.952382455
        0.952382455   0.952382455   0.530332229   0.530332229   0.952382455   0.530332229
        0.952382455   0.530332229   0.530332229   0.952382455   0.952382455   0.952382455
        0.952382455   0.530332229   0.952382455   0.530332229   0.530332229   0.530332229
        0.952382455   0.530332229   0.530332229   0.952382455   0.530332229   0.530332229
        0.530332229   0.952382455   0.530332229   0.952382455   0.952382455   0.952382455
        0.952382455   0.530332229   0.530332229   0.952382455
0.530332229   0.530332229   0.952382455   0.952382455   0.530332229   0.530332229
        0.530332229   0.530332229   0.952382455   0.530332229   0.952382455   0.952382455
        0.952382455   0.530332229   0.952382455   0.952382455   0.530332229   0.952382455
        0.952382455   0.952382455   0.530332229   0.952382455   0.530332229   0.530332229
        0.530332229   0.530332229   0.952382455   0.952382455   0.530332229   0.530332229
        0.530332229   0.952382455   0.952382455   0.530332229   0.530332229   0.530332229
        0.530332229   0.952382455   0.530332229   0.952382455   0.952382455   0.952382455
        0.530332229   0.952382455   0.952382455   0.530332229   0.952382455   0.952382455
        0.952382455   0.530332229   0.952382455   0.530332229   0.530332229   0.530332229
        0.530332229   0.952382455   0.952382455   0.530332229
];
n = 58;
   for i = 1:n
      for j = 1:n
p1(i,j) = (m(i,j)*cosd(angle(1,j))./0.172)*(sqrt(1-((2.54*2)/(18*2.54)))^(-1)) + 10;
p2(i,j) = (m(i,j)*cosd(angle(2,j))./0.172)*(sqrt(1-((2.54*2)/(18*2.54)))^(-1)) + 10;
p3(i,j) = (m(i,j)*cosd(angle(3,j))./0.172)*(sqrt(1-((2.54*2)/(18*2.54)))^(-1)) + 10;
p4(i,j) = (m(i,j)*cosd(angle(4,j))./0.172)*(sqrt(1-((2.54*2)/(18*2.54)))^(-1)) + 10;
p5(i,j) = (m(i,j)*cosd(angle(5,j))./0.172)*(sqrt(1-((2.54*2)/(18*2.54)))^(-1)) + 10;
p6(i,j) = (m(i,j)*cosd(angle(6,j))./0.172)*(sqrt(1-((2.54*2)/(18*2.54)))^(-1)) + 10;
p7(i,j) = (m(i,j)*cosd(angle(7,j))./0.172)*(sqrt(1-((2.54*2)/(18*2.54)))^(-1)) + 10;
p8(i,j) = (m(i,j)*cosd(angle(8,j))./0.172)*(sqrt(1-((2.54*2)/(18*2.54)))^(-1)) + 10;
p9(i,j) = (m(i,j)*cosd(angle(9,j))./0.172)*(sqrt(1-((2.54*2)/(18*2.54)))^(-1)) + 10;
p10(i,j) = (m(i,j)*cosd(angle(10,j))./0.172)*(sqrt(1-((2.54*2)/(18*2.54)))^(-1)) + 10;
p11(i,j) = (m(i,j)*cosd(angle(11,j))./0.172)*(sqrt(1-((2.54*2)/(18*2.54)))^(-1)) + 10;
p12(i,j) = (m(i,j)*cosd(angle(12,j))./0.172)*(sqrt(1-((2.54*2)/(18*2.54)))^(-1)) + 10;
p13(i,j) = (m(i,j)*cosd(angle(13,j))./0.172)*(sqrt(1-((2.54*2)/(18*2.54)))^(-1)) + 10;
p14(i,j) = (m(i,j)*cosd(angle(14,j))./0.172)*(sqrt(1-((2.54*2)/(18*2.54)))^(-1)) + 10;
```

```
p15(i,j) = (m(i,j)*cosd(angle(15,j))./0.172)*(sqrt(1-((2.54*2)/(18*2.54)))^(-1)) + 10;
p16(i,j) = (m(i,j)*cosd(angle(16,j))./0.172)*(sqrt(1-((2.54*2)/(18*2.54)))^(-1)) + 10;
p17(i,j) = (m(i,j)*cosd(angle(17,j))./0.172)*(sqrt(1-((2.54*2)/(18*2.54)))^(-1)) + 10;
p18(i,j) = (m(i,j)*cosd(angle(18,j))./0.172)*(sqrt(1-((2.54*2)/(18*2.54)))^(-1)) + 10;
p19(i,j) = (m(i,j)*cosd(angle(19,j))./0.172)*(sqrt(1-((2.54*2)/(18*2.54)))^(-1)) + 10;
p20(i,j) = (m(i,j)*cosd(angle(20,j))./0.172)*(sqrt(1-((2.54*2)/(18*2.54)))^(-1)) + 10;
p21(i,j) = (m(i,j)*cosd(angle(21,j))./0.172)*(sqrt(1-((2.54*2)/(18*2.54)))^(-1)) + 10;
p22(i,j) = (m(i,j)*cosd(angle(22,j))./0.172)*(sqrt(1-((2.54*2)/(18*2.54)))^(-1)) + 10;
p23(i,j) = (m(i,j)*cosd(angle(23,j))./0.172)*(sqrt(1-((2.54*2)/(18*2.54)))^(-1)) + 10;
p24(i,j) = (m(i,j)*cosd(angle(24,j))./0.172)*(sqrt(1-((2.54*2)/(18*2.54)))^(-1)) + 10;
p25(i,j) = (m(i,j)*cosd(angle(25,j))./0.172)*(sqrt(1-((2.54*2)/(18*2.54)))^(-1)) + 10;
p26(i,j) = (m(i,j)*cosd(angle(26,j))./0.172)*(sqrt(1-((2.54*2)/(18*2.54)))^(-1)) + 10;
p27(i,j) = (m(i,j)*cosd(angle(27,j))./0.172)*(sqrt(1-((2.54*2)/(18*2.54)))^(-1)) + 10;
p28(i,j) = (m(i,j)*cosd(angle(28,j))./0.172)*(sqrt(1-((2.54*2)/(18*2.54)))^(-1)) + 10;
p29(i,j) = (m(i,j)*cosd(angle(29,j))./0.172)*(sqrt(1-((2.54*2)/(18*2.54)))^(-1)) + 10;
p30(i,j) = (m(i,j)*cosd(angle(30,j))./0.172)*(sqrt(1-((2.54*2)/(18*2.54)))^(-1)) + 10;
p31(i,j) = (m(i,j)*cosd(angle(31,j))./0.172)*(sqrt(1-((2.54*2)/(18*2.54)))^(-1)) + 10;
p32(i,j) = (m(i,j)*cosd(angle(32,j))./0.172)*(sqrt(1-((2.54*2)/(18*2.54)))^(-1)) + 10;
p33(i,j) = (m(i,j)*cosd(angle(33,j))./0.172)*(sqrt(1-((2.54*2)/(18*2.54)))^(-1)) + 10;
p34(i,j) = (m(i,j)*cosd(angle(34,j))./0.172)*(sqrt(1-((2.54*2)/(18*2.54)))^(-1)) + 10;
p35(i,j) = (m(i,j)*cosd(angle(35,j))./0.172)*(sqrt(1-((2.54*2)/(18*2.54)))^(-1)) + 10;
p36(i,j) = (m(i,j)*cosd(angle(36,j))./0.172)*(sqrt(1-((2.54*2)/(18*2.54)))^(-1)) + 10;
p37(i,j) = (m(i,j)*cosd(angle(37,j))./0.172)*(sqrt(1-((2.54*2)/(18*2.54)))^(-1)) + 10;
p38(i,j) = (m(i,j)*cosd(angle(38,j))./0.172)*(sqrt(1-((2.54*2)/(18*2.54)))^(-1)) + 10;
p39(i,j) = (m(i,j)*cosd(angle(39,j))./0.172)*(sqrt(1-((2.54*2)/(18*2.54)))^(-1)) + 10;
p40(i,j) = (m(i,j)*cosd(angle(40,j))./0.172)*(sqrt(1-((2.54*2)/(18*2.54)))^(-1)) + 10;
p41(i,j) = (m(i,j)*cosd(angle(41,j))./0.172)*(sqrt(1-((2.54*2)/(18*2.54)))^(-1)) + 10;
p42(i,j) = (m(i,j)*cosd(angle(42,j))./0.172)*(sqrt(1-((2.54*2)/(18*2.54)))^(-1)) + 10;
p43(i,j) = (m(i,j)*cosd(angle(43,j))./0.172)*(sqrt(1-((2.54*2)/(18*2.54)))^(-1)) + 10;
p44(i,j) = (m(i,j)*cosd(angle(44,j))./0.172)*(sqrt(1-((2.54*2)/(18*2.54)))^(-1)) + 10;
p45(i,j) = (m(i,j)*cosd(angle(45,j))./0.172)*(sqrt(1-((2.54*2)/(18*2.54)))^(-1)) + 10;
p46(i,j) = (m(i,j)*cosd(angle(46,j))./0.172)*(sqrt(1-((2.54*2)/(18*2.54)))^(-1)) + 10;
p47(i,j) = (m(i,j)*cosd(angle(47,j))./0.172)*(sqrt(1-((2.54*2)/(18*2.54)))^(-1)) + 10;
p48(i,j) = (m(i,j)*cosd(angle(48,j))./0.172)*(sqrt(1-((2.54*2)/(18*2.54)))^(-1)) + 10;
p49(i,j) = (m(i,j)*cosd(angle(49,j))./0.172)*(sqrt(1-((2.54*2)/(18*2.54)))^(-1)) + 10;
p50(i,j) = (m(i,j)*cosd(angle(50,j))./0.172)*(sqrt(1-((2.54*2)/(18*2.54)))^(-1)) + 10;
p51(i,j) = (m(i,j)*cosd(angle(51,j))./0.172)*(sqrt(1-((2.54*2)/(18*2.54)))^(-1)) + 10;
p52(i,j) = (m(i,j)*cosd(angle(52,j))./0.172)*(sqrt(1-((2.54*2)/(18*2.54)))^(-1)) + 10;
p53(i,j) = (m(i,j)*cosd(angle(53,j))./0.172)*(sqrt(1-((2.54*2)/(18*2.54)))^(-1)) + 10;
p54(i,j) = (m(i,j)*cosd(angle(54,j))./0.172)*(sqrt(1-((2.54*2)/(18*2.54)))^(-1)) + 10;
p55(i,j) = (m(i,j)*cosd(angle(55,j))./0.172)*(sqrt(1-((2.54*2)/(18*2.54)))^(-1)) + 10;
p56(i,j) = (m(i,j)*cosd(angle(56,j))./0.172)*(sqrt(1-((2.54*2)/(18*2.54)))^(-1)) + 10;
p57(i,j) = (m(i,j)*cosd(angle(57,j))./0.172)*(sqrt(1-((2.54*2)/(18*2.54)))^(-1)) + 10;
p58(i,j) = (m(i,j)*cosd(angle(58,j))./0.172)*(sqrt(1-((2.54*2)/(18*2.54)))^(-1)) + 10;
      end
   end
```

```
p = [sum(p1);
sum(p2);
sum(p3);
sum(p4);
sum(p5);
sum(p6);
sum(p7);
sum(p8);
sum(p9);
sum(p10);
sum(p11);
sum(p12);
sum(p13);
sum(p14);
sum(p15);
sum(p16);
sum(p17);
sum(p18);
sum(p19);
sum(p20);
sum(p21);
sum(p22);
sum(p23);
sum(p24);
sum(p25);
sum(p26);
sum(p27);
sum(p28);
sum(p29);
sum(p30);
sum(p31);
sum(p32);
sum(p33);
sum(p34);
sum(p35);
sum(p36);
sum(p37);
sum(p38);
sum(p39);
sum(p40);
sum(p41);
sum(p42);
sum(p43);
sum(p44);
sum(p45);
sum(p46);
```

```
sum(p47);
sum(p48);
sum(p49);
sum(p50);
sum(p51);
sum(p52);
sum(p53);
sum(p54);
sum(p55);
sum(p56);
sum(p57);
sum(p58)];
q = 200;
for k = 1:q
    z = transpose(p).*lambda;
    y = a./(p.*lambda);
    x = z*y;
    lambda = x;
end
%lambda = circshift(lambda, [-20 15]);
imagesc(lambda)
```

REFERENCES

[1] M. Bourne, "Characterization of the CLYC detector for neutron and photon detection," Nuclear Instruments and Methods in Physics Research Section A: Accelerators, Spectrometers, Detectors and Associated Equipment, vol. 736, pp. 124-127, 2014.

[2] D. Reilly, H. S. Ensslin and S. Kreiner, "Passive Nondestructive Assay of Nuclear Materials," Los Alamos National Laboratory, Los Alamos, NM, 1991.

[3] B. Budden, "A Cs2LiYCl6:Ce-based advanced radiation monitoring device," Nuclear Instruments and Methods in Physics and Research A, vol. 784, pp. 97-104, 2015.

[4] "National Nuclear Data Center," [Online]. Available: http://www.nndc.bnl.gov/exfor/servlet/E4sGetTabSect?SectID=334216&req=29981&PenSectID=287141. [Accessed 26 August 2016].

[5] J. Glodo, W. M. Higgins, E. V. D. van Loef and S. Shah, "Scintillation Properties of 1 Inch Cs2LiYCl6:Ce Crystals"," in IEEE Transactions on Nuclear Science, 2008.

[6] N. D'Olympia, "Optimizing Cl2LiYCl6 for fast neutron spectroscopy," Nuclear Instruments and Methods in Physics Research A, vol. 694, pp. 140-146, 2012.

[7] P. Guss, T. Stampahar, S. Mukhopadhyay, J. Lee, K. Shah, M. Squillante and W. Higgins, "Novel Deployment of Elpasolites as a Duel Gamma-Neutron Directional Detector," Site Directed Research & Development, 2013.

[8] Gamma-Neutron Scintillator Properties CLYC, RMD, Inc., 2016.

[9] G. Knoll, Radiation Detection and Measurement, Wiley & Sons, 2010.

[10] G. e. al, "The CLYC-6 and CLYC-7 response to gamma-rays, fast and thermal neutrons," Nuclear Instruments and Methods in Physics Research A, vol. 810, pp. 132-139, 2016.

[11] N. D'Olympia, "Pulse-shape analysis of CLYC for thermal neutrons, fast neutrons, and gamma-rays," Nuclear Instruments and Methods in Physics Research A, vol. 714, pp. 121-127, 2013.

[12] U. Shirwadkar, "Investigating Scintillation Properties of Ce Doped Cs2LiYBr6," in IEEE Proc., 2010.

[13] J. Glodo, "Pulse Shape Discrimination with Selected Elpasolite Crystals," in IEEE Trans. on Nuclear Science, 2012.

[14] H. Kim, G. Rooh, H. Park and S. Kim, "Tl2LiYCl6(Ce3+): New Tl-based Elpasolite Scintillation Material," in IEEE Trans. on Nuclear Science, 2016.

[15] D. Shea and D. Morgan, "The Helium-3 Shortage: Supply, Demand, and Options for Congress," Federation of American Scientists, 2010.

[16] D. Cester, "A novel detector assembly for detecting thermal neutrons, fast neutrons and gamma rays," Nuclear Instruments and Methods in Physics Research A, vol. 830, pp. 191-196, 2016.

[17] "Evaluated Nuclear Data File (ENDF)," International Atomic Energy Agency, [Online]. Available: https://www.nds.iaea.org/exfor/endf.htm. [Accessed 14 March 2014].

[18] P. Holm, K. Perajarvi, S. Ristkari, T. Siiskonen and H. Toivonen, "A capture-gate neutron spectrometer for characterization of neutron sources and their shields," Nuclear Instruments and Methods in Physics Research A, vol. 751, pp. 48-54, 2014.

[19] F. Pino, "Detecting fast and thermal neutrons with a boron loaded liquid scintillator EJ-339A," Applied Radiation and Isotopes, vol. 92, pp. 6-11, 2014.

[20] N. Zaitseva, "Pulse shape discrimination with lithium-containing organic scintillators," Nuclear Instruments and Methods in Physics Research A, vol. 729, pp. 747-754, 2013.

[21] N. D'Olympia, "Fast neutron response of 6Li-depleted CLYC detectors up to 20 MeV," Nuclear Instruments and Methods in Physics Research A, vol. 763, pp. 433-441, 2014.

[22] L. Pellegri, "Thermal and fast neutron detection with two CLYC scintillators," in IEEE Proc., 2014.

[23] Giaz, "Fast neutron measurements with 7Li and 6Li enriched CLYC scintillators," Nuclear Instruments and Methods in Physics Research A, vol. 825, pp. 51-61, 2016.

[24] "InSpectorTM 1000 Digital Handheld Multichannel Analyzer," Canberra Industries, Inc., 2011.

[25] B. McDonald, "A wearable sensor based on CLYC scintillators," Nuclear Instruments and Methods in Physics Research A, vol. 821, pp. 73-80, 2016.

[26] "Target F500: Made for the mission," Target Systemelektronik GmbH & Co., [Online]. Available: http://target-sg.com/f500.html. [Accessed 1 November 2016].

[27] "RIIDEyeTM X/M Series Handheld Radiation Isotope Identifiers," Thermo Fisher Scientific, Inc., [Online]. Available: https://thermofisher.com/order/catalog/product/4250863. [Accessed 1 November 2016].

[28] Liu, P. Drouin, J. Deziel, M. Deziel and D. Waller, "Wireless Radiation Sensor Network with Directional Radiation Detectors," in IEEE Proc., 2014.

[29] A. Guckes, "Novel Deployment of Elpasolites as a Dual Neutron / Gamma-ray Directional Detector," University of Nevada, Las Vegas, 2014.

[30] J. Brennan, "Demonstration of two-dimensional time-encoded imaging of fast neutrons," Nuclear Instruments and Methods in Physics Research A, vol. 802, pp. 76-81, 2015.

[31] M. Cieslak, K. Gammage and R. Glover, "Coded-aperture imaging systems: Past, present and future development - A review," Radiation Measurements, vol. 92, pp. 59-71, 2016.

[32] L. Shepp and Y. Vardi, "Maximum Likelihood Reconstruction for Emission Tomography," IEEE Trans. on Medical Imaging, Vols. MI-1, no. 2, pp. 113-122, 1982.

[33] J. Lamarsh and A. Baratta, Introduction to Nuclear Engineering, Upper Saddle River, NJ: Prentice-Hall, Inc., 2001.

[34] J. J. D. Lima, "Imaging Methodologies," in Nuclear Medicine Physics, Boca Raton, FL, US, Taylor & Francis, 2011, p. 251.

[35] H. Liskien and A. Paulsen, "Neutron production cross sections and energies for the reactions T(p,n)3He, D(d,n)3He, and T(d,n)4He," Atomic Data and Nuclear Data Tables, vol. 11, no. 7, pp. 569-619, 1973.

[36] "Raspberry Pi 3 - Model B - ARMv8 with 1G RAM," Adafruit Industries, [Online]. Available: https://www.adafruit.com/products/3055. [Accessed 2017 February 27].

[37] "PiTFT Plus 480x320 3.5" TFT+Touchscreen for Raspberry Pi," Adafruit Industries, [Online]. Available: https://www.adafruit.com/products/2441. [Accessed 27 February 2017].

[38] "Morpho Data Server," Brideport Instruments (BPI), LLC, [Online]. Available: http://bridgeportinstruments.com/products/mds/mds.html. [Accessed 27 February 2017].

[39] I. Akkurt, K. GUnoglu and S. Arda, "Detection Efficiency of NaI(Tl) Detector in 511-1332 keV Energy Range," Science and Technology of Nuclear Installations, 2014.

[40] "National Nuclear Data Center," [Online]. Available: http://www.nndc.bnl.gov/exfor/servlet/E4sGetTabSect?SectID=334201&req=29982&PenSectID=287126. [Accessed 26 Aug 2016].

[41] "Gamma-Neutron Scintillator Properties CLYC," RMD, Inc., [Online]. Available: http://rmdinc.com/wp-content/uploads/2016/06/CLYC-Properties-5-10-16.pdf. [Accessed 22 march 2017].

[42] M. D. Team, "MCNP6, Version 1.0," Los Alamos National Laboratory, 2013.

CURRICULUM VITA

Amber Guckes

Contact Information

E-mail address: shield39@unlv.nevada.edu

Education

University of Nevada, Las Vegas
Ph.D., Mechanical Engineering with Concentration in Nuclear Engineering, May 2017
Dissertation Title: Applications of Elpasolites as a Mutlimode Radiation Sensor
M.S., Nuclear Engineering and Material Sciences, December 2014
Thesis Title: Deployment of Elpasolites as a Dual Neutron / Gamma-ray Directional Detection System
Graduate Certificate, Nuclear Criticality Safety Engineering, December 2014
Graduate Certificate, Nuclear Safeguards and Security, December 2014
B.S.M.E., Mechanical Engineering, December 2013

Employment

National Security Technologies, LLC
Nuclear Operations Directorate
Nuclear Safety Division
Nuclear Safety Engineer, June 2013 – August 2016

National Security Technologies, LLC
Nuclear Operations Directorate
Nuclear Safety Division
Unreviewed Safety Question (USQ) Lead Engineer, August 2016 - present

Publications

A. Guckes, A. Barzilov, D. Beller, T. Ward, "Monte Carlo Analysis of Neutron Multiplicity Detector System for WIMP Mass Measurement," Proc. of the American Nuclear Society 2014 Student Conference, Pennsylvania State University, State College, PA, USA, April 3 – 5, 2014.

A. Guckes, A. Barzilov, N. Richardson, "Modeling of Time-Correlated Detection of Fast Neutrons Emitted in Induced SNM Fission," Physics Procedia, 23rd Conference on Application of Accelerators in Research and Industry (CAARI), 2014.

P. Guss, T. Stampahar, A. Guckes, A. Barzilov, "Scintillation Properties of a $Cs_2LiLa(Br_6)90\%(Cl_6)10\%$:Ce (CLLBC) Crystal," Proc. SPIE, , Vol. 9215, San Diego, CA, USA September 2014.

P. Guss, T. Stampahar, A. Barzilov, A. Guckes, "Direction Detection of ^{239}Pu," Plutonium Futures: The Science 2014, Las Vegas, NV, USA, September 7-12, 2014.

A. Guckes, "Novel Deployment of Elpasolites as a Dual Neutron / Gamma-ray Directional Detector ," M.S. Thesis, University of Nevada, Las Vegas, December 2014.

P. Guss, T. Stampahar, S. Mukhopadhyay, A. Barzilov, A. Guckes, "Maximum Likelihood Source Localization Using Elpasolite Crystals as a Dual Gamma Neutron Directional Detector," Proc. SPIE, Radiation Detectors: Systems and Applications XVI, Vol. 9595, San Diego, CA, USA, August 27, 2015.

A. Guckes, A. Barzilov, P. Guss, "Directional Detection of Neutrons and Photons Using Elpasolites: Computational Study," submitted to Radiation Measurements, May 2017.

A. Guckes, A. Barzilov, P. Guss, "Directional Detection of Neutrons and Photons Using Elpasolites: Experimental Study," to be submitted, May 2017.

A. Guckes, A. Barilov, "Development and Deployment of the Collimated Directional Radiation Detection System," Proc. SPIE, San Diego, CA, USA, August 6-10, 2017.